

TSUNAMI HAZARD MAPS OF THE PUGET SOUND AND ADJACENT WATERS—MODEL RESULTS FROM AN EXTENDED L1 **M_w** 9.0 CASCADIA SUBDUCTION ZONE MEGATHRUST EARTHQUAKE SCENARIO

by Alexander Dolcimascolo, Daniel W. Eungard, Corina Allen,
Randall J. LeVeque, Loyce M. Adams, Diego Arcas,
Vasily V. Titov, Frank I. González, Christopher Moore,
Carrie E. Garrison-Laney, and Timothy J. Walsh

WASHINGTON
GEOLOGICAL SURVEY
Map Series 2021-01
April 2021

PEER REVIEWED



WASHINGTON STATE DEPARTMENT OF
NATURAL RESOURCES
WASHINGTON GEOLOGICAL SURVEY

TSUNAMI HAZARD MAPS OF THE PUGET SOUND AND ADJACENT WATERS—MODEL RESULTS FROM AN EXTENDED L1 **M_w** 9.0 CASCADIA SUBDUCTION ZONE MEGATHRUST EARTHQUAKE SCENARIO

by Alexander Dolcimascolo, Daniel W. Eungard, Corina Allen,
Randall J. LeVeque, Loyce M. Adams, Diego Arcas,
Vasily V. Titov, Frank I. González, Christopher Moore,
Carrie E. Garrison-Laney, and Timothy J. Walsh

WASHINGTON
GEOLOGICAL SURVEY
Map Series 2021-01
April 2021

This article has undergone a refereed review process with input from three of the author's subject-matter peers from outside the Washington Geological Survey who did not contribute toward the writing of the article.

This publication has also been subject to an iterative review process with Survey editors and cartographers and has been formatted by Survey staff.



WASHINGTON STATE DEPARTMENT OF
NATURAL RESOURCES
WASHINGTON GEOLOGICAL SURVEY

DISCLAIMER

Neither the State of Washington, nor any agency thereof, nor any of their employees, makes any warranty, express or implied, or assumes any legal liability or responsibility for the accuracy, completeness, or usefulness of any information, apparatus, product, or process disclosed, or represents that its use would not infringe privately owned rights. Reference herein to any specific commercial product, process, or service by trade name, trademark, manufacturer, or otherwise, does not necessarily constitute or imply its endorsement, recommendation, or favoring by the State of Washington or any agency thereof. The views and opinions of authors expressed herein do not necessarily state or reflect those of the State of Washington or any agency thereof.

This map product has been subjected to an iterative external and internal review process by agency geologists, cartographers, and editors and meets Map Series standards as defined by the Washington Geological Survey.

INDEMNIFICATION

This item was partially funded by the National Oceanic and Atmospheric Administration (NOAA) award no. NA19NWS4670017 to the Washington Geological Survey. This does not constitute an endorsement by NOAA.

WASHINGTON STATE DEPARTMENT OF NATURAL RESOURCES

Hilary S. Franz—*Commissioner of Public Lands*

WASHINGTON GEOLOGICAL SURVEY

Casey R. Hanell—*State Geologist*

Jessica L. Czajkowski—*Assistant State Geologist*

Ana Shafer—*Assistant State Geologist*

Washington State Department of Natural Resources Washington Geological Survey

Mailing Address:

MS 47007

Olympia, WA 98504-7007

Street Address:

Natural Resources Bldg, Rm 148

1111 Washington St SE

Olympia, WA 98501

Phone: 360-902-1450

Fax: 360-902-1785

Email: geology@dnr.wa.gov

Website: <http://www.dnr.wa.gov/geology>



Publications and Maps:

[www.dnr.wa.gov/programs-and-services/geology/
publications-and-data/publications-and-maps](http://www.dnr.wa.gov/programs-and-services/geology/publications-and-data/publications-and-maps)

Washington Geology Library Searchable Catalog:

[www.dnr.wa.gov/programs-and-services/geology/
washington-geology-library](http://www.dnr.wa.gov/programs-and-services/geology/washington-geology-library)

Suggested Citation: Dolcimascolo, Alexander; Eungard, D. W.; Allen, Corina; LeVeque, R. J.; Adams, L. M.; Arcas, Diego; Titov, V. V.; González, F. I.; Moore, Christopher; Garrison-Laney, C. E.; Walsh, T. J., 2021, Tsunami hazard maps of the Puget Sound and adjacent waters—Model results from an extended L1 Mw 9.0 Cascadia subduction zone megathrust earthquake scenario: Washington Geological Survey Map Series 2021-01, 16 sheets, scale 1:48,000, 49 p. text. [[https://fortress.wa.gov/dnr/geologydata/tsunami_hazard_maps/
ger_ms2021-01_tsunami_hazard_puget_sound.zip](https://fortress.wa.gov/dnr/geologydata/tsunami_hazard_maps/ger_ms2021-01_tsunami_hazard_puget_sound.zip)]



Daniel W Eungard

Daniel W. Eungard
April 2021

Contents

Introduction	1
Comparison of Tsunami Models	2
Modeling Approach	4
Results	9
Inundation	10
Current Speed.....	11
Timing of Tsunami Arrival and Initial Water Disturbance.....	11
Limitations of the Model.....	11
Conclusion.....	13
Acknowledgments.....	14
References	14
Appendix A. Tsunami Source Evidence and Models.....	18
Review of Evidence	19
Coastal Earthquake Subsidence.....	19
Tsunami Deposits.....	19
Deep-Sea Sediment Cores	19
Diatoms.....	21
Oral and Written Histories	21
Earthquake Slip Distributions and Tsunami Models.....	21
1700 Earthquake	21
Pre-1700 Earthquakes	22
Appendix B. Tide Gauge Comparison of the L1 and Extended L1 Scenarios.....	23
Appendix C. Tide Gauge Locations and Waveforms.....	23

FIGURES

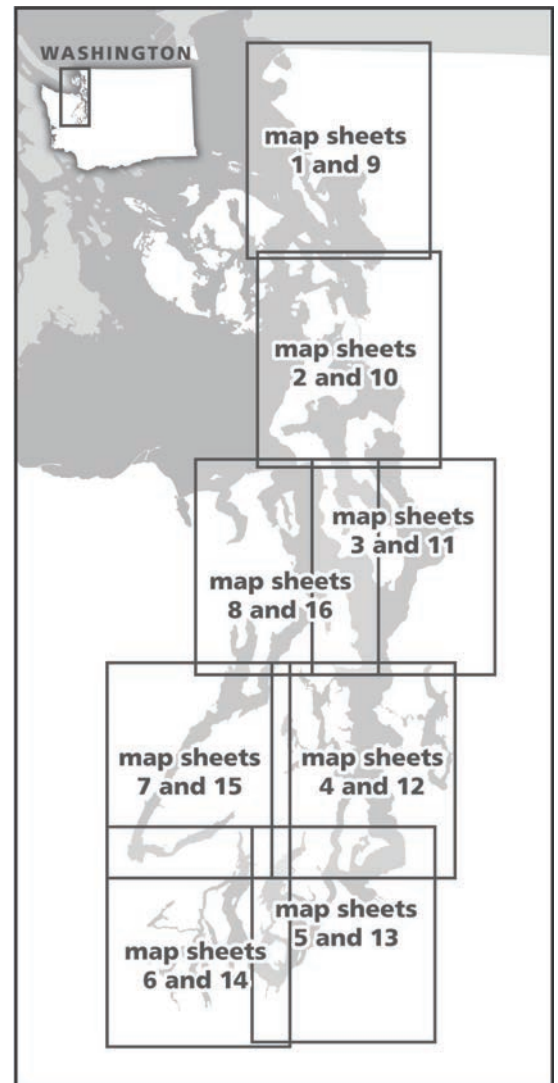
Figure 1. Tectonic overview of the Cascadia subduction zone	2
Figure 2. Map of the modeled area, showing the Cascadia subduction zone (CSZ) and major offshore channels	3
Figure 3. Comparison of vertical ground deformation for the Extended L1 scenario and the previous L1 scenario	5
Figure 4. Tsunami inundation depth shown in feet near Samish Bay from the L1 earthquake scenario and from the Extended L1 earthquake scenario.....	6
Figure 5. Map of new modeling compared to areas of previous modeling.....	7
Figure 6. Study areas modeled in this project	8
Figure 7. Map of initial ground and seafloor deformation from the Extended L1 scenario	9
Figure 8. Modeled tsunami wave variations over time for two simulated tide gauges.....	12
Figure 9. Schematic diagram of chronologic events following a CSZ earthquake and tsunami	13
Figure A1. Exposed sediments along the edge of the tidal marsh at Lynch Cove in Hood Canal	18
Figure A2. Schematic showing the formation of ghost forests over time.....	19
Figure A3. Two alternative schematic views of turbidity currents descending submarine canyons	20
Figure B1. Selected synthetic tide gauge locations simulated with both the L1 and Extended L1 earthquake scenarios.....	23
Figure B2. A comparison of modeled tsunami wave variations over time between the L1 and Extended L1 earthquake scenarios.....	23
Figure C1. Locations for each synthetic simulated tide gauge	26

TABLES

Table 1. Published tsunami hazard maps for Washington.....3
Table 2. Tsunami impacts from the CSZ Extended L1 scenario at key locations within the Puget Sound and adjacent waterways.....10
Table A1. Estimates of earthquake recurrence on the Cascadia subduction zone.....20
Table B1. Selected synthetic tide gauge locations simulated with both the L1 and Extended L1 earthquake scenarios23
Table C1. Additional synthetic simulated tide gauge key locations.....27

MAP SHEET

Map Sheet 1. Detailed tsunami inundation of the Puget Sound and adjacent waters—Strait of Georgia
 Map Sheet 2. Detailed tsunami inundation of the Puget Sound and adjacent waters—Whidbey Basin
 Map Sheet 3. Detailed tsunami inundation of the Puget Sound and adjacent waters—Admiralty Inlet
 Map Sheet 4. Detailed tsunami inundation of the Puget Sound and adjacent waters—East Passage
 Map Sheet 5. Detailed tsunami inundation of the Puget Sound and adjacent waters—Eastern South Sound
 Map Sheet 6. Detailed tsunami inundation of the Puget Sound and adjacent waters—Western South Sound
 Map Sheet 7. Detailed tsunami inundation of the Puget Sound and adjacent waters—Southern Hood Canal
 Map Sheet 8. Detailed tsunami inundation of the Puget Sound and adjacent waters—Northern Hood Canal
 Map Sheet 9. Tsunami maximum current speed of the Puget Sound and adjacent waters—Strait of Georgia
 Map Sheet 10. Tsunami maximum current speed of the Puget Sound and adjacent waters—Whidbey Basin
 Map Sheet 11. Tsunami maximum current speed of the Puget Sound and adjacent waters—Admiralty Inlet
 Map Sheet 12. Tsunami maximum current speed of the Puget Sound and adjacent waters—East Passage
 Map Sheet 13. Tsunami maximum current speed of the Puget Sound and adjacent waters—Eastern South Sound
 Map Sheet 14. Tsunami maximum current speed of the Puget Sound and adjacent waters—Western South Sound
 Map Sheet 15. Tsunami maximum current speed of the Puget Sound and adjacent waters—Southern Hood Canal
 Map Sheet 16. Tsunami maximum current speed of the Puget Sound and adjacent waters—Northern Hood Canal



Tsunami Hazard Maps of the Puget Sound and Adjacent Waters—Model Results from an extended L1 Mw 9.0 Cascadia Subduction Zone Megathrust Earthquake Scenario

by Alexander Dolcimascolo¹, Daniel W. Eungard¹, Corina Allen¹, Randall J. LeVeque², Loyce M. Adams², Diego Arcas³, Vasily V. Titov³, Frank I. González⁴, Christopher Moore³, Carrie E. Garrison-Laney⁵, and Timothy J. Walsh¹

¹ Washington Geological Survey
MS 47007
Olympia, WA
98504-7007

² Department of Applied Mathematics
University of Washington
Seattle, WA
98195-3925

³ National Oceanic and Atmospheric Administration
Pacific Marine Environmental Laboratory
7600 Sand Point Way NE
Seattle, WA
98115-6349

⁴ Department of Earth and Space Sciences
University of Washington
4000 15th Ave NE
Seattle, WA
98195-1310

⁵ Washington Sea Grant
University of Washington
3716 Brooklyn Ave NE
Seattle, WA
98105-6716

ABSTRACT

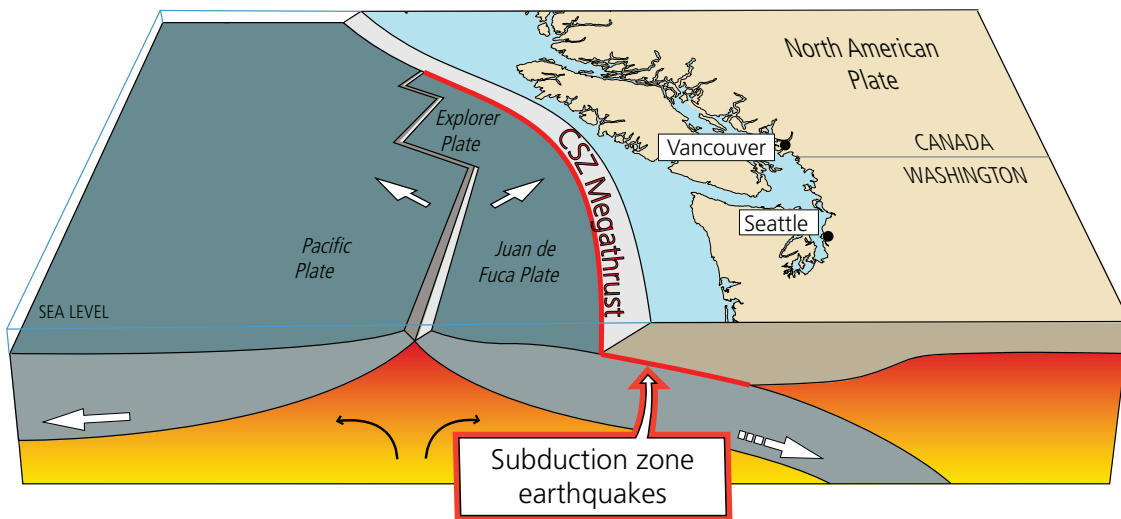
New tsunami modeling using a large earthquake scenario along the Cascadia subduction zone is now available for all areas within the Puget Sound and parts of the Strait of Georgia, some of which had not been modeled before. This modeling uses a simulated magnitude 9.0 earthquake that produces a tsunami that is unlikely to be exceeded in the next great earthquake. The intent of the modeling is to encourage hazard planning and increase community resilience. The earthquake scenario presented here is based on one that was recently used to estimate the hazard posed to Oregon by tsunamis. However, because tsunamis generated offshore must enter through the Strait of Juan de Fuca to reach Washington's inner coastline, our scenario adopts a fault geometry that extends farther north than the one used for Oregon. This extension better represents a tsunami generated offshore of northern Washington. The updated subduction zone geometry assumes a full-length rupture that spans ~775 mi from northern California to the northern end of Vancouver Island, Canada. Scientists inferred that this scenario encompasses ~95 percent of the variability of Cascadia tsunami simulations. Modeling results indicate that the tsunami would first arrive in all inner coastal waterway locations as a trough, with sea level gradually receding. The first tsunami wave generated by the earthquake would arrive on the west side of Whidbey Island approximately 1 hour and 30 minutes after the earthquake, with large wave crests in excess of 16 ft (5 m) traveling north into the Strait of Georgia and south through Puget Sound. Most other locations within Puget Sound and parts of the Strait of Georgia would encounter this first tsunami wave within 2–4 hours of the earthquake, leaving little time to issue official warnings, although any felt earthquake shaking is an immediate warning. Fast moving currents from the tsunami waves could locally exceed 9 knots in multiple harbors, inlets, and passages within the narrow waterways of Washington's inner coastline, presenting a significant navigational hazard to the maritime community. Tsunami wave inundation would likely continue over 14 hours and remain hazardous to maritime operations for more than 24 hours. This study is limited in that modeling does not account for tide stage, tidal currents, earthquake-induced landslides, seiches, liquefaction, or minor topographic changes that would locally modify the effects of tsunami waves. In addition, there are many assumptions associated with the scenario earthquake and its probability of occurrence modeled here. Due to these limitations, this modeling is unsuitable for site-specific tsunami inundation assessment or for determining effects on the built environment. Instead, we recommend using this modeling as a tool to assist with emergency preparations and evacuation planning prior to a Cascadia subduction zone event.

INTRODUCTION

The Cascadia subduction zone (CSZ), with the inclusion of the Explorer Plate to the north, stretches for about 775 mi along the Pacific Ocean from Cape Mendocino, California to just north of Vancouver Island, Canada. At the CSZ, the Juan de Fuca and Explorer oceanic plates slide beneath the North American

continental plate (Fig. 1), generating great earthquakes when strain builds up and abruptly releases. These earthquakes can produce tsunamis that pose a significant hazard to Washington.

Numerous workers found geologic evidence of tsunami deposits attributed to the CSZ in at least 59 localities from northern California to southern Vancouver Island (compiled in



Source	Maximum Size	Average Recurrence Interval	Major Past Earthquakes (Year)
— CSZ Megathrust	M 9	500-600 yr	1700

Figure 1. Tectonic overview of the Cascadia subduction zone (CSZ). The red line indicates the subduction zone interface that may host a megathrust earthquake. Strain builds up along this interface, where the Juan de Fuca and Explorer Plates subduct under the overriding North American Plate, generating earthquakes when it releases. This release of strain along the interface deforms the sea floor and represents the source of tsunamis for the CSZ (Figure modified from the U.S. Geological Survey).

Peters and others, 2003). The observed evidence of past seismicity and tsunamis suggests that not all earthquakes generated by the CSZ are the same. The preserved geologic record both onshore and offshore presents clues that help quantify the history of earthquakes along the CSZ. This information has become crucial for tsunami modeling and hazard preparedness, especially after recent events in Sumatra in 2004 and Japan in 2011, where the hazard was underestimated. The multitude of geologic findings (see *Appendix A* for a fuller discussion) and the history of past tsunami events in other parts of the world have now encouraged tsunami modelers and preparedness efforts to focus on more exceptional hazard scenarios than were previously considered.

Research over the last few decades illustrating the impacts of CSZ earthquakes and tsunamis along the shorelines of British Columbia (Hutchinson and Clague, 2017), Washington (Atwater, 1992; Atwater and others, 1995), Oregon (Kelsey and others, 2005), and northern California (Padgett and others, 2021) has led to concern that these events will leave little time for response. A key component of tsunami hazard assessment and the first step in developing evacuation plans is to identify areas subject to tsunami inundation (flooding caused by tsunami waves). This study focuses on modeling maximum tsunami inundation and current speeds for all areas within Washington’s Puget Sound and its adjacent waters (including parts of the Strait of Georgia, herein referred to as inner waterways, Fig. 2). The study results are based on a scenario earthquake and tsunami (the Extended L1 scenario described in the following section) estimated to encompass 95 percent of the inundation modeled in a suite of hypothetical CSZ tsunami scenarios

(Witter and others, 2011). This scenario produces a tsunami that is unlikely to be exceeded in the next CSZ event.

COMPARISON OF TSUNAMI MODELS

In this study we use the “Extended L1” earthquake scenario to model the impacts of a tsunami on the Puget Sound and adjacent waters. Previous tsunami modeling in Washington used other models that represent different scenarios, ones that are less conservative and may underestimate the hazard level for Washington. The tsunami modeling results presented in this publication include some areas with previously published tsunami inundation modeling using these alternate scenarios. For example, Walsh and others (2004, 2005) modeled impacts to the Bellingham and Anacortes–Whidbey Island areas using the CSZ “1A” scenario (Myers and others, 1999; Priest and others, 1997; Table 1). Researchers based the 1A scenario on the last CSZ event in 1700 (Myers and others, 1999), but successive research suggested that there were larger events than the event in the year 1700 (See *Appendix A*; Witter and others, 2011; Goldfinger and others, 2012; Witter and others, 2013).

Eungard and others (2018a) remodeled the Anacortes and Bellingham regions with the newer CSZ “L1” scenario of Witter and others (2011, 2013). These studies inferred higher variability in both the amount of slip and slip distribution from the paleotsunami record than the 1A scenario, producing larger tsunamis than the 1A scenario. Specifically, the L1 scenario assumes a greater amount of maximum slip at 88.6 ft (27 m) compared to the 1A scenario with 62 ft (19 m), and partitions slip to a splay fault (a thrust fault in the accretionary wedge)

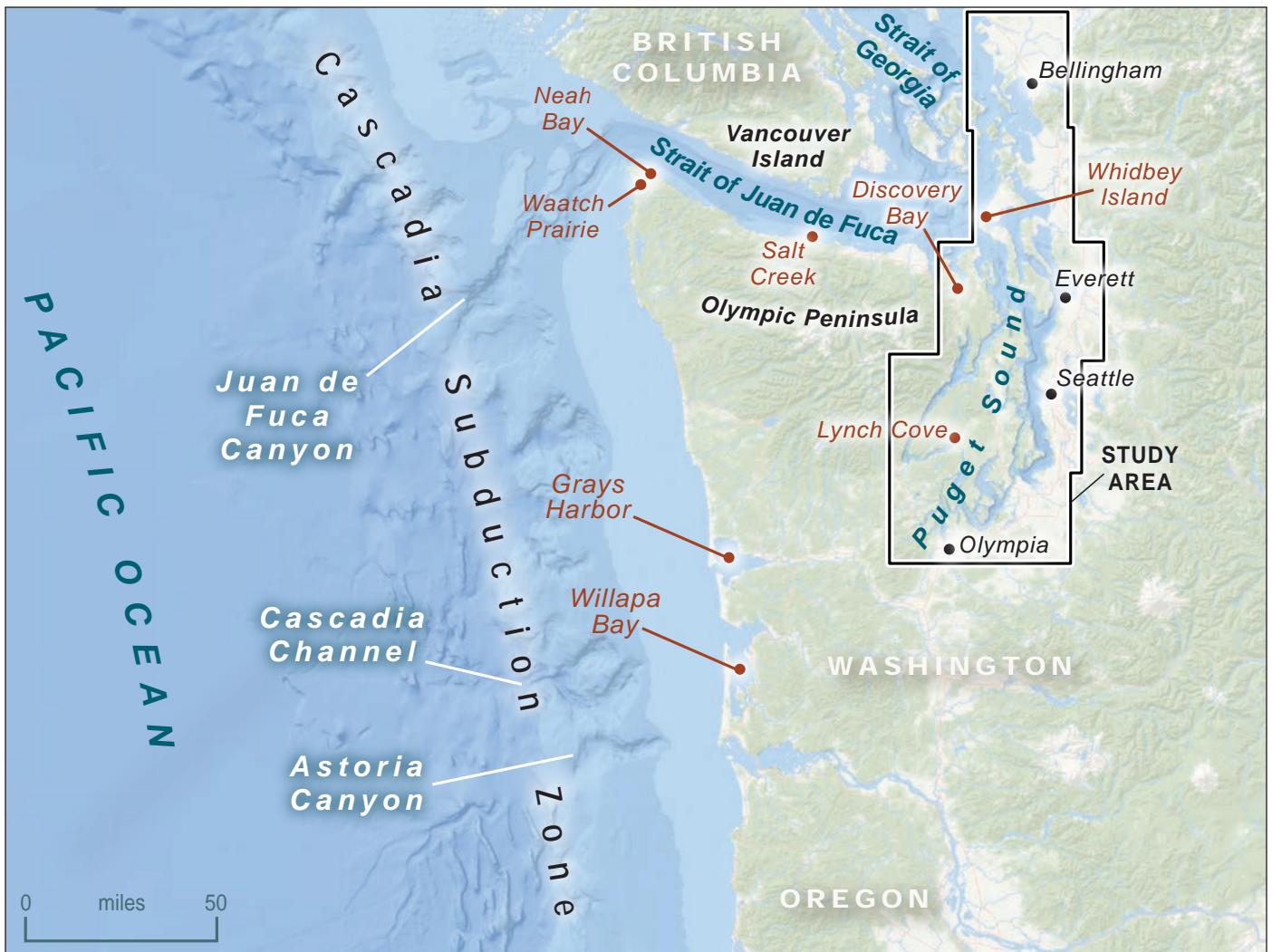


Figure 2. Map of the modeled area, showing the Cascadia subduction zone (CSZ) and major offshore channels. The black polygon outlines the study area that corresponds to the included map sheets. Locations marked in red circles contain sedimentary evidence of past tsunamis generated from the CSZ. This map does not show crustal faults crossing the Puget Sound or Strait of Georgia that may be capable of producing tsunamis (for example, the Seattle, Tacoma, Southern Whidbey Island, and Darrington–Devil’s Mountain fault zones). We do not discuss these potential tsunami sources in this publication.

Table 1. Published tsunami hazard maps for Washington. CSZ 1A with asperity models incorporate localized areas of offshore uplift.

Location	Reference	Modeled Scenario
Anacortes–Bellingham (superseded by this report)	Eungard and others (2018a)	CSZ L1
Port Angeles–Port Townsend	Eungard and others (2018c)	CSZ Extended L1
Southwest Washington	Eungard and others (2018b)	CSZ L1
San Juan Islands (in part superseded by this report)	Walsh and others (2016)	CSZ L1
Everett	Walsh and others (2014)	Seattle Fault
Tacoma	Walsh and others (2009)	Tacoma and Seattle faults
Anacortes–Whidbey Island	Walsh and others (2005)	CSZ 1A and 1A with asperity
Bellingham	Walsh and others (2004)	CSZ 1A and 1A with asperity
Neah Bay	Walsh and others (2003a)	CSZ 1A and 1A with asperity
Quileute area	Walsh and others (2003b)	CSZ 1A and 1A with asperity
Seattle	Walsh and others (2003c)	Seattle Fault
Port Angeles	Walsh and others (2002a)	CSZ 1A and 1A with asperity
Port Townsend	Walsh and others (2002b)	CSZ 1A and 1A with asperity
Southern Washington coast	Walsh and others (2000)	CSZ 1A and 1A with asperity

that intersects the seafloor at a higher angle than the 1A scenario (which places all slip on the subduction interface).

While Washington adopted the L1 scenario as a “maximum considered” tsunami scenario, it was not developed for Washington. In particular, the L1 scenario used by Eungard and others (2018a) depicts the earthquake rupture stopping at approximately 48 degrees north, the southern end of Vancouver Island. This truncated representation of the CSZ was designed originally for tsunami hazard assessment in Oregon and rupture farther north was assumed to have negligible effects for Oregon. The alternative Extended L1 scenario continues the rupture to account for the entire length of the subduction zone (Fig 3). A comparison of the L1 and the Extended L1 earthquake scenarios has shown that the truncated L1 scenario noticeably underestimates inundation in Washington’s inner waterways, such as within the Strait of Georgia and Whidbey Basin (Fig 4; *Appendix B*). This result is especially significant in coastal regions that are low in elevation and protected behind structures such as dikes and (or) levees, such as the Skagit Valley, where even the slightest increase in the waveform can lead to major increases in inundation extent. Due to the low-lying nature of this region, a tsunami has the potential to cause several miles of inland flooding if these structures become compromised by the earthquake or the tsunami. The Extended L1 scenario provides more realistic estimates of tsunami impacts to Washington from a northern or full CSZ rupture (See *Earthquake Slip Distributions and Tsunami Models* for more information on model scenarios in *Appendix A*) and is the more conservative choice.

The Extended L1 scenario uses a simplified extension of slip that follows the approximate strike of the CSZ along the coast of British Columbia, which includes the Explorer Plate to the north (Gica and Arcas, 2015). More rigorous treatment of this extension, including consideration of different rupture geometries, is presented in Gao and others (2018) and Sypus (2019). This publication does not test the differences in tsunami generation between these different northern rupture geometries. However, these variations would likely result in little difference to the tsunami waves entering the Strait of Juan de Fuca and model results within the study area. The Extended L1 model partitions slip into a splay fault that has an approximate 30-degree landward dip. This results in a much higher, narrower area of uplift than a fault rupture buried on the megathrust, which dips much more shallowly and reaches farther seaward than the splay fault.

Additionally, the newer modeling used here incorporates the most current topographic and bathymetric elevation data that were not yet available to Eungard and others (2018a), and as a result, supersedes that work for the Anacortes and Bellingham areas. Modeling presented here also partially overlaps with previous work completed around the San Juan Islands that uses the L1 scenario, included in Walsh and others (2016), and other areas noted in Figure 5. The newer modeling supersedes these areas of overlap in the San Juan Islands with the updated Extended L1 source.

MODELING APPROACH

This publication is a culmination of many years of collaboration between the National Oceanic and Atmospheric Administration (NOAA) Center for Tsunami Research at the Pacific Marine Environmental Laboratory (PMEL), the University of Washington’s (UW) tsunami modeling group within the Department of Applied Mathematics and Department of Earth & Space Sciences, and the Washington Geological Survey (WGS). The tsunami simulations presented here use one of two numerical modeling software packages. These packages are the Method of Splitting Tsunami (MOST) and GeoClaw. MOST was developed by PMEL and the University of Southern California (Titov and Synolakis, 1995; 1998; Titov and González, 1997), while GeoClaw is an open-source code that is part of the Clawpack software that was initiated at UW and is still being developed by the UW tsunami modeling group, in collaboration with other contributors (Clawpack Development Team, 2020). Both of these packages solve the same set of nonlinear shallow water equations that simulate tsunami generation, propagation, and inundation given specific earthquake and bathymetry inputs. Their main difference is in the numerical method employed.

The MOST package uses a grid of topographic and bathymetric elevations and calculates a water surface elevation and velocity for each cell at specified time intervals. A finite difference numerical scheme solves the nonlinear shallow water equations (Titov and others, 2016). This model also uses a set of three nested grids, referred to as A, B, and C grids, each of which becomes smaller in area and successively finer in resolution as they telescope into the community of interest.

The GeoClaw package uses a finite volume method that solves the nonlinear shallow water wave equations (George 2006; 2008; George and LeVeque, 2006; Berger and others, 2011; LeVeque and others, 2011; Mandli and others, 2016). The model uses an Adaptive Mesh Refinement (AMR) strategy to calculate water surface elevations and velocities on a fine grid covering the region of interest and monitors the maximum values over the full simulation time.

Both MOST and GeoClaw have been validated through benchmark tests and are approved by the National Tsunami Hazard Mitigation Program (NTHMP) for use in developing tsunami inundation models (Synolakis and others, 2007; González and others, 2011; Horrillo and others, 2015). To test the practical equivalence between the two software packages, a comparative test was set up to simulate model agreement for Bainbridge Island, Washington (Titov and others, 2018). The test revealed very close agreement between model results, and due to the collaborative nature of this project, we have used both models alternately for different locations.

Figure 6 illustrates the locations modeled either by MOST or GeoClaw. Since there is a transition from coarse to fine elevation grids for the tsunami models, the edges of the models where these grids transition can introduce erroneous results. We overlap our models to account for these, and opt for the more conservative results (larger maximum values). The vertical reference datum for all tsunami simulation results is the mean high water (MHW) tidal datum. This reference point stays static throughout the simulation by not including changes in the tides over time, leading to more conservative inundation values.

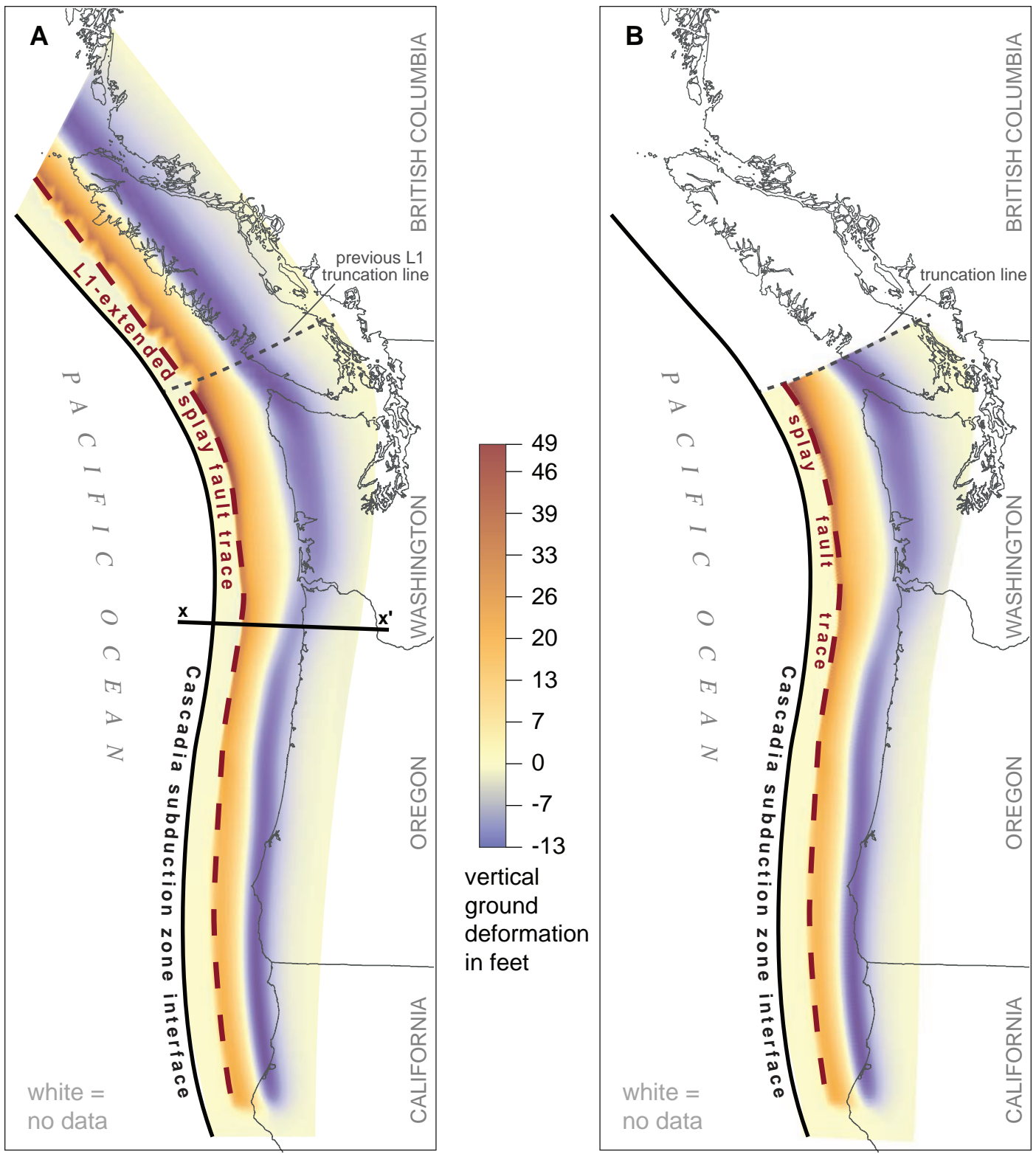


Figure 3. Comparison of vertical ground deformation for (A) the Extended L1 scenario modified by the National Oceanic and Atmospheric Administration (NOAA) Center for Tsunami Research at the Pacific Marine Environmental Laboratory (PMEL; Gica and Arcas, 2015) and (B) the previous L1 scenario of Witter and others (2011). This extension occurs along the northern edge of the fault from 48 degrees north to 51 degrees north, following the curvature of the known subduction zone. C. Splay fault model diagram corresponding to the X-X' line in subfigure A. The coseismic deformation is shown with approximately 2,500 times vertical exaggeration.

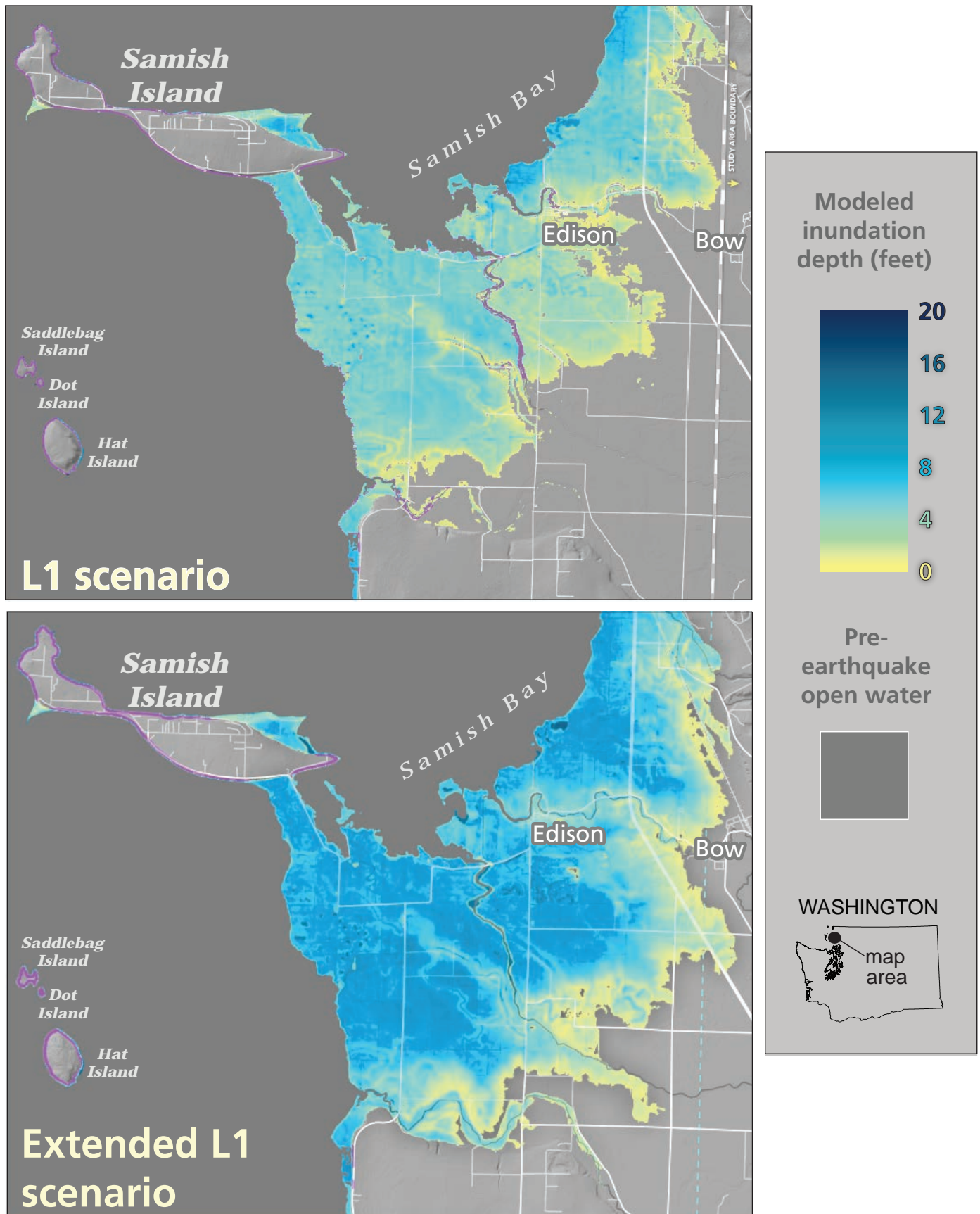


Figure 4. Tsunami inundation depth shown in feet near Samish Bay from the L1 earthquake scenario (top image; Eungard and others, 2018a) and from the Extended L1 earthquake scenario (bottom image; Map Sheet 2). The color bar range is the same in both cases. Tsunami modeling results show that the additional ground deformation present in the Extended L1 scenario contributes more tsunami wave energy into the Strait of Juan de Fuca, leading to larger modeled inundation depths and a larger tsunami inundation extent in the Strait of Georgia and Whidbey Basin. Refer to Appendix B for additional tide gauge comparisons between the two tsunami scenarios.

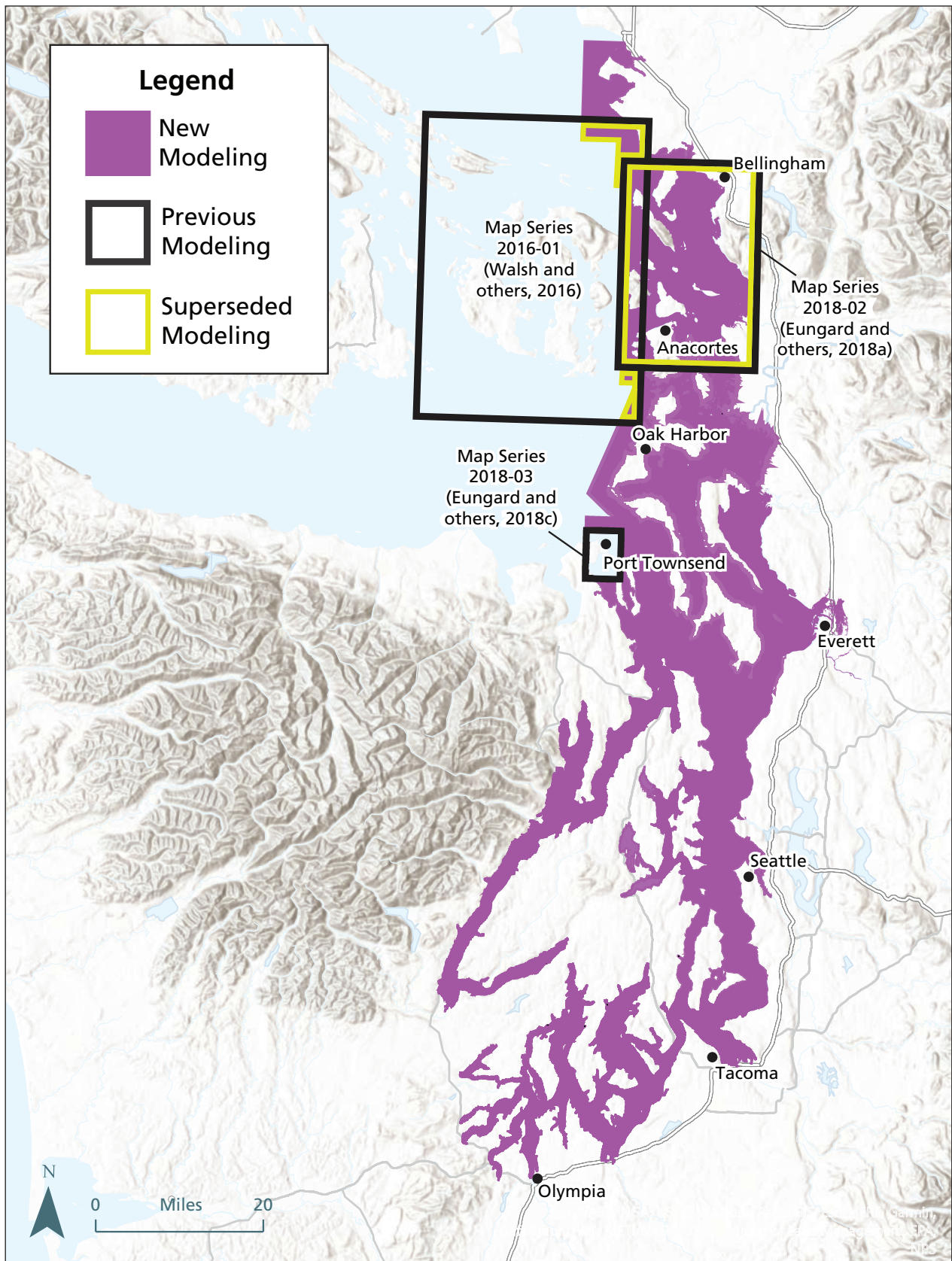


Figure 5. Map of new modeling (purple) compared to areas of previous modeling (black outline), and areas that were previously modeled and are being superseded by the model results presented here (yellow outline). New modeling supersedes Eungard and others (2018a) in the Bellingham and Anacortes region due to the use of the updated Extended L1 earthquake scenario. This modeling also partially supersedes data from Walsh and others (2016) in the San Juan Islands where there is overlap. The new data presented here also incorporates the previous data from Eungard and others (2018c) for Port Townsend because modeling from that publication used the Extended L1 earthquake scenario and the results are indistinguishable.

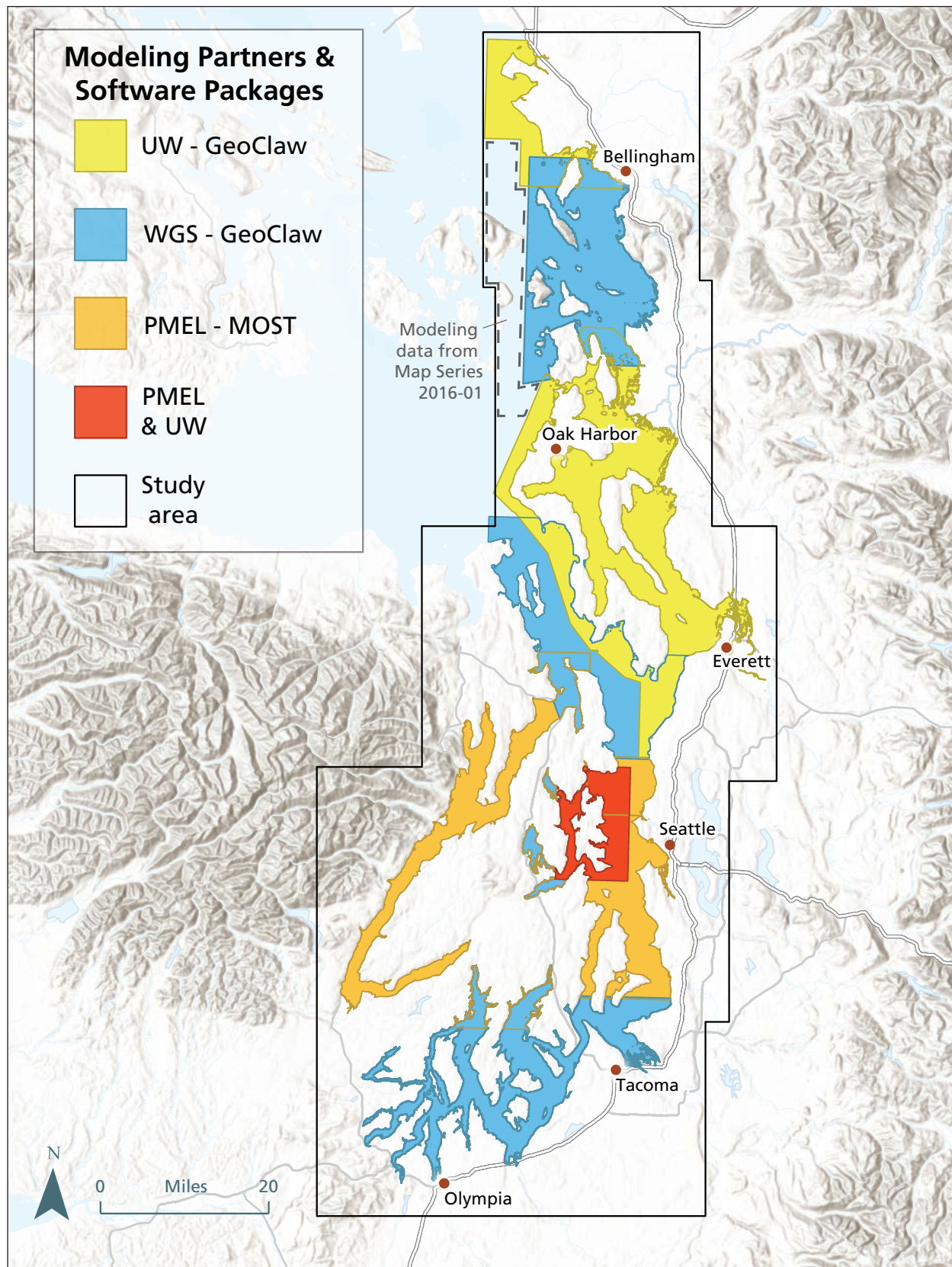


Figure 6. Study areas modeled in this project by the Tsunami Modeling Group at the University of Washington (UW), the NOAA Center for Tsunami Research at the Pacific Marine Environmental Laboratory (PMEL), and the Washington Geological Survey (WGS) at the Washington State Department of Natural Resources (WADNR). Regions of overlap used a compilation of all corresponding model results, prioritizing the maximum values. Both UW and WGS used the GeoClaw tsunami modeling software package while PMEL used the Method of Splitting Tsunami (MOST). The red region indicates the area modeled by both UW (GeoClaw) and PMEL (MOST), which served as a comparison between the two models (Titov and others, 2018). Areas that have two colors, for example near Bellingham where there is blue with yellow outlines, are areas that were modeled by two groups, in this case both UW and WGS.

The modeling presented in this project also uses high-resolution data from Digital Elevation Model (DEM) grids provided by NOAA's National Centers for Environmental Information (NOAA National Geophysical Data Center, 2011; 2014; 2015; Cooperative Institute for Research in Environmental Sciences (CIRES) at the University of Colorado, Boulder, 2014). Each grid cell on land within these DEM grids consists of 1/3 arc-second spacing in both the longitude and latitude directions (approximately 23 ft [7 m] and 33 ft [10 m] resolution, respectively).

These simulations also used the value 0.025-0.03 for Manning's Roughness Coefficient. This is a standard friction value used in tsunami modeling that assumes no vegetation and no structures on land, both of which can impede flow, leading our models to produce greater inundation. Impeded flow could also lead to deeper flow in certain areas with the tsunami wave advancing more slowly inland. Lastly, this assumption also neglects the localized effects that vegetation and structures can have on the path and flow of the tsunami. For example, locally faster current speeds may exist in heavily built-up urban environments where the surrounding buildings may channelize

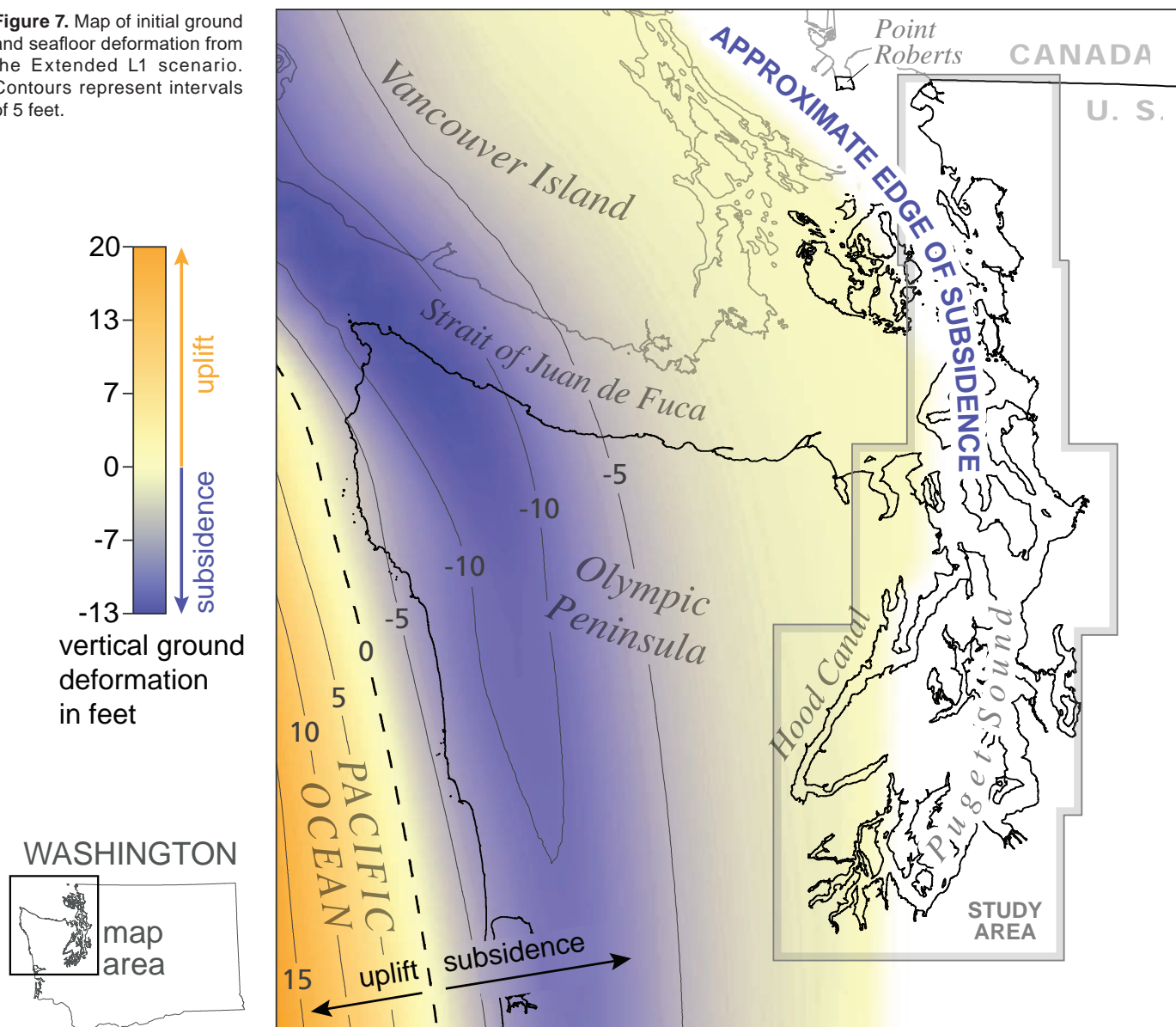
flow. A more accurate assessment of tsunami impacts in a built environment would require an additional site-specific study.

RESULTS

The modeling presented here provides tsunami inundation extent, maximum depth, and maximum current speed values using the CSZ Extended L1 scenario for the Puget Sound and adjacent waters. At this time, high-resolution topography and bathymetry around Point Roberts is not yet available, and therefore this project does not present model results for that location.

Land level change during an earthquake can have a large effect on modeled tsunami impacts. Most of the areas included within this study are too far from the subduction zone to experience land level change, though this is not true for areas on the outer coast. The Extended L1 scenario, like the previous truncated version, produces large amounts of land level change on the outer coast. For the inner waterways, the land surface along the Strait of Juan de Fuca would subside slightly during ground shaking, with subsidence decreasing eastward from

Figure 7. Map of initial ground and seafloor deformation from the Extended L1 scenario. Contours represent intervals of 5 feet.



the subduction zone (Fig. 7). The modeled deformation from the Extended L1 scenario also shows that the Hood Canal and parts of the south Puget Sound would experience a few inches or less of coseismic subsidence.

Tsunami waves from the Extended L1 scenario would impact communities from Blaine, Washington at the U.S.–Canada border to locations west of Olympia, Washington at the southern extent of the Puget Sound. The modeled tsunami wave would reach Blaine in approximately 2 hours and 5 minutes and Olympia approximately 4 hours after the earthquake, leaving limited time to issue official warnings. In this scenario, tsunami wave troughs would precede wave crests in all locations, which provides visual evidence, in addition to shaking, that a tsunami is imminent. A leading trough would look like a sudden drawdown of the ocean, similar to a low tide. The estimated wave arrival times listed throughout this report correspond to the first sign of water levels rising above the mean high water (MHW) tidal datum.

Map Sheets 1 through 8 depict maximum modeled tsunami inundation and Map Sheets 9 through 16 depict maximum

modeled current speed. These map sheets supplement a series of tsunami inundation maps produced over the past 21 years by WGS and the Washington Emergency Management Division as a contribution to the NTHMP (Table 1). These maps are a product of multiple computer simulations developed by the NOAA Center for Tsunami Research at PMEL, the tsunami modeling group of the Departments of Applied Mathematics and Earth and Space Sciences at UW, and WGS.

Inundation

Tsunami inundation (depth of tsunami-induced flooding over previously dry land) from the Extended L1 scenario floods many low-lying regions along the shoreline inside the Puget Sound and adjacent waters (Table 2). Inundation depths are dependent on surrounding topography and may reach or exceed 10 ft (2.4 m) in various locations throughout this study area. These include, but are not limited to, the Port of Bellingham, Fairhaven Station, Portage Bay, Flounder Bay, Deception Pass State Park, Joseph Whidbey State Park, Keystone Spit and Ferry Landing, Coon Bay,

Table 2. Tsunami impacts from the CSZ Extended L1 scenario at key locations within the Puget Sound and adjacent waterways (see "Map sheet number" column on far right of table). Maximum inundation depths and offshore current values refer to the entire simulation time. Note that the tsunami will affect all coastlines within the Puget Sound and Strait of Georgia to some extent. Inundation depth will vary based on local topographic changes. Refer to all map sheets for additional inundation points, current speeds, and wave arrival times.

General location and county	Approximate maximum inundation depth (ft)	Maximum offshore current speed (kn)	Estimated first rise above datum	Map sheet number
Blaine Marine Park, Whatcom	6.3	3–6	2 hr 5 min	1, 9
Bellingham, Whatcom	10.7	3–6	2 hr 15 min	1, 9
Deception Pass State Park, Island	11.7	9+	1 hr 45 min	2, 10
Oak Harbor, Island	6.7	3–6	2 hr 55 min	2, 10
Snohomish Delta, Snohomish	5.7	0–3	2 hr 20 min	3, 11
Point No Point Lighthouse, Kitsap	7.7	3–6	1 hr 55 min	3, 8, 11, 16
Harbor Island, King	3.7	0–3	2 hr 20 min	4, 12
Vashon Island Ferry Terminal, King	13	0–3	2 hr 30 min	4, 12
Port of Tacoma, Pierce	3.5	3–6	2 hr 45 min	5, 13
Nisqually Delta Boardwalk, Thurston	2.9	0–3	3 hr 10 min	5, 6, 13, 14
Port of Olympia, Thurston	0.5	0–3	4 hr	6, 14
Oyster Bay, Thurston	5.7	0–3	4 hr 15 min	6, 14
Belfair State Park, Kitsap	6.2	3–6	3 hr 40 min	7, 15
Dosewallips State Park, Kitsap	3.1	0–3	2 hr 25 min	7, 15
Indian Island Naval Magazine, Jefferson	10.7	9+	2 hr	8, 16
Shine Tidelands State Park, Jefferson	10	6–9	2 hr 10 min	8, 16

Blake Island Marine State Park, Vashon Island Ferry Terminal, Portage, Indian Island Naval Magazine, Irondale, Shine Tide Lands State Park, Eldon, and the Theler Wetlands near Belfair. Additionally, inundation may extend well into many other populated areas including the Skagit and Snohomish County lowlands, Birch Bay, Sandy Point, Useless Bay, Maxwelton, and the Port of Tacoma, to name a few. The CSZ Extended L1 scenario would also cause significant flooding up rivers and along floodplains within Washington's inner waterways such as the Lummi, Nooksack, Skagit, Stillaguamish, Snohomish, Quilcene, Duckabush, Skokomish, and Nisqually rivers. Refer to Table 2 and Map Sheets 1–8 for additional inundation values in key locations. The modeled study area does not encompass the entirety of all drainage basins. The extent of tsunami inundation would likely continue along river channels, exceeding the boundaries shown in the modeled map sheets (for example, at the Duwamish River and California/Dakota Creeks south of Blaine). Modeling does not account for opposing currents in rivers.

Current Speed

The modeled current speed maps (Map Sheets 9–16) show four ranges of speed in knots (a knot is equal to 1 nautical mile or ~1.15 land mi/hr): 0–3 knots, 3–6 knots, 6–9 knots, and >9 knots. These binned ranges follow the port damage categorization of Lynett and others (2014). The ranges approximate hazard to ships and docking facilities, representing the following amounts of damage: no expected damage (0–3 knots), minor/moderate damage possible (3–6 knots), major damage possible (6–9 knots), and extreme damage possible (>9 knots). Modeled current speeds locally exceed 9 knots, the maximum categorization, in many places within the study area. These locations include Drayton Harbor, Padilla Bay, Hat Island, Burrows Island, Deception Pass, Port Townsend Bay, Portage Canal, Port Gamble, Quartermaster Harbor, Gig Harbor, and around Point Glover, among others. Narrower waterway channels and nearshore locations where the tsunami-tide interactions are likely to be most significant should expect the highest speeds. Certain topographic features also produce strong currents with potential for the formation of vortices; examples of these features include entrances into harbors and around small islands or land spits with narrow passageways. On Map Sheets 9–16, the regions that show high-speed vortices may actually be much more widespread than currently shown. This is due to the sensitivity of current speeds in the tsunami modeling—small tweaks in the model setup cause these vortices to take slightly different paths. Thus, the spatial extents of these vortices are only estimates and people should avoid these general areas during a tsunami.

Timing of Tsunami Arrival and Initial Water Disturbance

Estimated wave arrival times for a given location correspond to the time elapsed from the beginning of earthquake shaking to the time when water first rises above the water surface datum (mean high water). This timing does not reflect the falling water levels that precede the first incoming wave at all simulated locations. For example, an estimated wave arrival of 2 hours and 35 minutes means the first wave above mean high tide

would arrive at that location 2 hours and 35 minutes after the earthquake begins. The arrival times shown on all map sheets are the arrival times of the first wave, which may not necessarily be the largest wave. Several minutes or even hours may pass between first wave arrival and another wave that brings maximum current speed, inundation depth, or inundation extent. Strong earthquake shaking may persist for as much as 5 minutes in this scenario, reducing the available time to evacuate. The tsunami wave would be generated at the subduction zone, travel to the outer coast, then travel through the Strait of Juan de Fuca and flow into the Puget Sound and Strait of Georgia. In this study area, the first wave would arrive on the west side of Whidbey Island at Fort Ebey State Park at approximately 1 hour and 30 minutes. Figure 8 shows a series of simulated synthetic tide gauge records in selected locations at the northern and southern extents of the study area (See *Appendix C* for all simulated tide gauge locations).

Simulated tide gauges estimate the approximate timing of the initial water disturbance. For example, just offshore of Ferndale (south of Cherry Point, Whatcom County), there is a gradual fall in sea level from a leading wave trough beginning approximately 1 hour after the earthquake shaking. Sea level drops ~3 ft (1 m) approximately 1 hour and 45 minutes after the earthquake (Fig. 8, Ferndale). A rapidly rising wave follows, reaching a peak of ~8 ft (2.4 m) above mean high water at approximately 2 hours and 15 minutes. Similarly, at North Point, Olympia, Thurston County, there is a gradual drop in sea level of ~3 ft (0.85 m) beginning approximately 3 hours after the start of the earthquake (Fig. 8, North Point). Much like all areas within the state's inner waterways, a rapidly rising wave follows this initial drawdown of water (Fig. 9), which crests at North Point, Olympia approximately 4 hours and 15 minutes after the earthquake with a wave height of ~3 ft (1 m). This location in Olympia is an example where the first wave is smaller in amplitude than a later wave. Although the first wave crest begins to arrive in North Point, Olympia just after 4 hours, the largest wave is the fourth wave (~4 ft) that arrives approximately 10 hours after the earthquake. Wave activity may last for 14 or more hours following the earthquake. Minor inundation and strong currents may pose a hazard to rescue and recovery operations and may continue for 24 or more hours after the earthquake. For comparison, the March 27, 1964, Mw 9.2 earthquake near Anchorage, Alaska affected local wave currents offshore of Alaska for days. This event also produced its most destructive wave in Washington (near Raymond and South Bend in Willapa Bay) about 12 hours after the first wave reached Washington's outer coast (Walsh and others, 2000). In addition, the January 26, 1700 earthquake along the CSZ produced a tsunami that may have lasted as many as 20 hours in Japan (Satake and others, 2003; Atwater and others, 2005).

LIMITATIONS OF THE MODEL

The rupture patterns of earthquakes on a given subduction zone often vary significantly from one earthquake sequence to the next. In addition, because there have been no direct observations of previous coseismic slip produced in a large CSZ earthquake, researchers do not have a strong understanding of

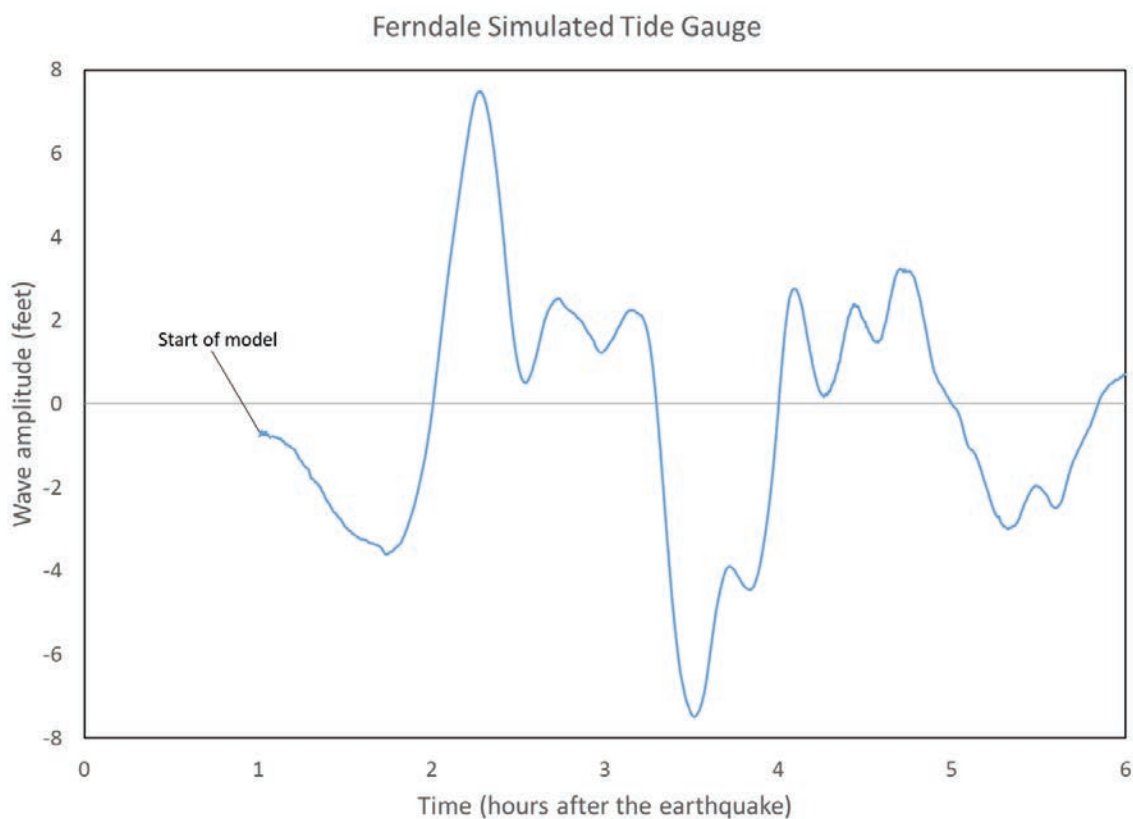
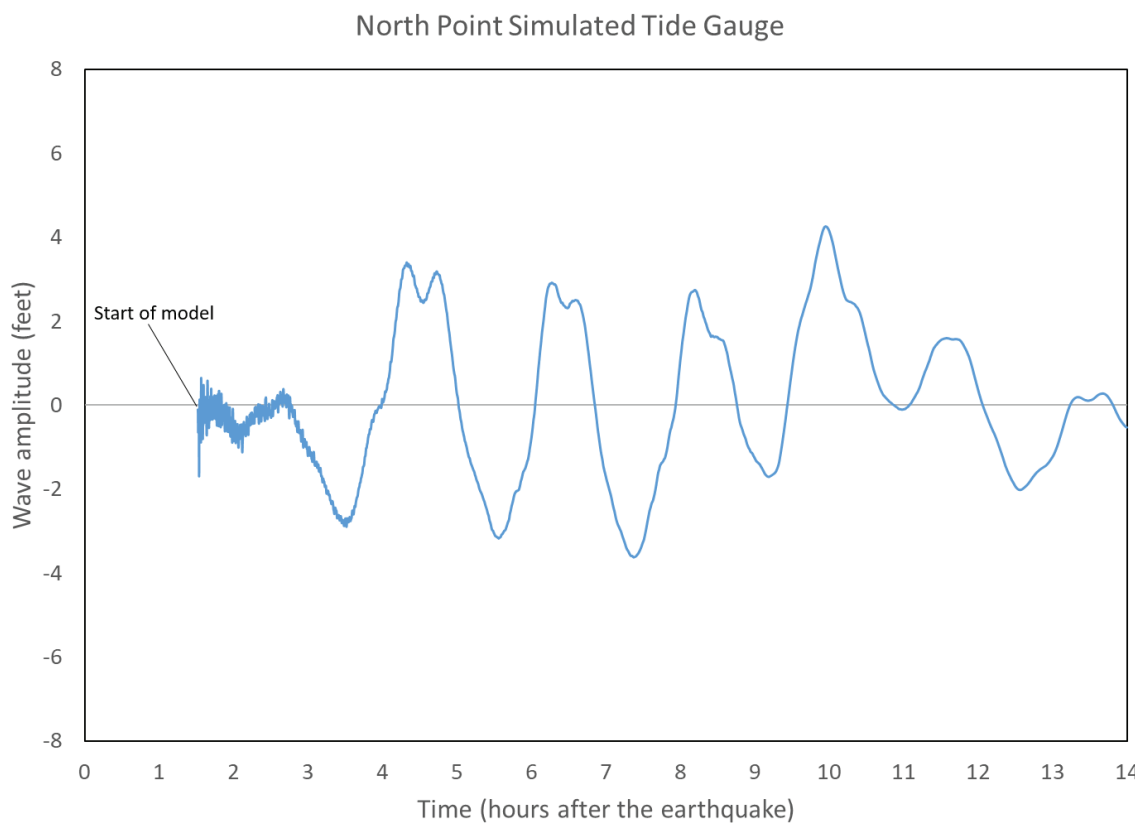
A**B**

Figure 8. Modeled tsunami wave variations over time (light blue lines) for two simulated tide gauges in the northern part of the study area near **(A)** Ferndale, Whatcom County (Cherry Point), and in the southern part of the study area, **(B)** North Point, Olympia, Thurston County. Gray horizontal lines indicate static mean high water elevation at simulated tide gauges. See Map Sheets 1 and 6, respectively for locations (see *Appendix C* for additional simulated tide gauge graphs at key locations within the study area). Note that there are high frequency oscillations at the beginning of the model in subfigure B. These do not affect the model results but are an artifact of the model initiation (see *Appendix C* for more information).

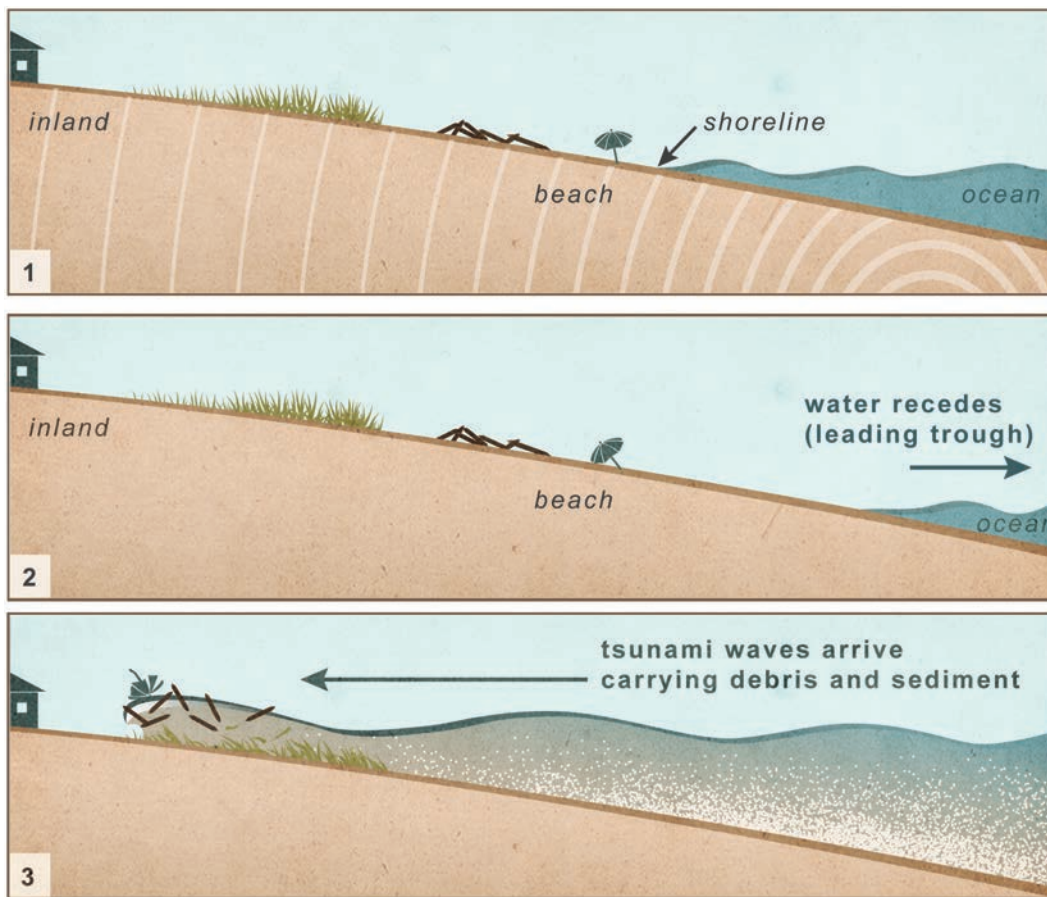


Figure 9. Schematic diagram of chronologic events following a CSZ earthquake and tsunami. **(1)** Large earthquake on the CSZ produces strong shaking that may last several minutes. **(2)** The first modeled indication of an incoming tsunami wave to all locations in the study area will be a gradual drop in water level prior to arrival of the first tsunami wave. However, submarine landslides triggered by seismic shaking are possible, which could result in locally generated tsunamis with leading wave peaks. **(3)** Tsunami waves begin to arrive. These powerful waves carry sediment and debris onshore and to higher elevations. The inundation may continue for at least 14 hours locally, posing a hazard to search, rescue, and recovery efforts.

the resultant pattern of seafloor deformation. Therefore, the Extended L1 scenario used in this study has a simplified regional slip distribution that only takes into account the static, vertical component of seafloor displacement for tsunami generation (Witter and others, 2011). This scenario does not include other potential components that could alter the tsunami generation such as material heterogeneity in the subduction zone, inelastic behavior, horizontal slip components, extensional faults within the subduction zone, or dynamic coseismic deformation. The largest source of uncertainty in this modeling is therefore the input earthquake deformation. The earthquake scenario used in this model consists of a surface-rupturing splay fault and was selected to approximate the 2 percent probability of exceedance in 50 years, but the next earthquake may have a more complex slip distribution and rupturing geometry than the CSZ Extended L1 scenario. For example, other megathrust earthquake scenarios that do not rupture an active splay fault (which in turn have their own uncertainty) are possible too (Wang and Tréhu, 2016). The Extended L1 scenario is a deterministic earthquake deformation model of a single large earthquake.

The tsunami modeling packages do not include the influences of changes in tides or projected sea-level rise. The tide stage can amplify or reduce the impact of a tsunami on a specific community. For example, the diurnal range (the difference in height between mean higher high water and mean lower low water) is 9.15 ft (2.79 m) at the Cherry Point tide gauge station in Whatcom County (NOAA, 2021). The model also does not include interaction with tidal currents, which can be additive, or if in opposite directions, can steepen the tsunami wave front

and cause a breaking wave (Zhang and others, 2011), nor does it include riverine flow.

The bathymetric and topographic data used to make the elevation grid limits the resolution of the modeling. A variety of data sources contributed to the elevation grid, with grid cells ranging from ~3 ft (1 m) for the topographic grid and 16–3,937 ft (5–1,200 m) for the bathymetric grid. Coarse grids do not capture small topographic features that can influence the tsunami locally. This generally leads to greater modeled inundation than would be produced by finer grids, except in narrow or constricted channels or along steep topographic features.

These model results do not account for the possibility of seismically induced seiches from the earthquake. Seiches are a series of standing waves that may occur in fully or partially enclosed bodies of water when earthquake waves pass through the area. These results also do not include potential tsunamis from coseismic landslides or ruptures on nearby crustal faults, both of which may be possible and could be triggered by a CSZ earthquake. Additionally, the modeling does not include any foreshocks or aftershocks, which may also trigger slope failures that could generate tsunamis in inland waters (including lakes). Local slope failures have the potential to generate tsunamis that arrive much earlier than the times estimated within this publication. This modeling does not incorporate localized topographic changes caused by sediment erosion or liquefaction, such as settlement or sand blows. All of these effects are beyond the scope of this study.

CONCLUSION

The new modeling presented here provides estimates of tsunami inundation extent, inundation depth, current speed, and first wave arrival times above mean high water for Washington's Puget Sound and adjacent interior waterways. Some of these areas had been modeled prior to this research, and some had not. For those areas that were previously modeled, we have updated the assumed tsunami source to the "Extended L1 scenario" which leads to the prediction of more severe future tsunami hazards that are relevant to the Puget Sound and adjacent areas. The Extended L1 scenario encompasses approximately 95 percent of the variability in CSZ tsunami sources, and produces a tsunami that is unlikely, though not impossible, to be exceeded. Modeling results suggest certain locations would experience inundation depths in excess of 10 feet, and some waterways would experience current speeds in excess of 9 knots. The first tsunami waves generated from the earthquake would reach Whidbey Island within 1 hour and 30 minutes, though the tsunami would arrive at most locations in this study area later, within 2–4 hours of the earthquake. Tsunami hazard zones should be evacuated immediately after the earthquake when safe to do so, and we emphasize that planning for tsunami hazards includes planning for earthquake hazards. Despite some limitations to our model, meaning that the model does not provide an exact representation of a tsunami generated by an earthquake on the Cascadia subduction zone, the results presented here are valuable for regional awareness and hazard planning. We hope this information will be used to increase community resilience to tsunamis in the Puget Sound region and its adjacent waters.

ACKNOWLEDGMENTS

The National Tsunami Hazard Mitigation Program (NTHMP) in cooperation with cities, counties, tribes, and the Washington Emergency Management Division supported this project. The NTHMP aims to reduce the impact of tsunamis through warning guidance, hazard assessment, and mitigation. This project was partially funded by NOAA Award #NA19NWS4670017. This does not constitute an endorsement by NOAA. This is PMEL contribution 5242.

We acknowledge the work of the WGS publications team for their effort in producing the map sheets, specifically Daniel Coe and Maria Furtney. We also would like to acknowledge the computing time provided by the CU-CSDMS High-Performance Computing Cluster, and by the Applied Mathematics Department at the University of Washington. We are further thankful for reviews by Brian Atwater (USGS), Kelin Wang (Geological Survey of Canada), and Robert Witter (USGS) which greatly improved this publication. This work would also not be possible without the seminal work done regarding the Cascadia subduction zone earthquake source model by Witter and others (2011).

REFERENCES

- Adams, John, 1990, Paleoseismicity of the Cascadia subduction zone: Evidence from turbidites off the Oregon–Washington margin: *Tectonics*, v. 9, no. 4, p. 569–583. [https://doi.org/10.1029/TC009i004p00569]
- Gica, Edison; Arcas, Diego, 2015, Tsunami inundation modeling of Seattle and Tacoma due to a Cascadia subduction zone earthquake: National Oceanic and Atmospheric Administration Center for Tsunami Research unpublished report, 44 p.
- Atwater, B. F., 1992, Geologic evidence for earthquakes during the past 2,000 years along the Copalis River, southern coastal Washington: *Journal of Geophysical Research*, v. 97, no. B2, p. 1901–1919. [https://doi.org/10.1029/91JB02346]
- Atwater, B. F.; Carson, R. C.; Griggs, G. B.; Johnson, H. P.; Salmi, M. S., 2014, Rethinking turbidite paleoseismology along the Cascadia subduction zone: *Geology*, v. 42, no. 9, p. 827–830. [https://doi.org/10.1130/G35902.1]
- Atwater, B. F.; Hemphill-Haley, Eileen, 1997, Recurrence intervals for great earthquakes of the past 3,500 years at northeastern Willapa Bay, Washington: U.S. Geological Survey Professional Paper 1576, 108 p. [https://doi.org/10.3133/pp1576]
- Atwater, B. F.; Nelson, A. R.; Clague, J. J.; Carver, G. A.; Yamaguchi, D. K.; Bobrowsky, P. T.; Bourgeois, Joanne; Darienzo, M. E.; Grant, W. C.; Hemphill-Haley, Eileen; Kelsey, H. M.; Jacoby, G. C.; Nishenko, S. P.; Palmer, S. P.; Peterson, C. D.; Reinhart, M. A., 1995, Summary of coastal geologic evidence for past great earthquakes at the Cascadia subduction zone: *Earthquake Spectra*, v. 11, no. 1, p. 1–18. [https://doi.org/10.1193/1.1585800]
- Atwater, B. F.; Musumi-Rokkaku, Satoko; Satake, Kenji; Tsuji, Yoshinobu; Ueda, Kazue; Yamaguchi, D. K., 2005, The orphan tsunami of 1700—Japanese clues to a parent earthquake in North America: University of Washington Press and U.S. Geological Survey Professional Paper 1707, 133 p. [https://pubs.usgs.gov/pp/pp1707/pp1707_front.pdf]
- Atwater, B. F.; Yamaguchi, D. K., 1991, Sudden, probably coseismic submergence of Holocene trees and grass in coastal Washington State: *Geology*, v. 19, no. 7, p. 706–709. [https://doi.org/10.1130/0091-7613(1991)019<0706:SPCSOH>2.3.CO;2]
- Bucknam, R. C.; Leopold, E. B.; Hemphill-Haley, Eileen; Ekblaw, D. E.; Atwater, B. F.; Benson, B. E.; Phipps, J. B., 1994, Holocene tectonics in western Washington. *In* Swanson, D. A.; Haugerud, R. A., editors, *Geologic field trips in the Pacific Northwest*: University of Washington Department of Geological Sciences, v. 2, p. 2C1–2C15.
- Berger, M. J.; George, D. L.; LeVeque, R. J.; Mandli, K. T., 2011, The GeoClaw software for depth-averaged flows with adaptive refinement: *Advances in Water Resources*, v. 34, no. 9, p. 1195–1206. [https://doi.org/10.1016/j.advwatres.2011.02.016]
- Clawpack Development Team, 2020, Clawpack Versions 5.5.0–5.7.0, <http://www.clawpack.org>. [https://doi.org/10.17605/osf.io/kmw6h]
- Cooperative Institute for Research in Environmental Sciences (CIRES) at the University of Colorado, Boulder, 2014, Continuously Updated Digital Elevation Model (CUDEM) - 1/9 Arc-Second Resolution Bathymetric-Topographic Tiles, Bellingham, 2020: NOAA National Centers for Environmental Information. [accessed Sep. 29, 2020 at <https://doi.org/10.25921/ds9v-ky35>]
- Eungard, D. W.; Forson, Corina; Walsh, T. J.; Gica, Edison; Arcas, Diego, 2018a, Tsunami hazard maps of the Anacortes–Bellingham area, Washington—Model results from a ~2,500-year Cascadia subduction zone earthquake scenario: Washington Geological Survey Map Series 2018-02, 6 sheets, scale 1:30,000, 10 p. text. [https://www.dnr.wa.gov/publications/ger_ms2018-02_tsunami_hazard_anacortes_bellingham.zip]

- Eungard, D. W.; Forson, Corina; Walsh, T. J.; Gica, Edison; Arcas, Diego, 2018b, Tsunami hazard maps of southwest Washington—Model results from a ~2,500-year Cascadia subduction zone earthquake scenario: Washington Geological Survey Map Series 2018-01, originally published March 2018, 6 sheets, scale 1:48,000, 11 p. text. [http://www.dnr.wa.gov/publications/ger_ms201801_tsunami_hazard_southwest_washington.zip]
- Eungard, D. W.; Forson, Corina; Walsh, T. J.; González, F. I.; LeVeque, R. J.; Adams, L. M., 2018c, Tsunami hazard maps of Port Angeles and Port Townsend, Washington—Model results from a ~2,500-year Cascadia subduction zone earthquake scenario: Washington Geological Survey Map Series 2018-03, 6 sheets, scale 1:11,000 and 1:16,000, 11 p. text. [http://www.dnr.wa.gov/publications/ger_ms201803_tsunami_hazard_pt_angeles_pt_townsend.zip]
- Flück, Paul; Hyndman, R. D.; Wang, Kelin, 1997, Three-dimensional dislocation model for great earthquakes of the Cascadia subduction zone: *Journal of Geophysical Research: Solid Earth*, v. 102, no. B9, p. 20539–20550. [<https://doi.org/10.1029/97JB01642>]
- Gao, Dawei; Wang, Kelin; Insua, T. L.; Sypus, Matthew; Riedel, Michael; Sun, Tianhaozhe, 2018, Defining megathrust tsunami source scenarios for northernmost Cascadia: *Natural Hazards*, v. 94, no. 1, p. 445–469. [<https://doi.org/10.1007/s11069-018-3397-6>]
- Garrison-Laney, C. E., 2017, Tsunamis and sea levels of the past millennium in Puget Sound, Washington: University of Washington Doctor of Philosophy thesis, 166 p.
- Garrison-Laney, C. E.; Miller, Ian, 2017, Tsunamis in the Salish Sea: Recurrence, sources, hazards. *In* Haugerud, R. A.; Kelsey, H. M., editors, 2017, From the Puget Lowland to east of the Cascade Range—Geologic excursions in the Pacific Northwest: Geological Society of America Field Trip Guide v. 49, p. 67–78. [[https://doi.org/10.1130/2017.0049\(04\)](https://doi.org/10.1130/2017.0049(04))]
- George, D. L., 2008, Augmented Riemann solvers for the shallow water equations over variable topography with steady states and inundation: *Journal of Computational Physics*, v. 227, no. 6, p. 3089–3113. [<https://doi.org/10.1016/j.jcp.2007.10.027>]
- George, D. L., 2006, Finite volume methods and adaptive refinement for tsunami propagation and inundation: University of Washington Doctor of Philosophy thesis, 167 p.
- George, D. L.; LeVeque, R. J., 2006, Finite volume methods and adaptive refinement for global tsunami propagation and local inundation: *Science of Tsunami Hazards*, v. 24, no. 5, p. 319–328. [<http://tsunamisociety.org/245george.pdf>]
- Griggs, G. B., 1968, Cascadia Channel: The anatomy of a deep-sea channel: Oregon State University Doctor of Philosophy thesis, 185 p.
- Griggs, G. B.; Kulm, L. D., 1970, Sedimentation in Cascadia deep-sea channel: *Geological Society of America Bulletin*, v. 81, no. 5, p. 1361–1384. [[https://doi.org/10.1130/0016-7606\(1970\)81\[1361:SICDC\]2.0.CO;2](https://doi.org/10.1130/0016-7606(1970)81[1361:SICDC]2.0.CO;2)]
- Goldfinger, Chris; Galer, Steve; Beeson, Jeffrey; Hamilton, Tark; Black, Bran; Romsos, Chris; Patton, Jason; Nelson, C. H.; Hausmann, Rachel; Morey, Ann, 2017, The importance of site selection, sediment supply, and hydrodynamics—A case study of submarine paleoseismology on the northern Cascadia margin, Washington, USA: *Marine Geology*, v. 384, 36 p. [<https://doi.org/10.1016/j.margeo.2016.06.008>]
- Goldfinger, Chris; Morey, A. E.; Black, Bran; Beeson, Jeffrey; Nelson, C. H.; Patton, Jason, 2013, Spatially limited mud turbidites on the Cascadia margin: segmented earthquake ruptures?: *Natural Hazards and Earth System Sciences*, v. 13, no. 8, p. 2109–2146. [<https://doi.org/10.5194/nhess-13-2109-2013>]
- Goldfinger, Chris; Nelson, C. H.; Morey, A. E.; Johnson, J. E.; Patton, J. R.; Karabanov, Eugene; Gutierrez-Pastor, Julia; Eriksson, A. T.; Gracia, Eulalia; Dunhill, Gita; Enkin, R. J.; Dallimore, Audrey; Vallier, Tracy, 2012, Turbidite event history—Methods and implications for Holocene paleoseismicity of the Cascadia subduction zone: U.S. Geological Survey Professional Paper 1661-F, 170 p., 64 figures. [<https://pubs.usgs.gov/pp/pp1661f/>]
- González, F. I.; LeVeque, R. J.; Chamberlain, Paul; Hirai, Bryant; Varkovitsky, Jonathan; George, D. L., 2011, Validation of the GeoClaw model—NTHMP MMS tsunami inundation model validation workshop: University of Washington, 84 p. [<https://depts.washington.edu/clawpack/links/nthmp-benchmarks/geo-claw-results.pdf>]
- Heaton, T. H.; Snavely, P. D., Jr., 1985, Possible tsunami along the northwestern coast of the United States inferred from Indian traditions: *Seismological Society of America Bulletin*, v. 75, no. 5, p. 1455–1460. [<https://pubs.geoscienceworld.org/ssa/bssa/article/75/5/1455/102218>]
- Horrillo, Juan; Grilli, S. T.; Nicolsky, Dmitry; Roeber, Volker; Zhang, Joseph, 2015, Performance benchmarking tsunami models for NTHMP's inundation mapping activities: *Pure and Applied Geophysics*, v. 172, no. 3–4, p. 869–884. [<https://doi.org/10.1007/s00024-014-0891-y>]
- Hutchinson, Ian; Peterson, C. D.; Sterling, S. L., 2013, Late Holocene tsunami deposits at Salt Creek, Washington, USA: *Science of Tsunami Hazards*, v. 32, p. 221–235. [<http://archives.pdx.edu/ds/psu/12419>]
- Hutchinson, Ian; Clague, John, 2017, Were they all giants? Perspectives on late Holocene plate-boundary earthquakes at the northern end of the Cascadia subduction zone: *Quaternary Science Reviews*, v. 169, p. 29–49. [<https://doi.org/10.1016/j.quascirev.2017.05.015>]
- International Code Council, 2015, International Building Code 2015, 690 p. [<https://codes.iccsafe.org/content/IBC2015>]
- Jacoby, G. C.; Bunker, D. E.; Benson, B. E., 1997, Tree-ring evidence for an A.D. 1700 Cascadia earthquake in Washington and northern Oregon: *Geology*, v. 25, no. 11, p. 999–1002. [[https://doi.org/10.1130/0091-7613\(1997\)025<0999:TREFAA>2.3.CO;2](https://doi.org/10.1130/0091-7613(1997)025<0999:TREFAA>2.3.CO;2)]
- Kelsey, H. M.; Nelson, A. R.; Hemphill-Haley, Eileen; Witter, R. C., 2005, Tsunami history of an Oregon coastal lake reveals a 4600 yr record of great earthquakes on the Cascadia subduction zone: *Geological Society of America*, v. 117, no. 7–8, p. 1009–1032. [<https://doi.org/10.1130/B25452.1>]
- Kelsey, H. M.; Witter, R. C.; Hemphill-Haley, Eileen, 2002, Plate boundary earthquakes and tsunamis of the past 5,500 yr, Sixes River estuary, southern Oregon: *Geological Society of America Bulletin*, v. 114, no. 3, p. 298–314. [[https://doi.org/10.1130/0016-7606\(2002\)114<0298:PBEATO>2.0.CO;2](https://doi.org/10.1130/0016-7606(2002)114<0298:PBEATO>2.0.CO;2)]
- LeVeque, R. J.; George, D. L.; Berger, M. J., 2011, Tsunami modelling with adaptively refined finite volume methods: *Acta Numerica*, v. 20, p. 211–289. [<https://doi.org/10.1017/S0962492911000043>]
- Ludwin, R. S., 2002, Cascadia megathrust earthquakes in Pacific Northwest Indian myths and legends: *TsuInfo Alert*, v. 4, no. 2, p. 6–10. [https://www.dnr.wa.gov/publications/ger_tsuinfo_2002_v4_no2.pdf]
- Lynett, P. J.; Borrero, Jose; Son, Sangyoung; Wilson, Rick; Miller, Kevin, 2014, Assessment of the tsunami-induced current hazard, *Geophysical Research Letters*, v. 41, no. 6, p. 2048–2055. [<https://doi.org/10.1002/2013GL058680>]
- Mandli, K. T.; Ahmadi, A. J.; Berger, Marsha; Calhoun, Donna; George, D. L.; Hadjimichael, Yiannis; Ketcheson, D. I.; Lemoine, G. I.; LeVeque, R. J., 2016, Clawpack: Building an open source ecosystem for solving hyperbolic PDEs: *PeerJ Computer Science*, v. 2, no. e68, 27 p. [<https://doi.org/10.7717/peerj-cs.68>]

- Morton, R. A.; Gelfenbaum, Guy; Jaffe, B. E., 2007, Physical criteria for distinguishing sandy tsunami and storm deposits using modern examples: *Sedimentary Geology*, v. 200, no. 3–4, p. 184–207. [https://doi.org/10.1016/j.sedgeo.2007.01.003]
- Myers, E. P., III; Baptista, A. M.; Priest, G. R., 1999, Finite element modeling of potential Cascadia subduction zone tsunamis: *Science of Tsunami Hazards*, v. 17, no. 1, p. 3–18. [https://library.lanl.gov/tsunami/ts171.pdf]
- National Oceanic and Atmospheric Administration, 2021, Datums for 9449424, Cherry Point WA [webpage]: National Oceanic and Atmospheric Administration. [accessed Apr. 15, 2021 at https://tidesandcurrents.noaa.gov/datums.html?id=9449424]
- Nelson, A. R.; Kelsey, H. M.; Witter, R. C., 2006, Great earthquakes of variable magnitude at the Cascadia subduction zone: *Quaternary Research*, v. 65, no. 3, p. 354–365. [https://doi.org/10.1016/j.yqres.2006.02.009]
- NOAA National Geophysical Data Center, 2011, Port Townsend, Washington 1/3 Arc-second MHW Coastal Digital Elevation Model: NOAA National Centers for Environmental Information, [accessed Oct. 22, 2020 at https://www.ncei.noaa.gov/metadata/geoportal/rest/metadata/item/gov.noaa.ngdc.mgg.dem:1786/html].
- NOAA National Geophysical Data Center, 2014, Puget Sound, Washington 1/3 Arc-second MHW Coastal Digital Elevation Model: NOAA National Centers for Environmental Information. [accessed Oct. 22, 2020 at https://www.ncei.noaa.gov/metadata/geoportal/rest/metadata/item/gov.noaa.ngdc.mgg.dem:5165/html].
- NOAA National Geophysical Data Center, 2015, Strait of Juan de Fuca, Washington 1/3 Arc-second NAVD88 Coastal Digital Elevation Model: NOAA National Centers for Environmental Information. [accessed Oct. 22, 2020 at https://www.ncei.noaa.gov/metadata/geoportal/rest/metadata/item/gov.noaa.ngdc.mgg.dem:11514/html].
- Padgett, J. S.; Engelhart, S. E.; Kelsey, H. M.; Witter, R. C.; Cahill, Niamh; Hemphill-Haley, Eileen, 2021, Timing and amount of southern Cascadia earthquake subsidence over the past 1700 years at northern Humboldt Bay, California, USA: *Geological Society of America Bulletin*, in press. [https://doi.org/10.1130/B35701.1]
- Peters, Robert; Jaffe, B. E.; Gelfenbaum, Guy; Peterson, C. D., 2003, Cascadia tsunami deposit database: U.S. Geological Survey Open-File Report 03-13, 25 p. [https://doi.org/10.3133/ofr0313]
- Petersen, M. D.; Moschetti, M. P.; Powers, P. M.; Mueller, C. S.; Haller, K. M.; Frankel, A. D.; Zeng, Yuehua; Rezaeian, Sanaz; Harmsen, S. C.; Boyd, O. S.; Field, E. H.; Chen, Rui; Rukstales, K. S.; Luco, Nico; Wheeler, R. L.; Williams, R. A.; and Olsen, A. H., 2014, Documentation for the 2014 update of the United States national seismic hazard maps: U. S. Geological Survey Open-File Report 2014–1091, 243 p. [https://doi.org/10.3133/ofr20141091]
- Peterson, C. D.; Cruikshank, K. M. ; Darienzo, M. E. ; Wessen, G. C.; Butler, V. L.; Sterling, S. L., 2013, Coseismic subsidence and paleotsunami run-up records from latest Holocene deposits in the Waatch Valley, Neah Bay, northwest Washington, U.S.A.—Links to great earthquakes in the northern Cascadia margin: *Journal of Coastal Research*, v. 29, no. 1, p. 157–172. [https://doi.org/10.2112/JCOASTRES-D-12-00031.1]
- Plafker, George, 1969, Tectonics of the March 27, 1964, Alaska earthquake: U.S. Geological Survey Professional Paper 543-1, 74 p., 2 sheets, scales 1:2,000,000 and 1:500,000. [https://pubs.usgs.gov/pp/0543i/].
- Plafker, George; Savage, J. C., 1970, Mechanism of the Chilean earthquakes of May 21 and 22, 1960: *Geological Society of America Bulletin*, v. 81, no. 4, p. 1001–1030. [https://doi.org/10.1130/0016-7606(1970)81[1001:MOTCEO]2.0.CO;2]
- Priest, G. R.; Myers, E. P., III; Baptista, A. M.; Flück, Paul; Wang, Kelin; Kamphaus, R. A.; Peterson, C. D., 1997, Cascadia subduction zone tsunamis—Hazard mapping at Yaquina Bay, Oregon: Oregon Department of Geology and Mineral Industries Open-File Report O-97-34, 144 p. [http://www.oregongeology.org/pubs/ofr/O-97-34.pdf]
- Priest, G. R.; Zhang, Yinglong; Witter, R. C.; Wang, Kelin; Goldfinger, Chris; Stimely, Laura, 2014, Tsunami impact to Washington and northern Oregon from segment ruptures on the southern Cascadia subduction zone: *Natural Hazards*, v. 72, no. 2, p. 849–870. [https://doi.org/10.1007/s11069-014-1041-7]
- Satake, Kenji; Shimazaki, Kunihiko; Tsuji, Yoshinobu; Ueda, Kazue, 1996, Time and size of a giant earthquake in Cascadia inferred from Japanese tsunami records of January 1700: *Nature*, v. 379, no. 6562, p. 246–249. [https://doi.org/10.1038/379246a0]
- Satake, Kenji; Wang, Kelin; Atwater, B. F., 2003, Fault slip and seismic moment of the 1700 Cascadia earthquake inferred from Japanese tsunami description: *Journal of Geophysical Research*, v. 108, no. B11, 17 p. [https://doi.org/10.1029/2003JB002521]
- Synolakis, C. E.; Bernard, E. N.; Titov, V. V.; Kânoğlu, Utku; González, F. I., 2007, Standards, criteria, and procedures for NOAA evaluation of tsunami numerical models: National Oceanic and Atmospheric Administration Technical Memorandum OAR PMEL-135, 60 p. [https://repository.library.noaa.gov/view/noaa/11073/noaa_11073_DS1.pdf]
- Sypus, Matthew, 2019, Models of tsunamigenic earthquake rupture along the west coast of North America: University of Victoria Doctor of Philosophy thesis, 100 p. [http://hdl.handle.net/1828/11436]
- Titov, V. V.; Arcas, Diego; Moore, C. W.; LeVeque, R. J.; Adams, L. M.; González, F. I., 2018, Tsunami hazard assessment of Bainbridge Island, Washington—Project Report: Washington State Emergency Management Division, 43 p. [http://depts.washington.edu/ptha/WA_EMD_Bainbridge/BainbridgelslandTHA.pdf].
- Titov, V. V.; Kânoğlu, Utku; Synolakis, C. E., 2016, Development of MOST for real-time tsunami forecasting: *Journal of Waterway, Port, Coastal, and Ocean Engineering*, v. 142, no. 6, 48 p. [https://doi.org/10.1061/(ASCE)WW.1943-5460.0000357]
- Titov, V. V.; González, F. I., 1997, Implementation and testing of the Method of Splitting Tsunami (MOST) model: NOAA Technical Memorandum ERL PMEL-112 (PB98-122773), 11 p. [https://www.pmel.noaa.gov/pubs/PDF/tito1927/tito1927.pdf]
- Titov, V. V.; Synolakis, C. E., 1995, Modeling of breaking and nonbreaking long-wave evolution and runup using VTCS-2: *Journal of Waterway, Port, Coastal, and Ocean Engineering*, v. 121, no. 6, p. 308–316.
- Titov, V. V.; Synolakis, C. E., 1998, Numerical modeling of tidal wave runup: *Journal of Waterway, Port, Coastal and Ocean Engineering*, v. 124, no. 4, p. 157–171. [https://doi.org/10.1061/(ASCE)0733-950X(1998)124:4(157)]
- Walsh, T. J.; Arcas, Diego; Titov, V. V.; Chamberlin, C. C., 2014, Tsunami hazard map of Everett, Washington: Model results for magnitude 7.3 and 6.7 Seattle fault earthquakes: Washington Division of Geology and Earth Resources Open File Report 2014-03, 1 plate, scale 1:32,000. [http://www.dnr.wa.gov/publications/ger_ofr2014-03_tsunami_hazard_everett.pdf]
- Walsh, T. J.; Arcas, Diego; Venturato, A. J.; Titov, V. V.; Mofjeld, H. O.; Chamberlin, C. C.; González, F. I., 2009, Tsunami hazard map of Tacoma, Washington—Model results for Seattle fault and Tacoma fault earthquake tsunamis: Washington Division of Geology and Earth Resources Open File Report 2009-9, 1 sheet, scale 1:24,000. [http://www.dnr.wa.gov/publications/ger_ofr2009-9_tsunami_hazard_tacoma.pdf]

- Walsh, T. J.; Caruthers, C. G.; Heinritz, A. C.; Myers, E. P., III; Baptista, A. M.; Erdakos, G. B.; Kamphaus, R. A., 2000, Tsunami hazard map of the southern Washington coast—Modeled tsunami inundation from a Cascadia subduction zone earthquake: Washington Division of Geology and Earth Resources Geologic Map GM-49, 1 sheet, scale 1:100,000, with 12 p. text. [http://www.dnr.wa.gov/publications/ger_gm49_tsunami_hazard_southern_coast.zip]
- Walsh, T. J.; Gica, Edison; Arcas, Diego; Titov, V. V.; Eungard, D. W., 2016, Tsunami hazard maps of the San Juan Islands, Washington—Model results from a Cascadia subduction zone earthquake scenario: Washington Division of Geology and Earth Resources Map Series 2016-01, 4 sheets, scale 1:24,000 and 1:48,000, 9 p. text. [http://www.dnr.wa.gov/publications/ger_ms2016-01_tsunami_hazard_san_juan_islands.zip]
- Walsh, T. J.; Myers, E. P., III; Baptista, A. M., 2002a, Tsunami inundation map of the Port Angeles, Washington area: Washington Division of Geology and Earth Resources Open File Report 2002-1, 1 sheet, scale 1:24,000. [http://www.dnr.wa.gov/publications/ger_ofr2002-1_tsunami_hazard_portangeles.pdf]
- Walsh, T. J.; Myers, E. P., III; Baptista, A. M., 2002b, Tsunami inundation map of the Port Townsend, Washington area: Washington Division of Geology and Earth Resources Open File Report 2002-2, 1 sheet, scale 1:24,000. [http://www.dnr.wa.gov/publications/ger_ofr2002-2_tsunami_hazard_porttownsend.pdf]
- Walsh, T. J.; Myers, E. P., III; Baptista, A. M., 2003a, Tsunami inundation map of the Neah Bay, Washington, area: Washington Division of Geology and Earth Resources Open File Report 2003-2, 1 sheet, scale 1:24,000. [http://www.dnr.wa.gov/publications/ger_ofr2003-2_tsunami_hazard_neahbay.pdf]
- Walsh, T. J.; Myers, E. P., III; Baptista, A. M., 2003b, Tsunami inundation map of the Quileute, Washington, area: Washington Division of Geology and Earth Resources Open File Report 2003-1, 1 sheet, scale 1:24,000. [http://www.dnr.wa.gov/publications/ger_ofr2003-1_tsunami_hazard_quileute.pdf]
- Walsh, T. J.; Titov, V. V.; Venturato, A. J.; Mofjeld, H. O.; González, F. I., 2003c, Tsunami hazard map of the Elliott Bay area, Seattle, Washington—Modeled tsunami inundation from a Seattle Fault earthquake: Washington Division of Geology and Earth Resources Open File Report 2003-14, 1 sheet, scale 1:50,000. [http://www.dnr.wa.gov/publications/ger_ofr2003-14_tsunami_hazard_elliottbay.pdf]
- Walsh, T. J.; Titov, V. V.; Venturato, A. J.; Mofjeld, H. O.; González, F. I., 2004, Tsunami hazard map of the Bellingham area, Washington—Modeled tsunami inundation from a Cascadia subduction zone earthquake: Washington Division of Geology and Earth Resources Open File Report 2004-15, 1 sheet, scale 1:50,000. [http://www.dnr.wa.gov/publications/ger_ofr2004-15_tsunami_hazard_bellingham.pdf]
- Walsh, T. J.; Titov, V. V.; Venturato, A. J.; Mofjeld, H. O.; González, F. I., 2005, Tsunami hazard map of the Anacortes-Whidbey Island area, Washington—Modeled tsunami inundation from a Cascadia subduction zone earthquake: Washington Division of Geology and Earth Resources Open File Report 2005-1, 1 sheet, scale 1:62,500. [http://www.dnr.wa.gov/publications/ger_ofr2005-1_tsunami_hazard_anacortes_whidbey.pdf]
- Wang, P.-L.; Engelhart, S. E.; Wang, Kelin; Hawkes, A. D.; Horton, B. P.; Nelson, A. R.; Witter, R. C., 2013, Heterogeneous rupture in the great Cascadia earthquake of 1700 inferred from coastal subsidence estimates: *Journal of Geophysical Research Solid Earth*, v. 118, no. 5, p. 2460–2473. [<https://doi.org/10.1002/jgrb.50101>]
- Wang, Kelin; Tréhu, A. M., 2016, Invited review paper: Some outstanding issues in the study of great megathrust earthquakes—The Cascadia example: *Journal of Geodynamics*, v. 98, p. 1–18. [<https://doi.org/10.1016/j.jog.2016.03.010>]
- Williams, H. F. L.; Hutchinson, Ian, 2000, Stratigraphic and microfossil evidence for late Holocene tsunamis at Swantown Marsh, Whidbey Island, Washington: *Quaternary Research*, v. 54, no. 2, p. 218–227. [<https://doi.org/10.1006/qres.2000.2162>]
- Williams, H. F. L.; Hutchinson, Ian; Nelson, A. R., 2005, Multiple sources for late-Holocene tsunamis at Discovery Bay, Washington State, USA: *The Holocene*, v. 15, no. 1, p. 60–73. [<https://doi.org/10.1191/0956683605hl784rp>]
- Witter, R. C.; Kelsey, H. M.; Hemphill-Haley, Eileen, 2003, Great Cascadia earthquakes and tsunamis of the past 6,700 years, Coquille River estuary, southern coastal Oregon: *Geological Society of America Bulletin*, v. 115, no. 10, p. 1289–1306. [<https://doi.org/10.1191/0956683605hl784rp>]
- Witter, R. C.; Zhang, Y. J.; Wang, Kelin; Goldfinger, Chris; Priest, G. R.; Allan, J. C., 2012, Coseismic slip on the southern Cascadia megathrust implied by tsunami deposits in an Oregon lake and earthquake-triggered marine turbidites: *Journal of Geophysical Research*, v. 117, no. B10303, 17 p. [<https://doi.org/10.1029/2012JB009404>]
- Witter, R. C.; Zhang, Y. J.; Wang, Kelin; Priest, G. R.; Goldfinger, Chris; Stimely, L. L.; English, J. T.; Ferro, P. A., 2011, Simulating tsunami inundation at Bandon, Coos County, Oregon, using hypothetical Cascadia and Alaska earthquake scenarios: *Oregon Department of Geology and Mineral Industries Special Paper 43*, 57 p. [<http://www.oregongeology.org/pubs/sp/p-SP-43.htm>]
- Witter, R. C.; Zhang, Y. J.; Wang, Kelin; Priest, G. R.; Goldfinger, Chris; Stimely, Laura; English, J. T.; Ferro, P. A., 2013, Simulated tsunami inundation for a range of Cascadia megathrust earthquake scenarios at Bandon, Oregon, USA: *Geosphere*, v. 9, no. 6, p. 1783–1803. [<https://doi.org/10.1130/GES00899.1>]
- Yamaguchi, D. K.; Atwater, B. F.; Bunker, D. E.; Benson, B. E.; Reid, M. S., 1997, Tree-ring dating the 1700 Cascadia earthquake: *Nature*, v. 389, p. 922–923. [<https://doi.org/10.1038/40048>]
- Zhang, Y. J.; Witter, R. C.; Priest, G. R., 2011, Tsunami–tide interaction in 1964 Prince William Sound tsunami: *Ocean Modelling*, v. 40, no. 3–4, p. 246–259. [<https://doi.org/10.1016/j.ocemod.2011.09.005>]

Appendix A. Tsunami Source Evidence and Models

Applying evidence of past tsunamis is the best way to prepare for future tsunamis. One important piece of geologic evidence for past tsunamis is the deposits they leave behind. Tsunami deposits are typically preserved in tidal-marsh stratigraphy and consist of normally graded sand beds that may contain marine microfossils (Morton and others, 2007). There are many locations containing tsunami deposits within Washington, mostly preserved along the Pacific coast, which suggests a nearby source like the Cascadia subduction zone (CSZ; Peters and others, 2003). Researchers have also found tsunami deposits within Washington's inner waterways that correlate to the same approximate timing, indicating that the

CSZ is capable of producing powerful tsunamis that penetrate into the Salish Sea. These locations include the Strait of Juan de Fuca at Salt Creek (Hutchinson and others, 2013), Discovery Bay (near Port Townsend; Williams and others, 2005), the west shore of Whidbey Island (Fig. 2; Williams and Hutchison, 2000), and as far south as Lynch Cove at the terminus of Hood Canal (Lynch Cove stratigraphy interpreted in Fig. A1; Garrison-Laney, 2017).

This appendix reviews past evidence for earthquakes and their resultant tsunamis that have impacted Washington's inner and outer coastlines. This includes a discussion of evidence from the geologic record that was used to calculate recurrence

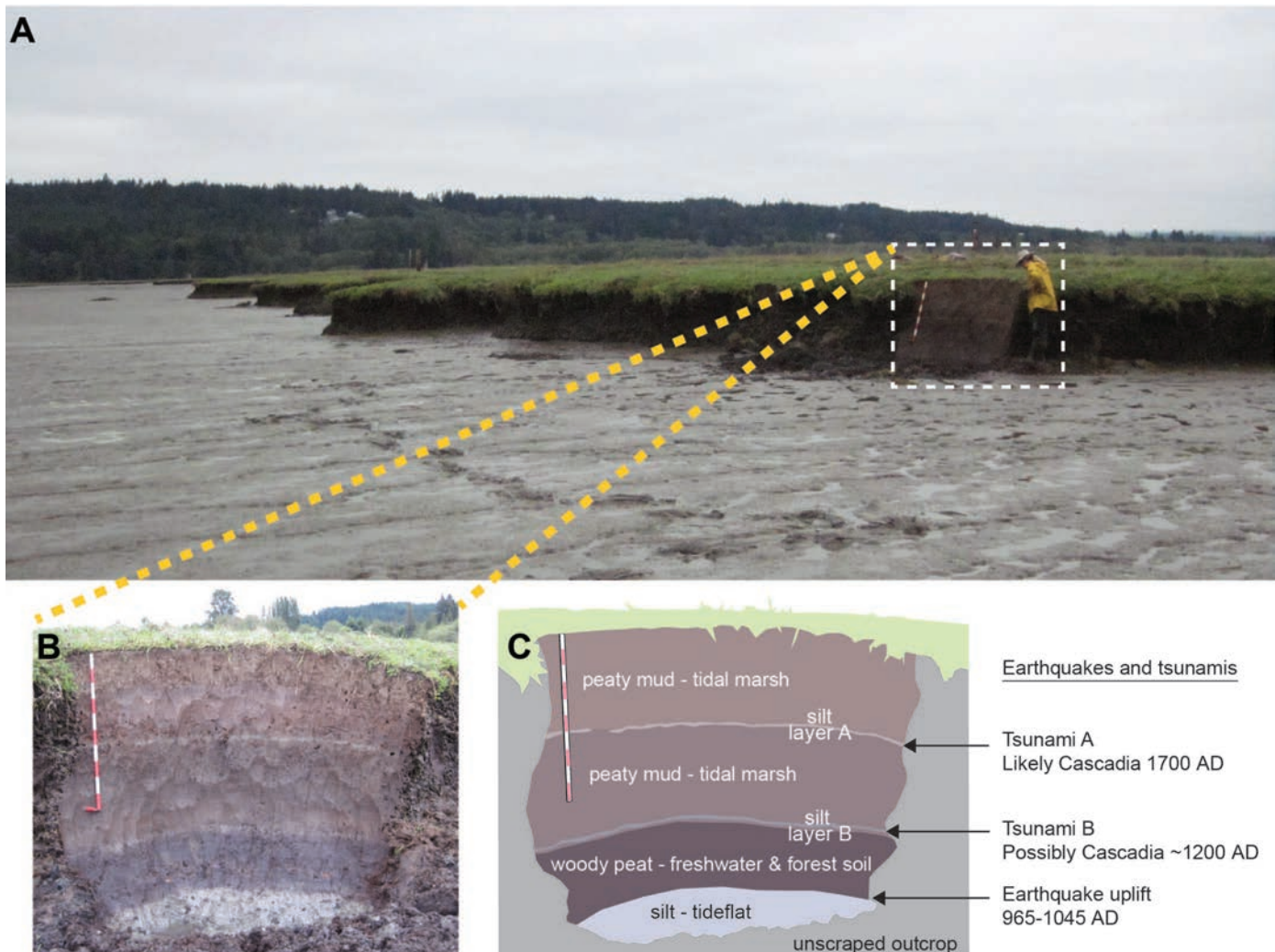


Figure A1. **A.** Exposed sediments along the edge of the tidal marsh at Lynch Cove in Hood Canal. **B.** Outcrop of tidal marsh sediments scraped clean. The red and white meter stick increments are ~4 in. (10 cm) long. **C.** Schematic diagram of the outcrop in B labeled with interpretation of how the environment has changed over time based off the layers of the sediment. The oldest gray silt layer on the bottom was a tidal mudflat until one or more earthquakes uplifted it up out of the intertidal zone between the years 965–1045 (Bucknam and others, 1994). Trees and freshwater marshes colonized the uplifted tidal flat, forming the woody peat layer over time. The forested areas gradually converted to tidal marshes as relative sea level rose, covering the woody peat with marsh deposits. During this sea level rise, tsunamis flooded the area at least twice, leaving behind silty layers A and B, interpreted as tsunami deposits. The radiocarbon ages of layers A and B overlap with the date ranges of the last two Cascadia subduction zone earthquakes. Layer A is dated between the years of 1690–1830 and likely represents the most recent Cascadia earthquake from the year 1700 (Atwater and others, 2005). Layer B is dated between the years 1170–1230 and may possibly represent the next oldest Cascadia earthquake (although not all published ages for the poorly dated earthquake overlap with layer B's age; Garrison-Laney, 2017).

COASTAL EARTHQUAKE SUBSIDENCE

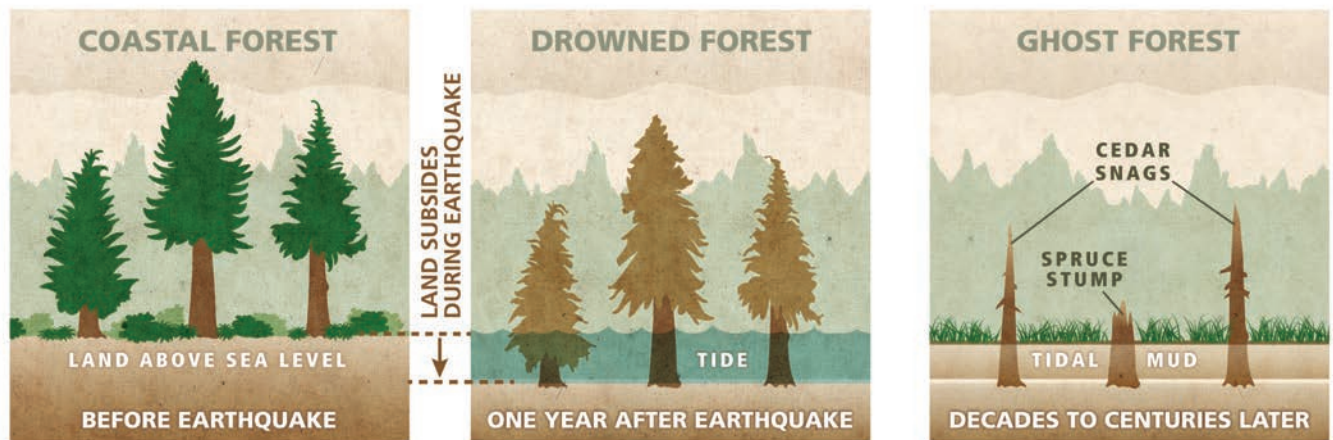


Figure A2. Schematic showing the formation of ghost forests over time as described in Atwater and Yamaguchi (1991), Atwater (1992), and Atwater and others (1995; 2005). Trees that were once above sea level may subside to below the tidal level following an earthquake. These trees die by saltwater intrusion, leaving behind distinctive cedar snags seen in coastal and tidal areas (spruce stumps shown here are exaggerated and are not typically seen protruding through tidal mud). Dendrochronology techniques can reveal when the sudden subsidence occurred. Between earthquake events, the land level slowly rebounds to elevations similar to pre-earthquake conditions (the land may not recover all elastic deformation) and a forest once again grows. This cycle then repeats itself following the next earthquake event.

intervals for the CSZ (the frequency of how often earthquakes occur). Recurrence intervals and the characterization of past tsunamis come from many lines of evidence, including coastal earthquake subsidence, tsunami deposits, deep-sea sediment cores, marine microfossils (diatoms), and oral and written histories. All of this evidence points to numerous earthquakes and tsunamis that originated from the CSZ, and researchers believe that Washington has experienced both moderate to large tsunamis in the past.

REVIEW OF EVIDENCE

Coastal Earthquake Subsidence

Great subduction zone earthquakes commonly cause coincident land-level changes, known as coseismic subsidence and uplift (Plafker, 1969; Plafker and Savage, 1970). Coastal subsidence during great earthquakes causes sudden sea-level rise and drops salt marshes and uplands into lower intertidal environments; the sudden submergence is recorded geologically by stratigraphic sequences that show sharp contacts between buried marsh peat or upland soil and overlying estuarine mud (Atwater, 1992). Some coastal regions such as the banks of the Copalis River in southwest Washington also contain “ghost forests,” or dead standing trees and other vegetation that were suddenly submerged in seawater (Fig. A2; Atwater, 1992). Dendrochronology and radiocarbon dating techniques reveal when these submergence events occurred and allow for reconstructions of past great earthquake events (Jacoby and others, 1997; Yamaguchi and others, 1997). Atwater and Hemphill-Haley (1997) reported six sudden submergence events in Willapa Bay over the last 3,500 years. Their data imply an average recurrence interval of about 520 years for earthquakes on the CSZ. However, individual intervals for each earthquake have varied between ~100 and ~1,300 years (Atwater and Hemphill-Haley, 1997).

Tsunami Deposits

Researchers working in Oregon have found a somewhat different record farther south. Using marsh stratigraphy and inferred tsunami deposits, Kelsey and others (2002) found a 5,500-year record of 11 earthquake events at Sixes River in southern Oregon. These records also include an abrupt subsidence event not observed on the southern Washington coast. Kelsey and others (2005) examined Bradley Lake on the southern Oregon coast near Bandon and found that it included probable tsunami deposits with an average recurrence interval of ~390 years. The shorter recurrence interval in southern Oregon implies that some earthquakes on the CSZ did not produce abrupt subsidence in southern Washington. A possible explanation is that the CSZ earthquakes recorded in Oregon did not rupture the entire length of the subduction zone, resulting in a spatially heterogeneous response in the geologic record. Nelson and others (2006) examined the degree of overlap and amount of abrupt subsidence at eight sites along the Oregon and Washington coasts. They concluded that rupture area (and therefore earthquake magnitudes) varied—ruptures along the northern CSZ are generally longer, whereas ruptures along the southern CSZ are more variable in both length and recurrence interval.

Deep-Sea Sediment Cores

Another approach to inferring recurrence intervals is the correlation of turbidites—deposits of sediment gravity flows, or turbidity currents—out on the abyssal plain (Griggs and Kulm, 1970). Adams (1990) inferred that great earthquakes triggered turbidity currents in Cascadia Channel and Astoria Canyon (Fig. A3). Oregon State University researchers logged 13 turbidites in both Cascadia Channel and Astoria Canyon from multiple deep-sea cores, suggesting 13 CSZ ruptures (Griggs, 1968; Adams, 1990). All 13 turbidite deposits

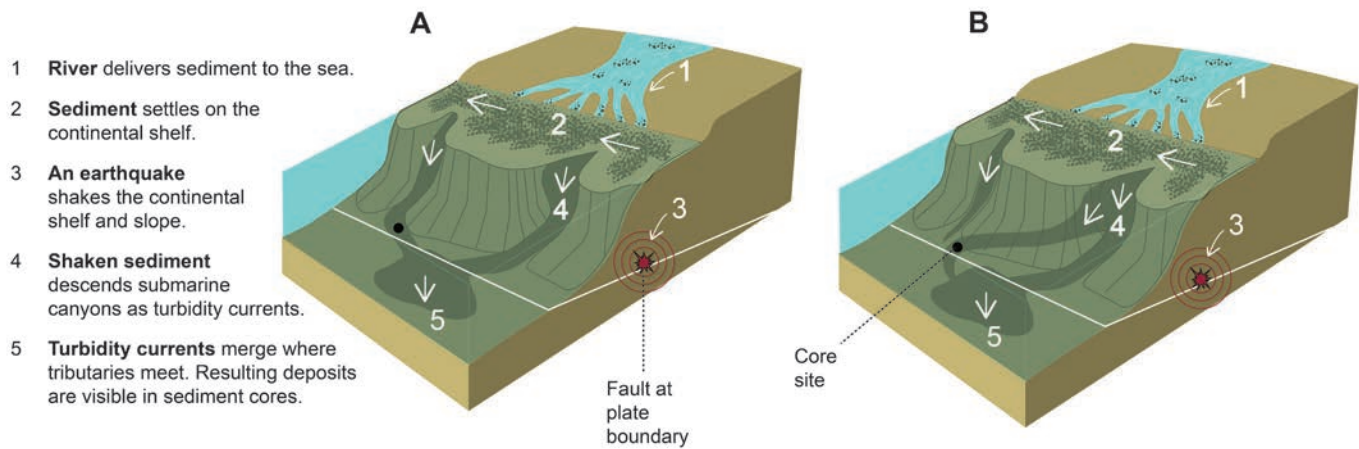


Figure A3. Two alternative schematic views of turbidity currents descending submarine canyons. **A.** Turbidity current flows produced by seismic shaking (modified from Adams; 1990). Extensive shaking enables turbidity currents to descend different submarine channels at the same time and merge. **B.** Turbidity current flows influenced more by differences in sediment supply than by seismic shaking (modified from Atwater and others; 2014). Turbidite stratigraphy at a specific core site at one submarine canyon may suggest that accumulation occurs by way of latitudinal spillover from other submarine canyons with differing sediment supply to canyon heads. In this case, shaking from the upper canyon shown may also have limited sediment supply and produce few, if any turbidity currents before merging where the tributaries meet. These contrasting views require future research focused on sediment supply, flow initiations, and downstream pathways.

Table A1. Estimates of earthquake recurrence on the Cascadia subduction zone.

Events over time interval	Average recurrence interval in years; range if given	Section of CSZ	Reference	Major evidence
6 submergence events in 3,500 years	500–540 average, 100–300 to 1,300	northern	Atwater and Hemphill-Haley (1997)	submergence events
11 submergence events in 5,500 years	510	southern	Kelsey and others (2002)	marsh stratigraphy and tsunami deposits
13 tsunami deposits, 17 disturbances in 7,000 years	390 average for local tsunamis entering Bradley Lake; ~500 year average for ruptures along the southern margin	southern	Kelsey and others (2003)	marine incursions and disturbance events in Bradley Lake
13 turbidites post Mazama ash (6,845 years BP [calibrated to ~7,700 cal yr BP])	590 ±170	northern	Adams (1990)	turbidites in Astoria Canyon and Cascadia Channel
19 or 20 full-margin turbidites in 10,000 years; 22 turbidites restricted to the south	500–530 average for full-margin rupture, ~240 full-margin plus southern only	whole and partial	Goldfinger and others (2012)	turbidites along Cascadia margin
20 full-margin turbidites in 10,000 years; 3 turbidites on a segment running from northern California to Juan de Fuca Channel; 1 turbidite off Washington and British Columbia only	500–530 average for full-margin rupture; ~434 full-margin plus shorter ruptures adjacent to Washington	whole and partial	Goldfinger and others (2017)	turbidites along Cascadia margin

were located stratigraphically above the Mazama ash (erupted from Mount Mazama volcano), implying that they are younger than the Mazama ash. Radiometric dating of the Mazama ash suggests an age of $6,845 \pm 50$ radiocarbon years before present (BP; Adams, 1990). These findings indicate that earthquakes on the CSZ have an average recurrence interval of 590 ± 170 years (Table A1; Adams, 1990).

Goldfinger and others (2012) supplemented Griggs' (1968) turbidite data that Adams (1990) correlated to the CSZ by collecting numerous additional cores in the seafloor along

the Cascadia continental margin. From this updated record, Goldfinger and others (2012) concluded that the CSZ is capable of both full-length and partial ruptures of different sizes. They proposed that full-length ruptures offshore of northern California to British Columbia have a recurrence interval of 500 to 530 years offshore Washington and British Columbia, similar to the previous estimates of Adams (1990), Atwater (1992), and Atwater and Hemphill-Haley (1997). Goldfinger and others (2012) additionally estimated a recurrence interval of ~240 years for

partial ruptures, which include earthquakes offshore of Oregon and northern California.

Earthquakes that rupture only the northern part of the CSZ (including Washington) are also a possibility. Goldfinger and others (2017) selected additional sites for coring and seismic assessment offshore of the Washington continental shelf. Results from these new sites suggested a slight revision of their CSZ rupture model, extending several rupture boundaries from central Oregon farther north to include southwest Washington. They also inferred an additional event offshore of Washington and southern British Columbia only, although their revision may still require further data collection. As a result, these findings led to minor variations in their interpretation on CSZ recurrence intervals. In their updated interpretation, recurrence for most of the Washington coast decreased to 434 years, with the exception of the northernmost section (possible recurrence interval of 430–500 years) where turbidites of recent millennia are inconspicuous or absent (Goldfinger and others, 2017). This proposed change in interpretation suggests that there is a 10–17 percent chance that Washington experiences a CSZ earthquake within the next 50 years (probability estimate based off Gaussian and log-normal time-dependent distributions; Goldfinger and others, 2017). However, Atwater and others (2014) argued that the absence of core data and turbidites along the northern CSZ does not necessarily disprove ground shaking. Differences in sediment supply and flow paths down tributary channels may prohibit turbidites in this section of the CSZ (Fig. A3). Atwater and others (2014) further questioned the rupture lengths proposed by Goldfinger and others (2012). These rupture lengths were determined based on age correlations of widely spaced core sites, but the ages of each core site could not always be adequately determined.

Diatoms

Further studies on Discovery Bay, located on the northeast part of the Olympic Peninsula, detected nine muddy sand beds bearing marine microfossils (diatoms) that interrupt a 2,500-year-old sequence of peat deposits beneath a tidal marsh (Williams and others, 2005). Diatoms can assist in characterizing past earthquake events and are a useful proxy for land level and sea level change over time. This is because different species of diatoms occupy diverse environmental niches, and thereby researchers can use any changes in diatom assemblages over time to infer changes in the coastal environment. The ages of four of these beds, more precisely determined by Garrison-Laney and Miller (2017), overlap with inferred late-Holocene tsunamis generated by full-length ruptures of the CSZ (Goldfinger and others, 2012). Diatoms found in peat deposits bracketing these four beds do not indicate a concurrent change in sea level and elevation at Discovery Bay. This suggests that CSZ-associated coseismic subsidence has been negligible as far east as Discovery Bay. Other sand sheets in the sequence may represent tsunamis generated by partial ruptures of the CSZ, by upper plate fault earthquakes, or by landslides (Garrison-Laney and Miller, 2017), none of which triggered turbidity currents. This implies either that some CSZ earthquakes do not leave turbidite deposits in Cascadia Channel (Atwater and others, 2014), or that other events

such as local earthquakes or landslides generated some tsunami deposits, both of which are plausible.

Oral and Written Histories

Subduction zone earthquakes can generate tsunamis that are capable of crossing oceans. A key historical component of documenting the timing of the last CSZ-induced tsunami comes from historical reports in Japan. According to the Japanese record, accounts of unusual seas, flooded fields, damaged property, and damaged freight were reported on January 27/28th, 1700. Although there was abnormal flooding in Japan's coastal areas, many writers were resistant to call it a tsunami because they did not feel earthquake shaking. Instead, they called it a "high tide" (Atwater and others, 2005). Abnormal flooding events had occurred many other times in Japan, though researchers were able to attribute them to other locations of known distant earthquakes, such as South America. Uniquely, the event in 1700 later became known as the "orphan tsunami" (Atwater and others, 2005) because it lacked an apparent earthquake source. On the other side of the Pacific Ocean, histories passed down through native oral storytelling also mention powerful waves and shaking throughout the Pacific Northwest around this time (Ludwin, 2002). For example, Heaton and Snavely (1985) reported that Makah Tribal histories describe what could be a tsunami flowing through Waatch Prairie near Cape Flattery (Fig. 2).

EARTHQUAKE SLIP DISTRIBUTIONS AND TSUNAMI MODELS

1700 Earthquake

Nearly 300 years passed before researchers attributed the flooding that occurred in 1700 in Japan to possible fault activity within the CSZ (Satake and others, 1996). Satake and others (2003) tested various possible rupture dimensions and slip amounts to match the observed tsunami wave heights recorded in Japan. They assumed that this event ruptured the full 684 mi (~1,100 km; Flück and others, 1997) length of the CSZ and inferred 62 ft (19 m) of uniform, coseismic slip within the full-slip zone. The average slip over the whole subduction zone, including the full-slip and down-dip partial slip zone, equaled 46 ft (14m), suggesting a magnitude of 8.7 to 9.2 (Satake and others, 2003). They inferred that the most likely magnitude was 9.0 based on the correlation between estimates of coseismic subsidence from paleo-seismic studies and the subsidence predicted by their models.

While these early rupture models assumed a uniform slip distribution along the megathrust, all instrumentally recorded subduction zone earthquakes ruptured heterogeneously (for example, 2004 Sumatra, 2010 Chile, and 2011 Japan). Wang and others (2013) developed a heterogeneous earthquake deformation scenario for the 1700 CSZ earthquake. Their models allow slip to vary both along strike and in the dip direction, which correlates with the more precise estimates of subsidence and uplift constrained by detailed tidal microfossil studies than the uniform slip models. Better estimates of paleoseismic deformation are useful for delineating future earthquake and tsunami behavior,

but a heterogeneous slip distribution is challenging to predict and model.

Pre-1700 Earthquakes

PARTIAL-LENGTH RUPTURE MODELS

The magnitudes and slip distributions of earlier CSZ earthquakes are not as well constrained. Inferences of shorter ruptures that affect only the southern part of the CSZ generally imply smaller magnitude earthquakes. Priest and others (2014) modeled tsunamis from several postulated shorter ruptures limited to the southern part of the CSZ and concluded that the tsunamis they generated were significantly smaller in Washington than those generated by full-length ruptures. A partial CSZ rupture restricted to the north was suggested by Goldfinger and others (2013) and Peterson and others (2013). Goldfinger and others (2017) later substantiated this northern rupture, but there is insufficient paleo-seismic data to generate a tsunami model (see figs. 9 and 18 in Goldfinger and others, 2017). Therefore, the study presented here does not consider these smaller events.

FULL-LENGTH RUPTURE MODELS

Witter and others (2012) hypothesized that the earthquakes generated by the CSZ over the last 10,000 years have been highly variable, with some larger than the last one in the year 1700. This deduction comes from synthesizing multiple data including: (1) the turbidite data from Goldfinger and others (2012); (2) the correlation of inferred tsunami deposits with turbidites in Bradley Lake, Oregon (Witter and others, 2012); and (3) interpretation of tsunami deposits in the Coquille River estuary at Bandon, Oregon that extend as much as 6.2 mi (10 km) farther inland than the tsunami deposits from the 1700 event (Witter and others, 2003). Previously, Witter and others (2011) constructed 15 scenarios of full-length ruptures where they adjusted vertical seafloor deformation to simulate tsunami differences in inundation at Bandon, Oregon. These rupture scenarios included slip partitioned to a splay fault in the accretionary wedge as well as scenarios that varied the up-dip limit of slip on a buried megathrust fault. In tsunami modeling, the water column moves as an incompressible fluid, suggesting that any seafloor deformation will directly influence tsunami generation (Berger and others, 2011). Since splay fault ruptures breach the seafloor directly, they consequently could generate larger tsunamis than other types of earthquakes buried on the megathrust that do not and only cause seafloor deformation through elastic deformation of the upper plate. Thus, modeling a splay fault rupture effectively boosts tsunami generation. However, researchers have not decisively confirmed the existence of a splay fault in the CSZ, although some indirect structural evidence hints at this possibility on parts of the margin (Wang and Tréhu, 2016). To assess these rupture scenarios, Witter and others (2011, 2012) performed numerical tsunami simulations for Bradley Lake and Bandon. They used a logic tree approach to rank model consistency by comparing the results of each simulation with geophysical and geological data from the distribution of inferred tsunami deposits. Witter and others (2011) found that the observational tsunami data were broadly compatible with their larger scenarios.

Of the 15 CSZ scenarios modeled by Witter and others (2011), scenario L1—a splay fault model with a maximum slip of 88.6 ft (27 m) and an average slip of 42.6 ft (13 m)—produced a tsunami that encompassed 95 percent of the variability in their simulations. In other words, the L1 scenario produces tsunami inundation as extensive as, or more extensive than most (95 percent) other models along the Oregon coast. We have inferred these model results to be the same for the Puget Sound (disregarding potential tsunamis from crustal fault or landslide sources). Witter and others (2011) tied the assumed rate of plate convergence to the existing turbidite paleoseismic records (Goldfinger and others, 2011). They did this to estimate the size of the earthquakes that generated the turbidites, which were assigned to 19 stratigraphic units. However, Goldfinger and others (2012) debatably correlated these units among widely separated cores along the full length of the CSZ margin. These earthquake sizes were further constrained from tsunami simulations at Bradley Lake, Oregon (Witter and others, 2013). They concluded that three earthquakes in the last ~10,000 years were probably similar to scenario ‘L’ and only one was larger (Table 1 in Witter and others, 2011). The intervals between the inferred ‘L’ and larger earthquakes are ~1,800 to ~4,600 years apart. Another way to estimate recurrence frequency is that if four earthquakes in the last 10,000 years are L or larger, then these type of events have an average recurrence interval between 2,500 and 5,000 years.

Witter and others (2011) recommended considering the L1 scenario for land-use planning and revisions to coastal building codes. If the L1 scenario represents 95 percent of the hazard over a 10,000-year period, then scenario ‘L’ earthquakes have a long recurrence interval with a probability of occurrence that is on the same order as the International Building Code (seismic standard of 2 percent probability of exceedance in 50 years; International Code Council, 2015). Much of the geological evidence presented in this publication that justifies the use of the (Extended) L1 scenario, such as the turbidite record and tsunami deposits, have also been included in efforts to create the United States Geological Survey (USGS) national seismic hazard maps (Petersen and others, 2014).

Appendix B. Tide Gauge Comparison of the L1 and Extended L1 Scenarios

This appendix features the locations of supplemental simulated tide gauges (Fig. B1; Table B1) that compare the waveforms produced by the L1 and Extended L1 scenarios (Fig. B2). In all cases, the Extended L1 scenario produced a larger, broader tsunami waveform than the L1 scenario. Thus, the Extended L1 scenario pushes a larger volume of water into Washington’s inner waterways of the Salish Sea than the L1 scenario, which greatly worsens estimated flooding. This suggests that using the Extended L1 scenario for tsunami hazard assessment is the more conservative choice.

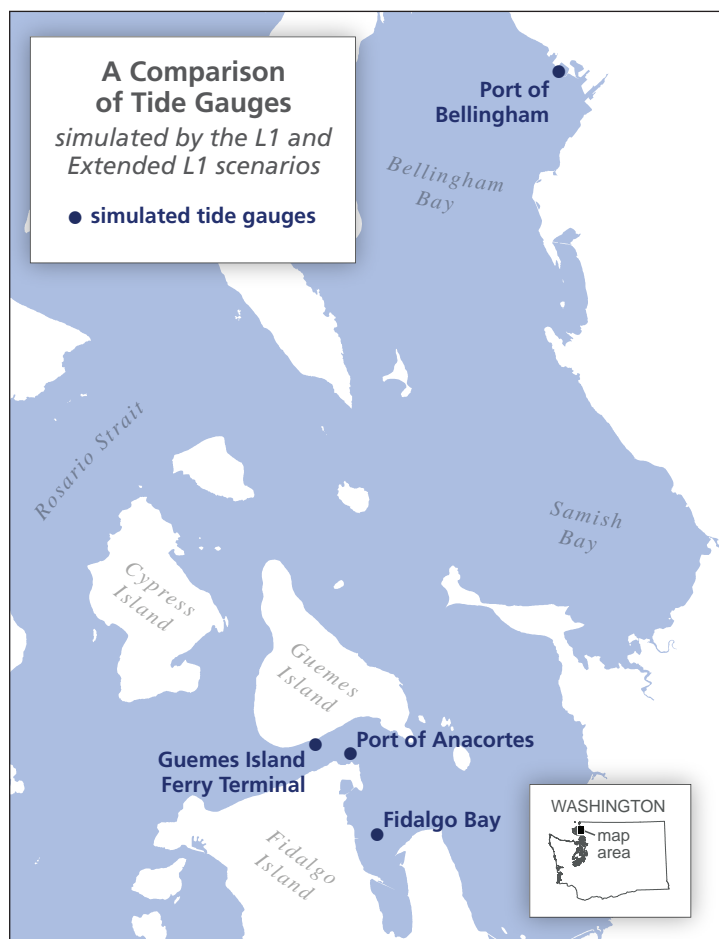


Figure B1. Selected synthetic tide gauge locations simulated with both the L1 and Extended L1 earthquake scenarios.

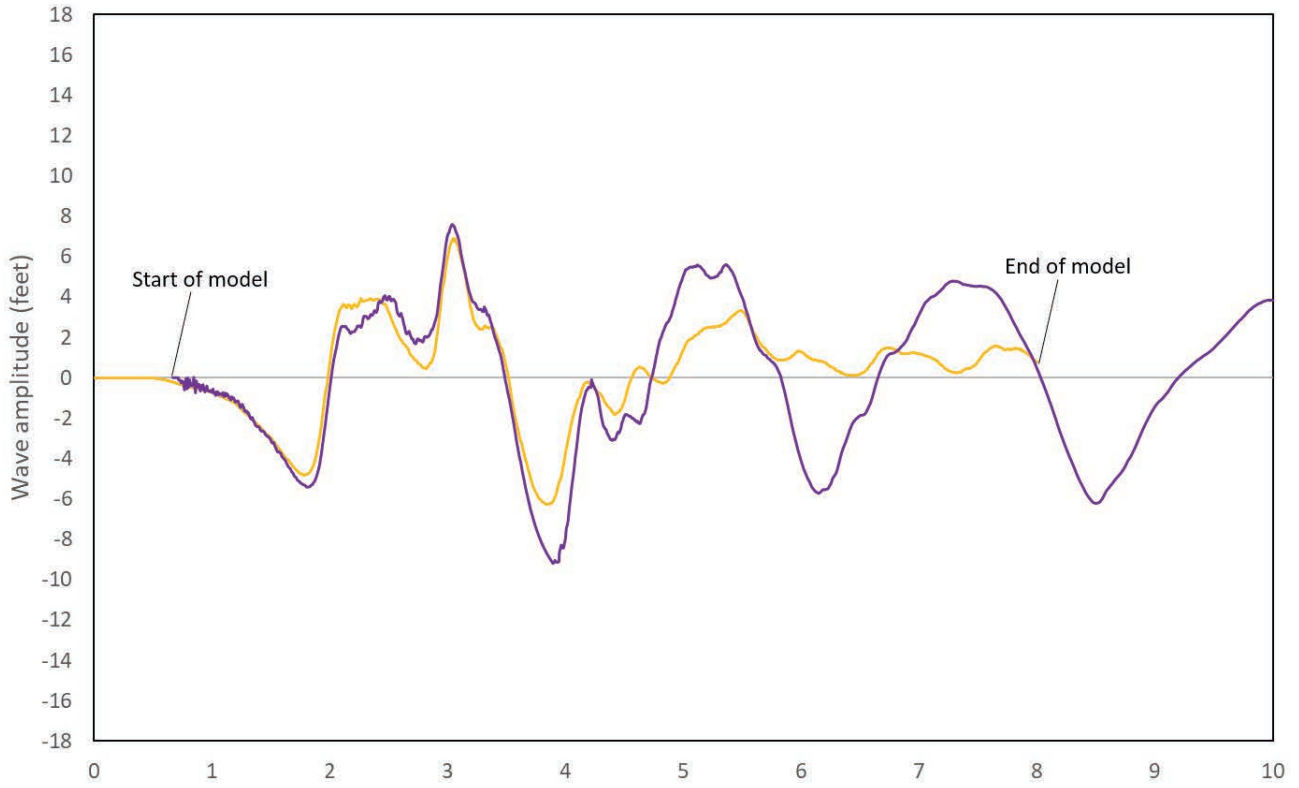
Table B1. Selected synthetic tide gauge locations simulated with both the L1 and Extended L1 earthquake scenarios.

Location Name	Longitude	Latitude
Fidalgo Bay	-122.589401	48.496899
Guemes Island Ferry Terminal	-122.623840	48.519768
Port of Anacortes	-122.612183	48.523102
Port of Bellingham	-122.512176	48.751991

Figure B2. (next pages) A comparison of modeled tsunami wave variations over time between the L1 (yellow) and Extended L1 (purple) earthquake scenarios at specified locations. Gray horizontal lines indicate static mean high water elevation at simulated tide gauges. While the L1 scenario may produce a higher initial wave amplitude than the Extended L1 in some instances, the Extended L1 produces both higher peak amplitudes and broader waveforms for following waves. **A** shows the simulated tide gauge for Fidalgo Bay, **B** shows the same for Guemes Island Ferry Terminal, **C** shows the Port of Anacortes, and **D** shows the Port of Bellingham.

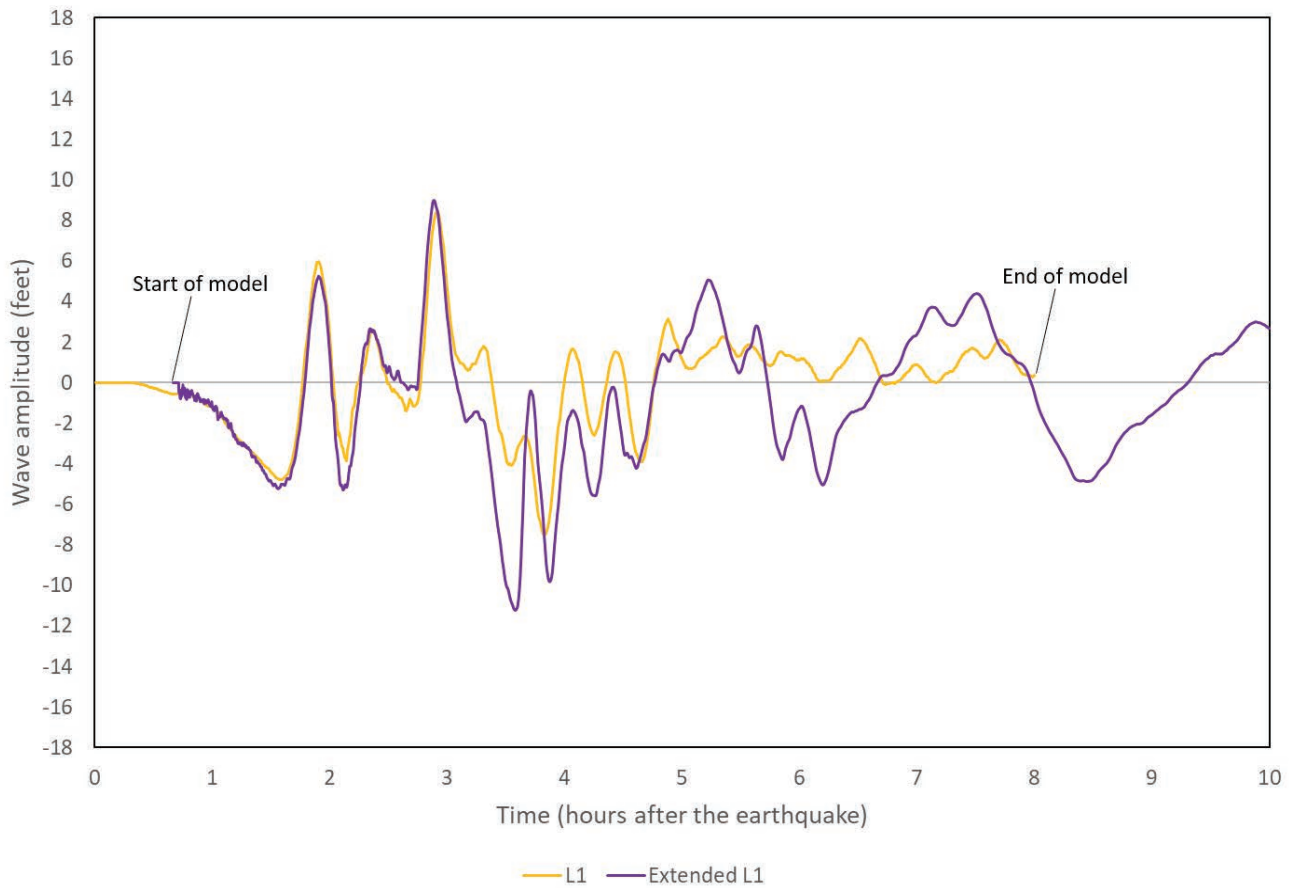
A

Fidalgo Bay Simulated Tide Gauge



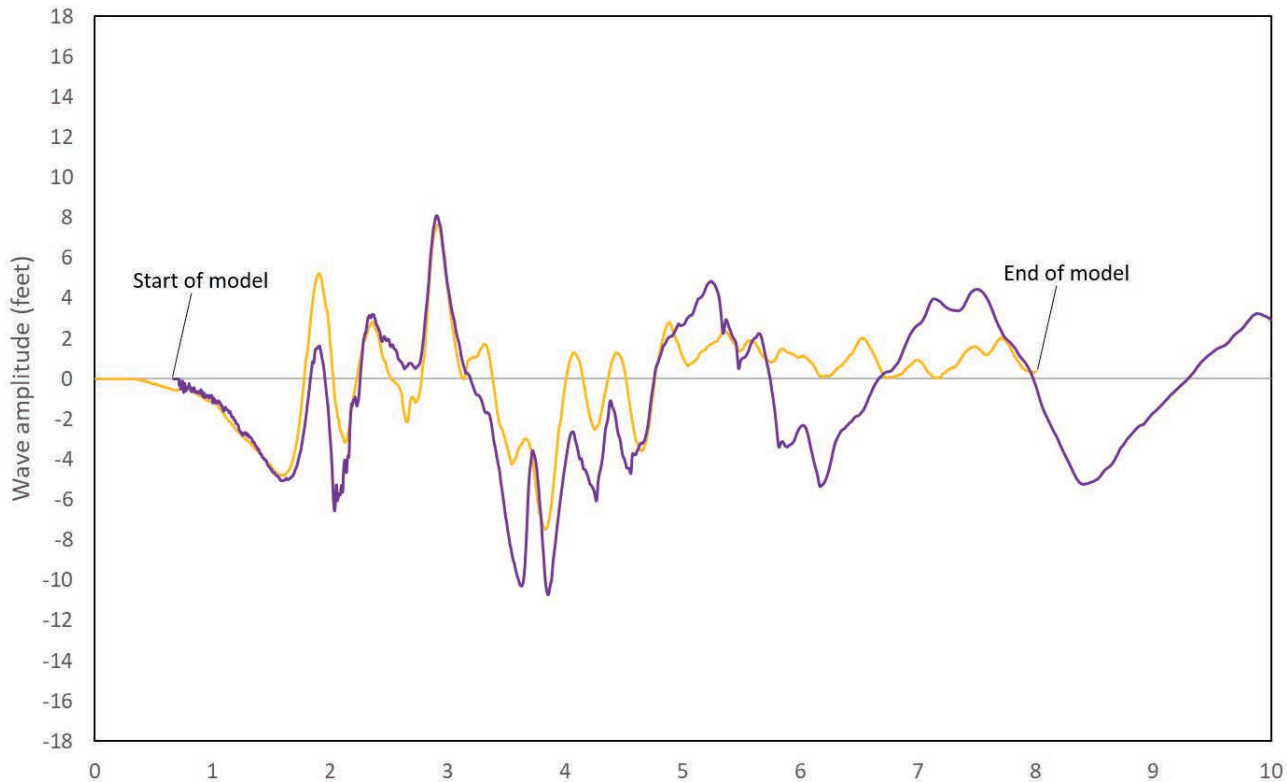
B

Guemes Island Terminal Simulated Tide Gauge



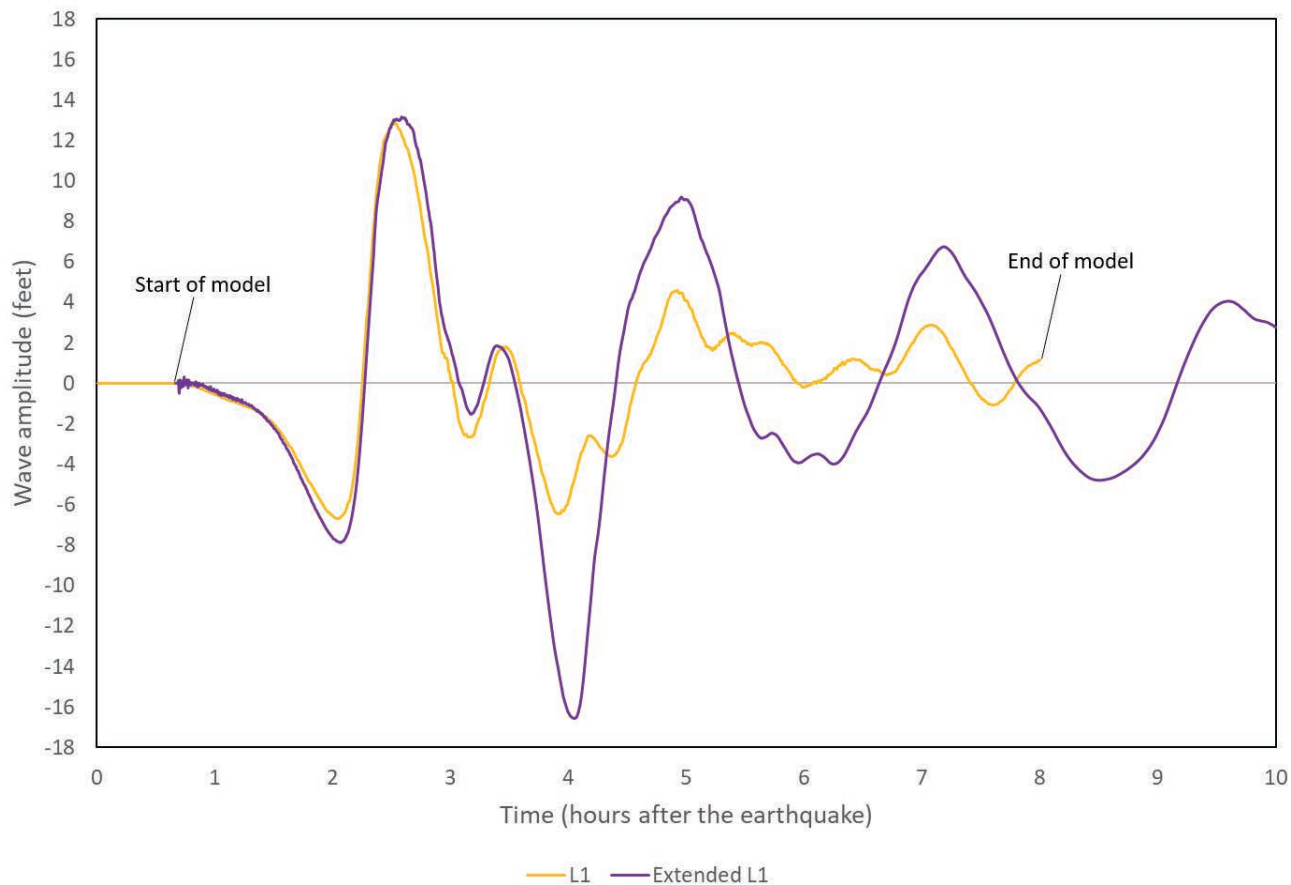
C

Port of Anacortes Simulated Tide Gauge



D

Port of Bellingham Simulated Tide Gauge



Appendix C. Tide Gauge Locations and Waveforms

This appendix shows the waveforms of synthetic simulated tide gauges at key locations (Fig. C1; Table C1) produced by the Extended L1 scenario included in this project. Refer to Map Sheets 1 through 8 for a more detailed view of these specified locations.

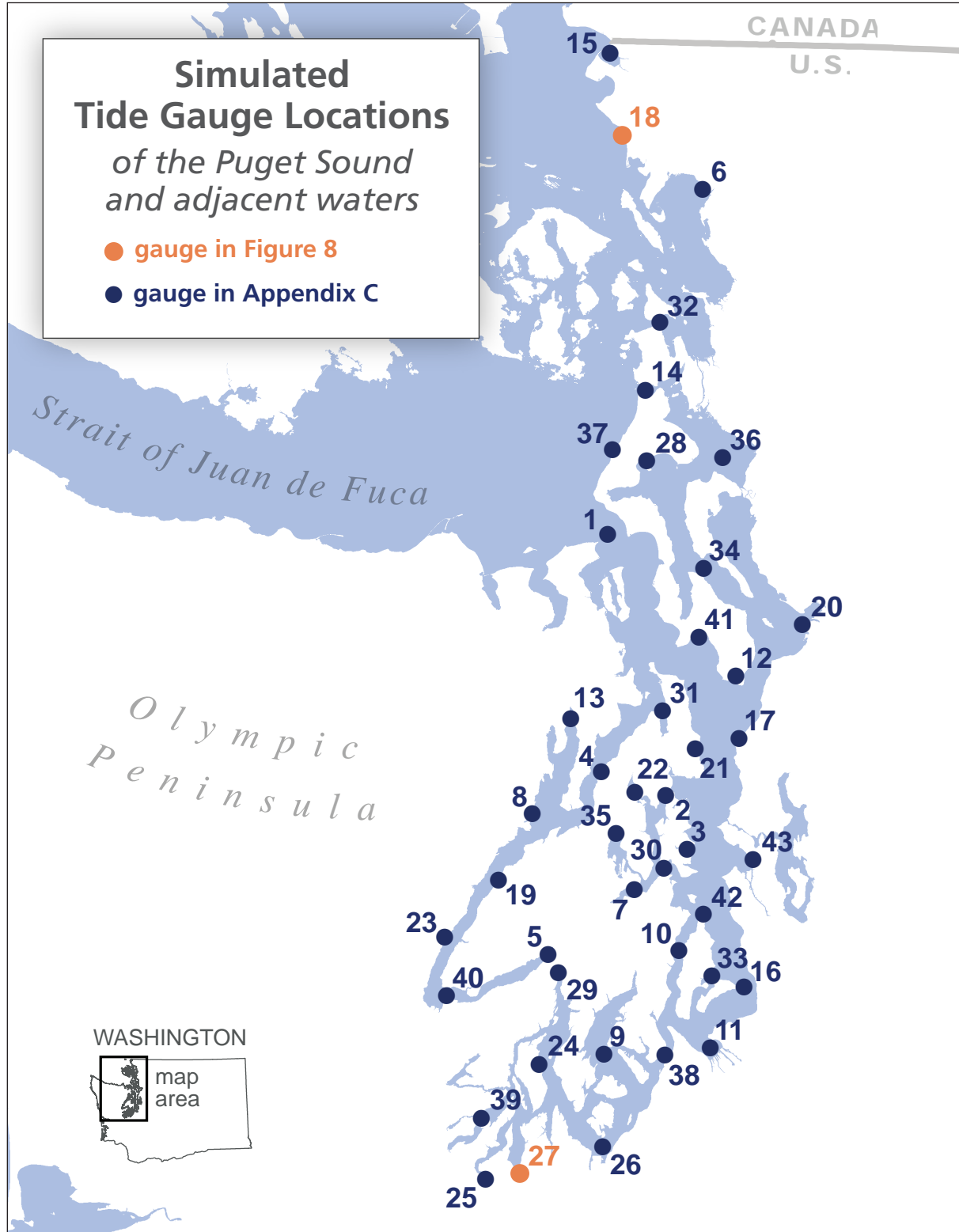


Figure C1. Locations for each synthetic simulated tide gauge included in this publication. Numbers correspond to the I.D. Number listed in Table C1.

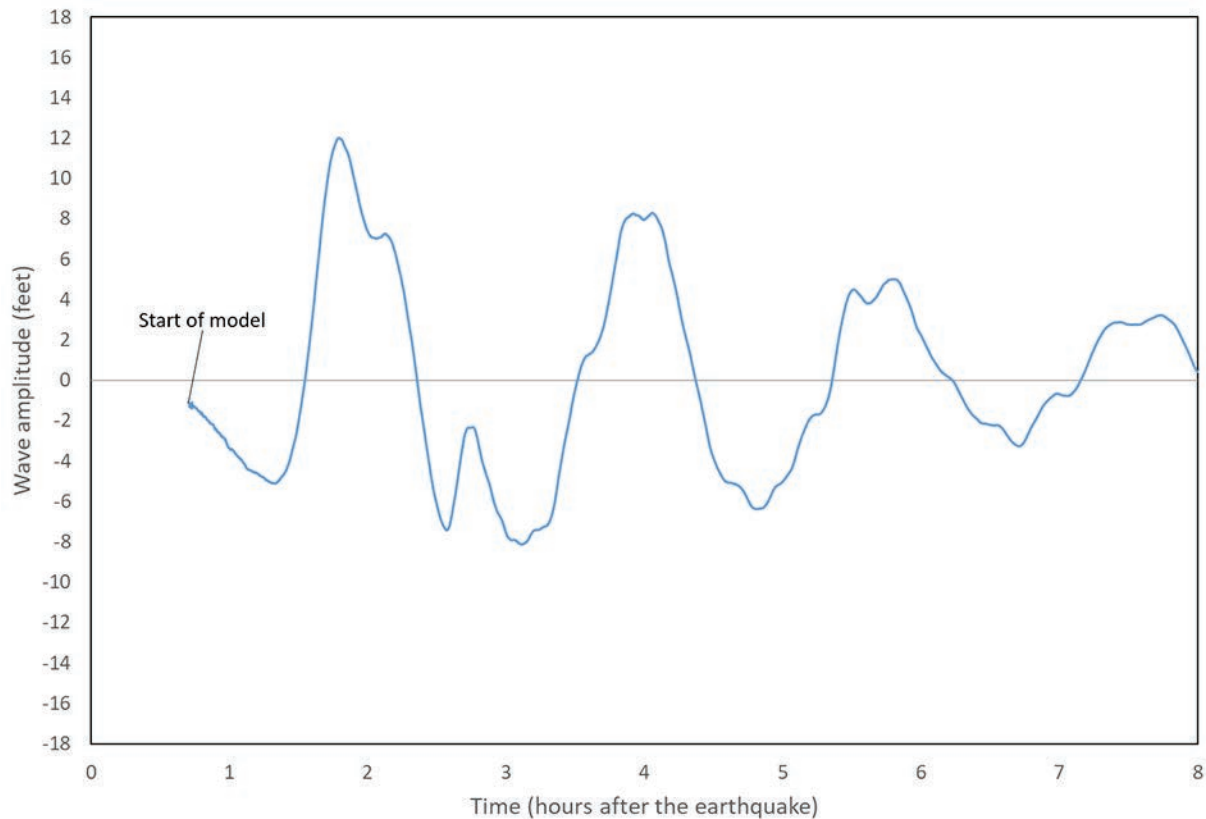
Table C1. Additional synthetic simulated tide gauge key locations. For those sites listed as 'Y' in the column 'In Results Section', their simulated tide gauge plots are in the *Results* section of this pamphlet, whereas the sites listed with 'N' have tide gauge plots in *Appendix C*.

I.D. Number	Longitude	Latitude	Description	Map Sheet Number	In Results Section
1	-122.7303854	48.156564	Admiralty Inlet North	2, 3, 8	N
2	-122.5660484	47.712355	Agate Passage	4	N
3	-122.5088982	47.622218	Bainbridge Island Ferry Terminal	4	N
4	-122.73	47.75	Bangor	4, 7, 8	N
5	-122.85	47.435	Belfair	7	N
6	-122.5121765	48.751991	Bellingham Bay	1	N
7	-122.6377825	47.550383	Bremerton Sinclair Inlet	4	N
8	-122.9	47.675	Brinnon	7	N
9	-122.703042	47.267174	Carr Inlet	5, 6	N
10	-122.522827	47.447914	Colvos Passage	4	N
11	-122.438477	47.282547	Commencement Bay	5	N
12	-122.3969815	47.921388	Cultus Bay	3	N
13	-122.81	47.84	Dabob	8	N
14	-122.644615	48.406156	Deception Pass	2	N
15	-122.76	48.98	Drayton Harbor	1	N
16	-122.357545	47.388009	East Passage	4, 5	N
17	-122.38494	47.81348	Edmonds Ferry Terminal	3	N
18	-122.72225	48.840728	Ferndale	1	Y
19	-122.98	47.56	Holly	7	N
20	-122.231	48.011	Jetty Island	3	N
21	-122.493943	47.794489	Kingston Ferry Terminal	3, 8	N
22	-122.6436578	47.717569	Liberty Bay	4	N
23	-123.11	47.46	Lilliwaup	7	N
24	-122.864215	47.246826	McMicken Island	6	N
25	-122.988964	47.046593	Mud Bay	6	N
26	-122.699153	47.108896	Nisqually Reach	5, 6	N
27	-122.90373	47.058869	North Point	6	Y
28	-122.637081	48.285134	Oak Harbor	2	N
29	-122.822627	47.403829	Point Victor	6, 7	N
30	-122.5663415	47.588581	Point White	4	N
31	-122.579219	47.857715	Port Gamble	3, 8	N
32	-122.6121826	48.523102	Port of Anacortes	2	N
33	-122.438883	47.406022	Portage	4, 5	N
34	-122.4850591	48.103136	Saratoga Passage	3, 8	N
35	-122.6884468	47.64518	Silverdale	4, 7	N
36	-122.4437215	48.294548	Skagit Bay	2	N
37	-122.7253316	48.30252	Swantown	2	N
38	-122.551071	47.268749	Tacoma Narrows	5	N
39	-123.004425	47.151723	Totten Inlet	6	N
40	-123.1	47.36	Union	7	N
41	-122.4923357	47.985482	Useless Bay	3, 8	N
42	-122.463435	47.511609	Vashon Ferry Terminal	4	N
43	-122.342772	47.606734	Waterfront Park, Seattle	4	N

The following graphs show modeled tsunami wave variations over time (light blue lines) at key locations. The numbers in the upper left corners correspond with the I.D. numbers listed on Table C1. Gray horizontal lines indicate static mean high water elevation at synthetic simulated tide gauges. Many gauges appear to have high-frequency oscillations at the start. This is due to a bug in the specific version of the GeoClaw code at the time of the modeling. This bug causes a few grid cells near the shoreline to initialize as dry, despite having elevation values below mean high water (MHW). This then causes water to immediately flow into these cells by the adjacent wet cells along the shoreline at the start of the modeling simulation, resulting in the creation of small waves moving away from the shore. These small waves generate the oscillations seen in some tide gauges as the waves reflect along the shore. The size of these oscillations are dependent on the steepness of the topography near the simulated tide gauge. For example, coastal areas with flat topography generate smaller erroneous waves than areas with steep topography. The oscillations also last longer in areas consisting of narrow bays and passageways where the erroneous waves reflect back and forth for a longer time than open areas offshore where the waves dissipate more quickly. This is only a problem with the simulated tide gauge plots and do not affect the reported results on the map sheets, which only record the maximum wave heights and speeds during the simulation. The waves generated from the earthquake create both larger and faster moving waves than this initial wave from the bug in the code.

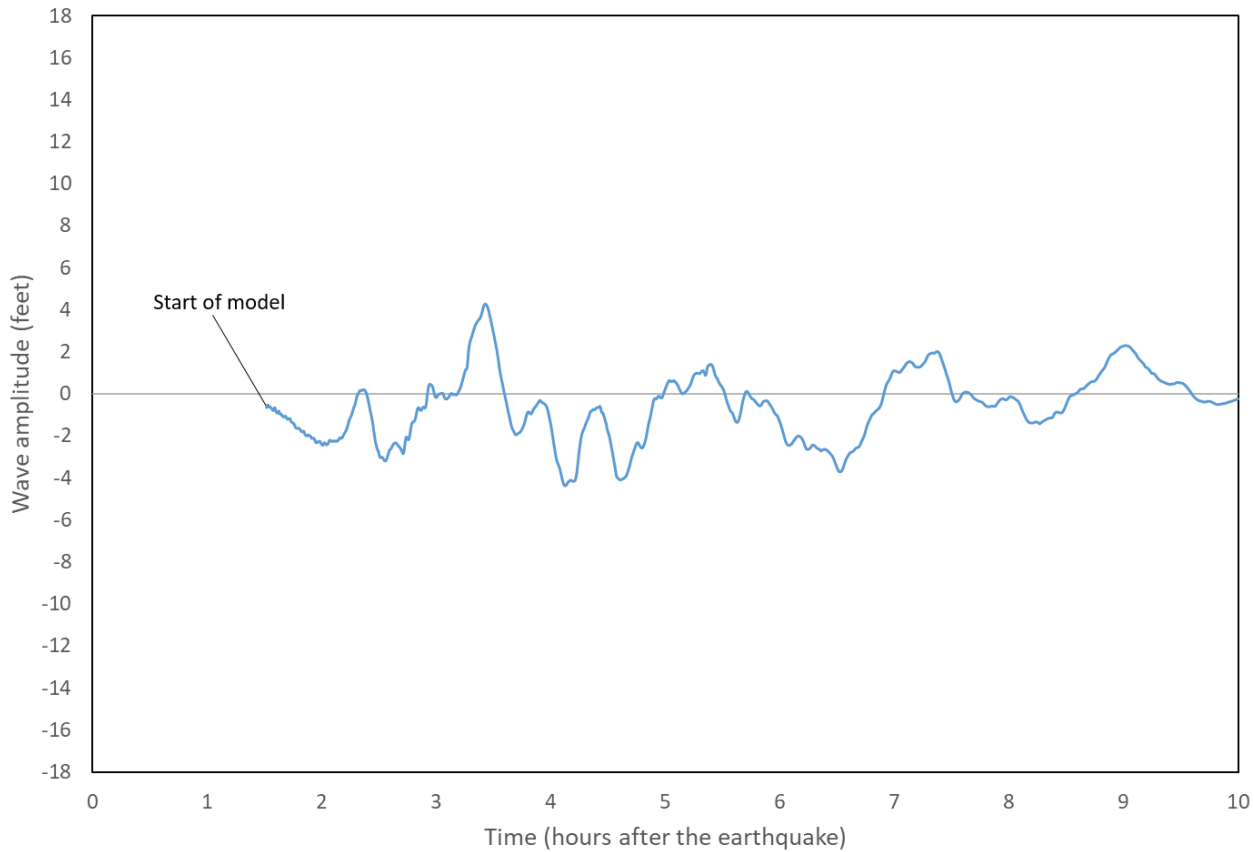
1

Admiralty Inlet North Simulated Tide Gauge



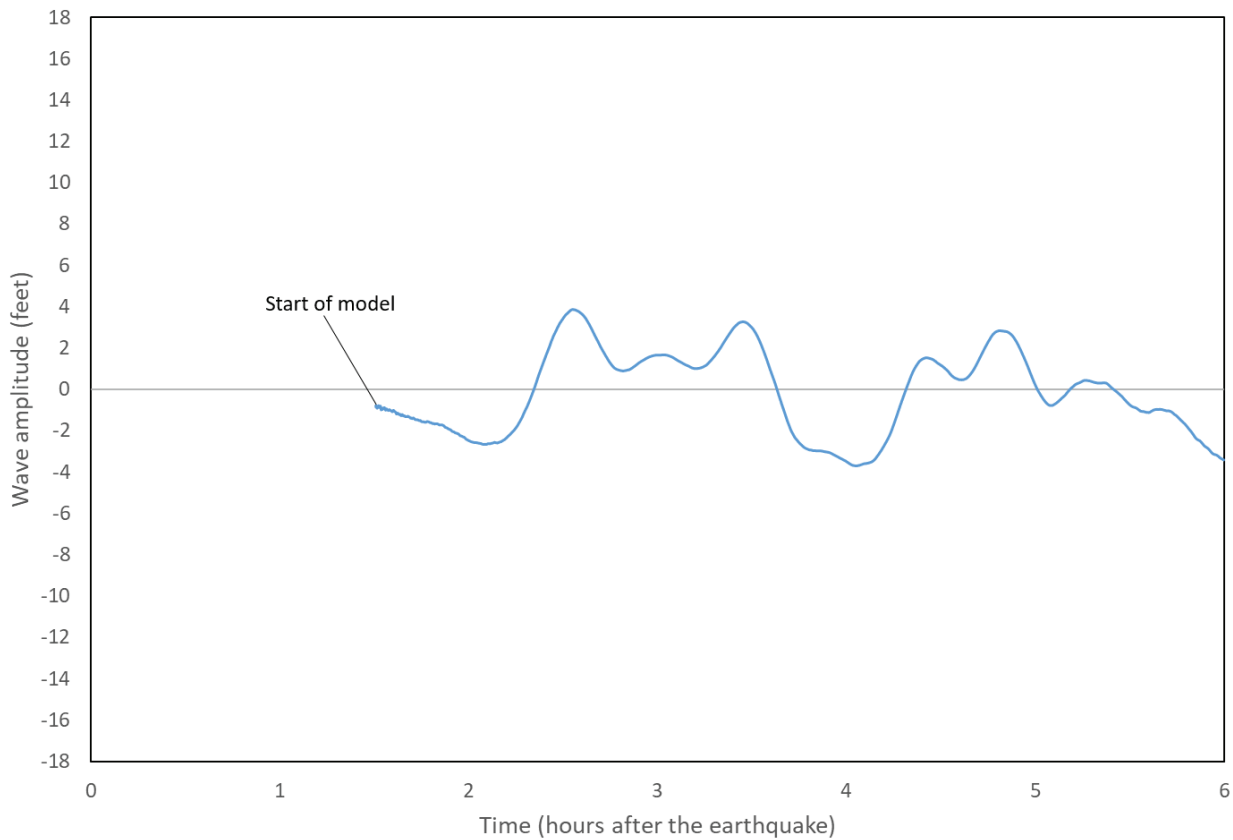
2

Agate Passage Simulated Tide Gauge



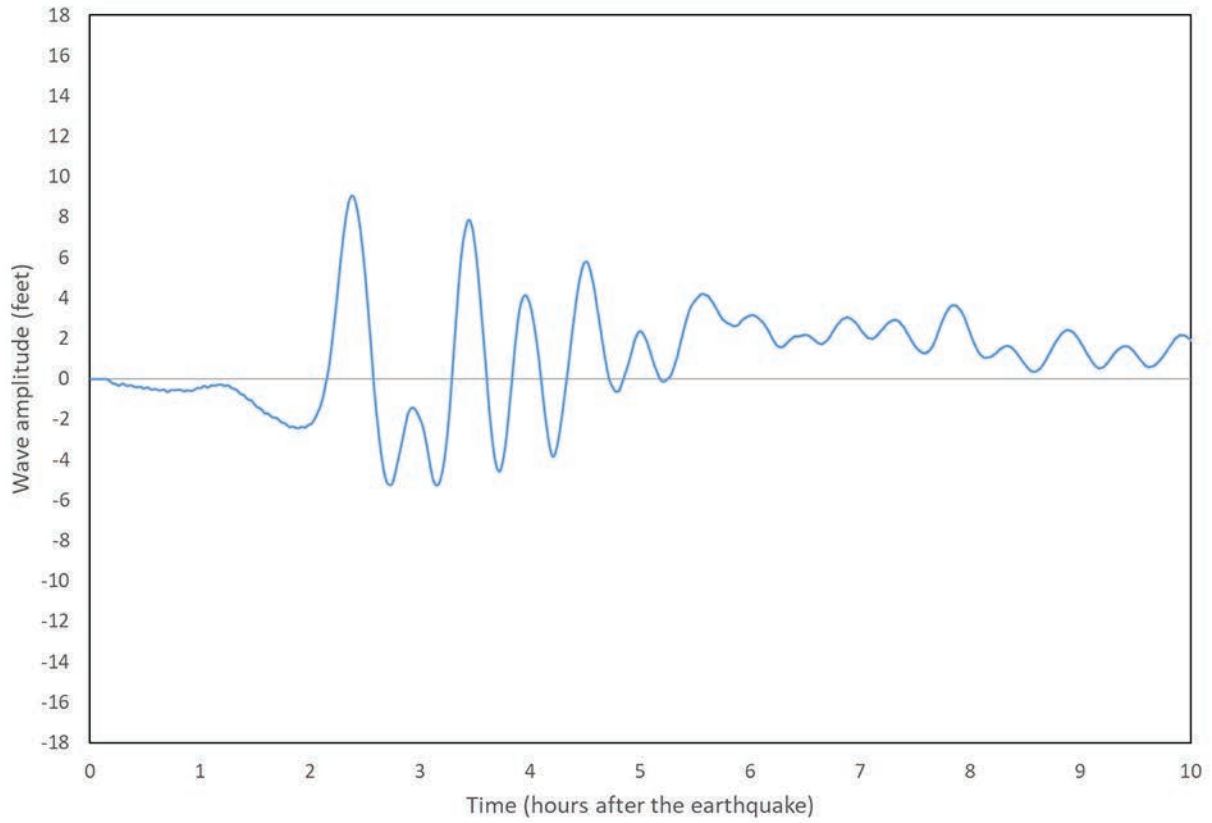
3

Bainbridge Island Ferry Terminal Simulated Tide Gauge



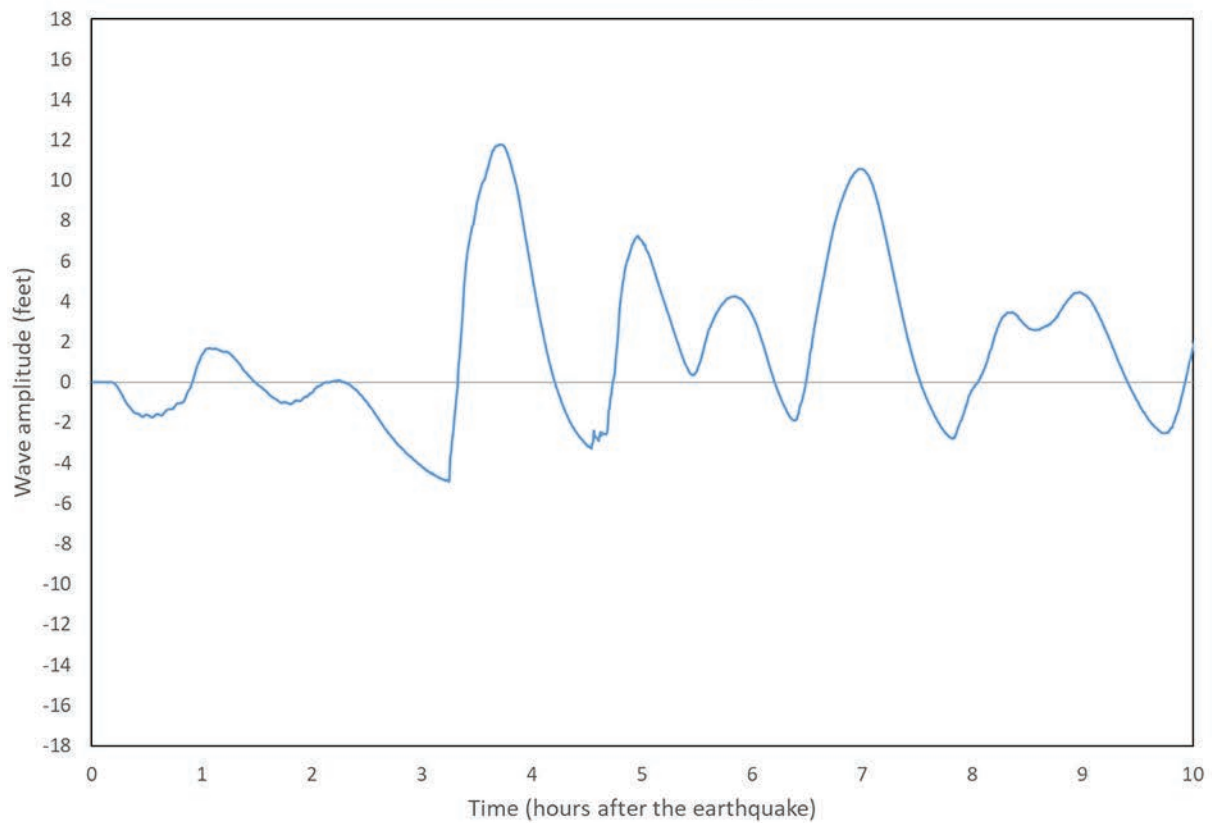
4

Bangor Simulated Tide Gauge



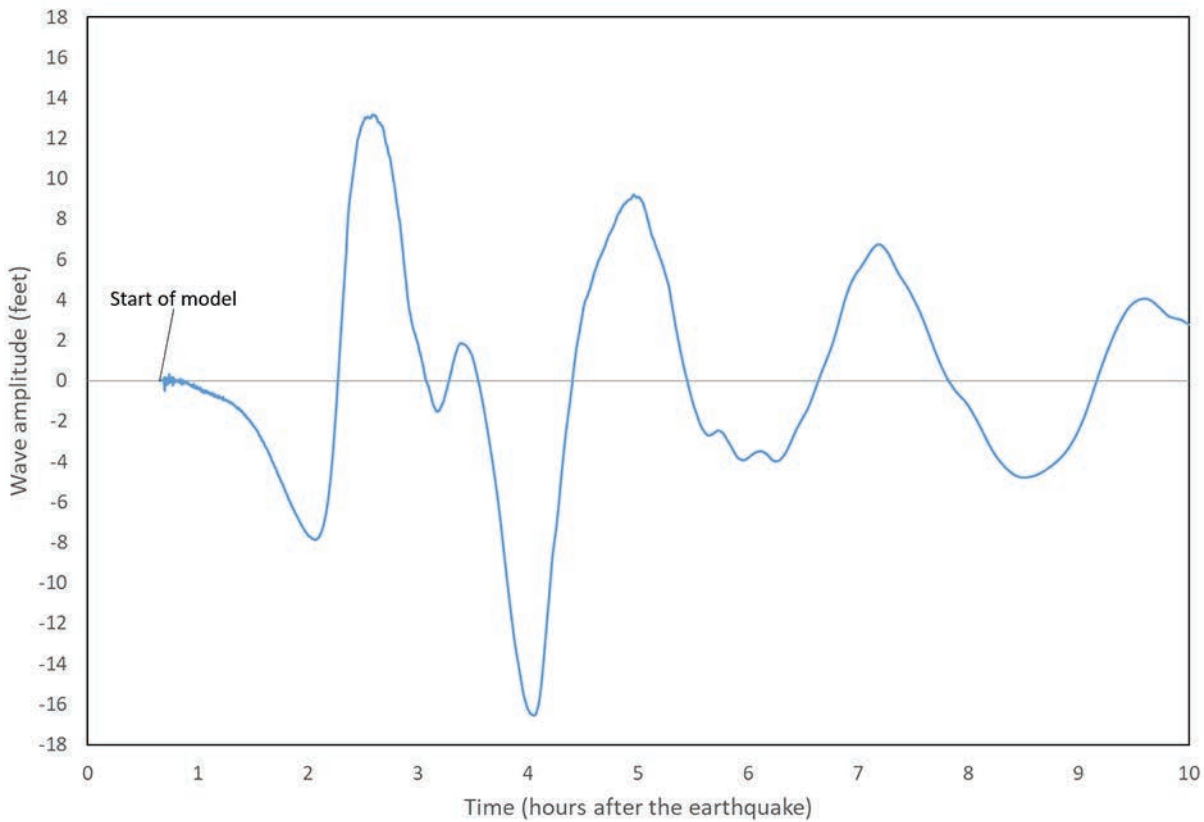
5

Belfair Simulated Tide Gauge



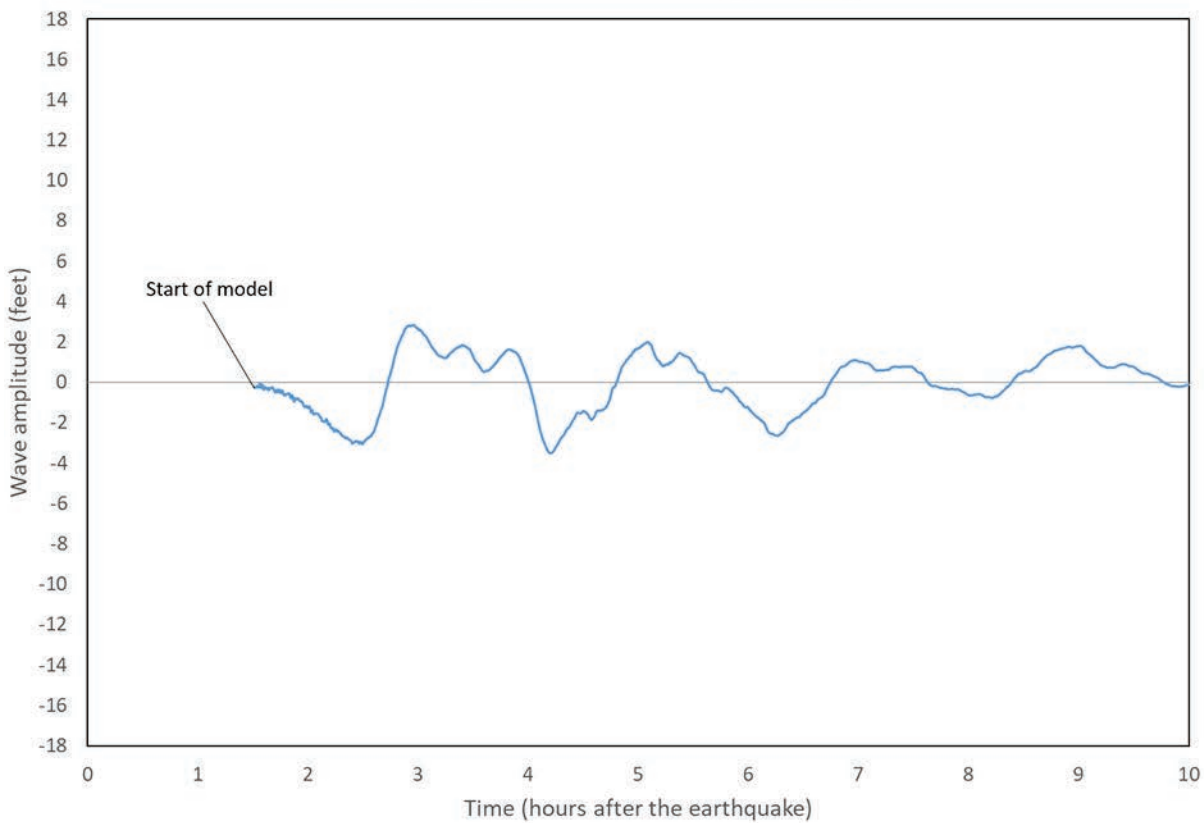
6

Bellingham Bay Simulated Tide Gauge

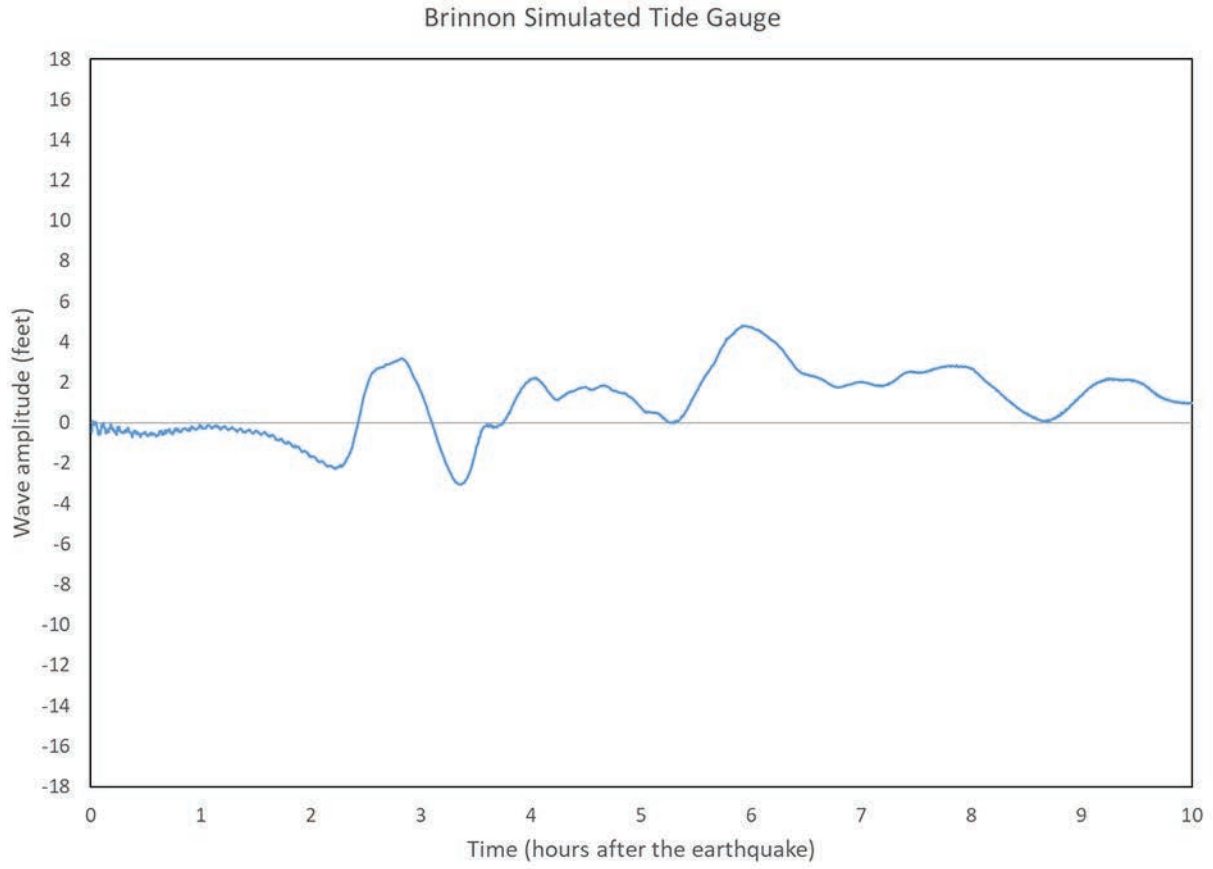


7

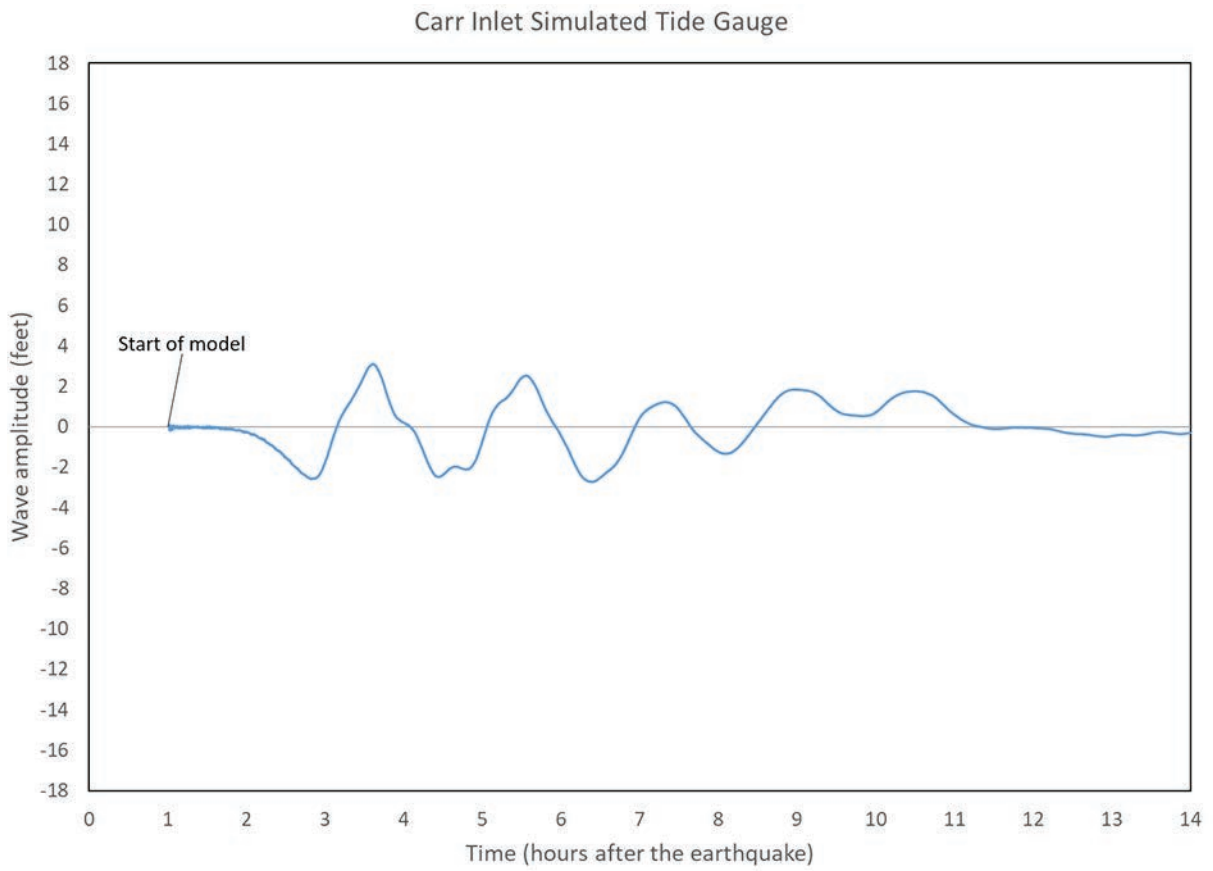
Bremerton Sinclair Inlet Simulated Tide Gauge



8

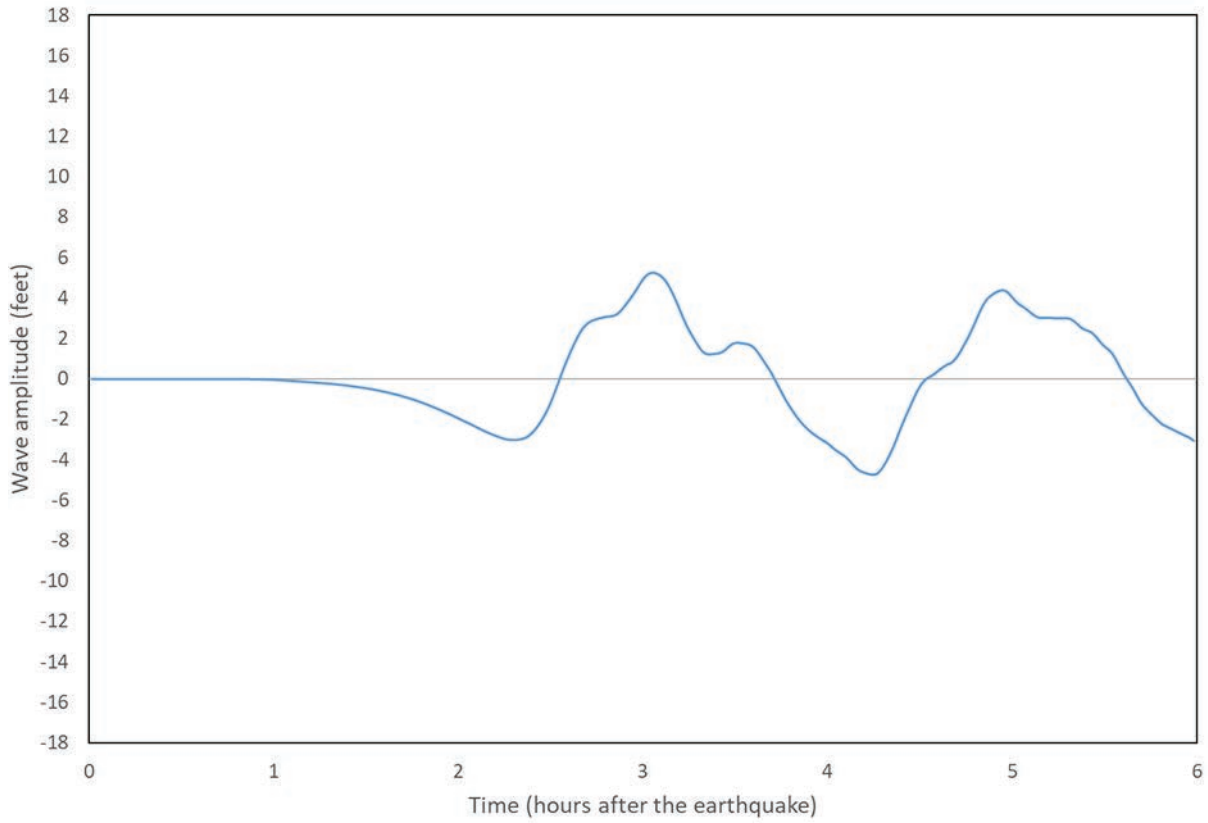


9



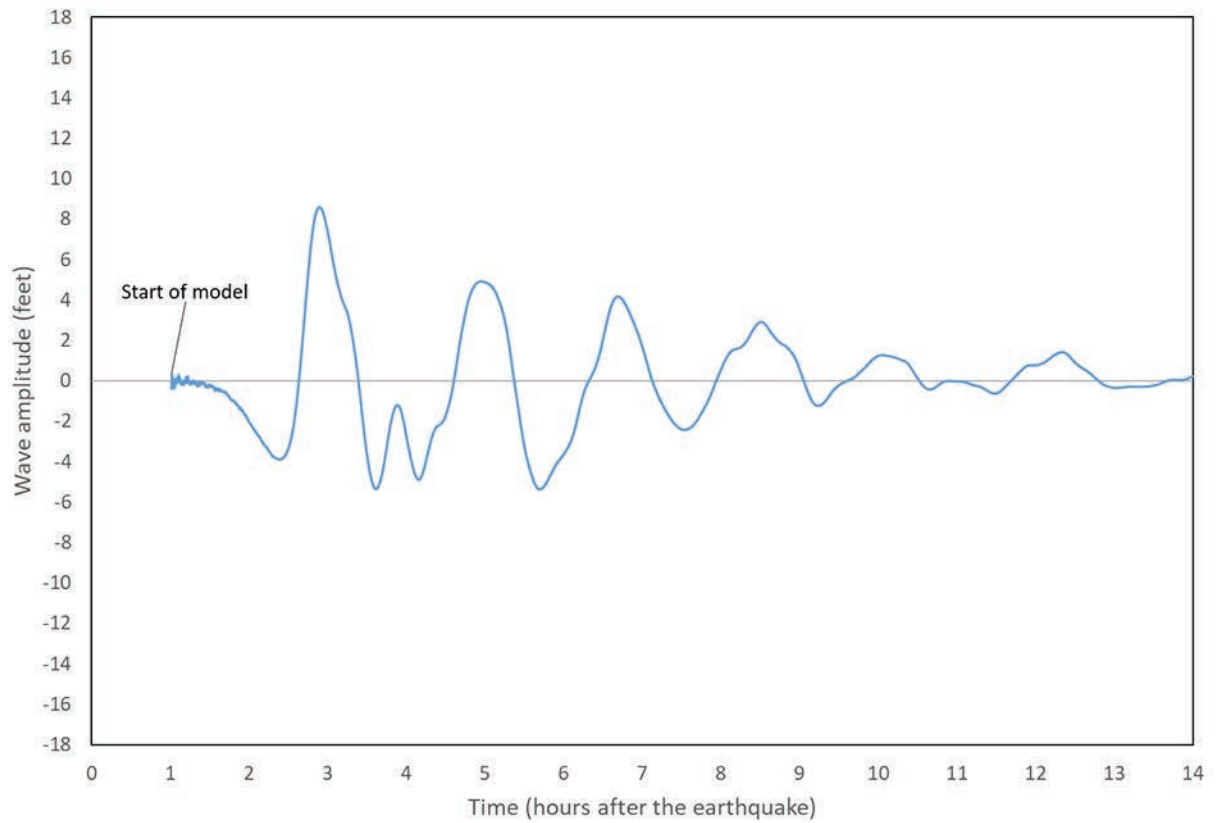
10

Colvos Passage Simulated Tide Gauge



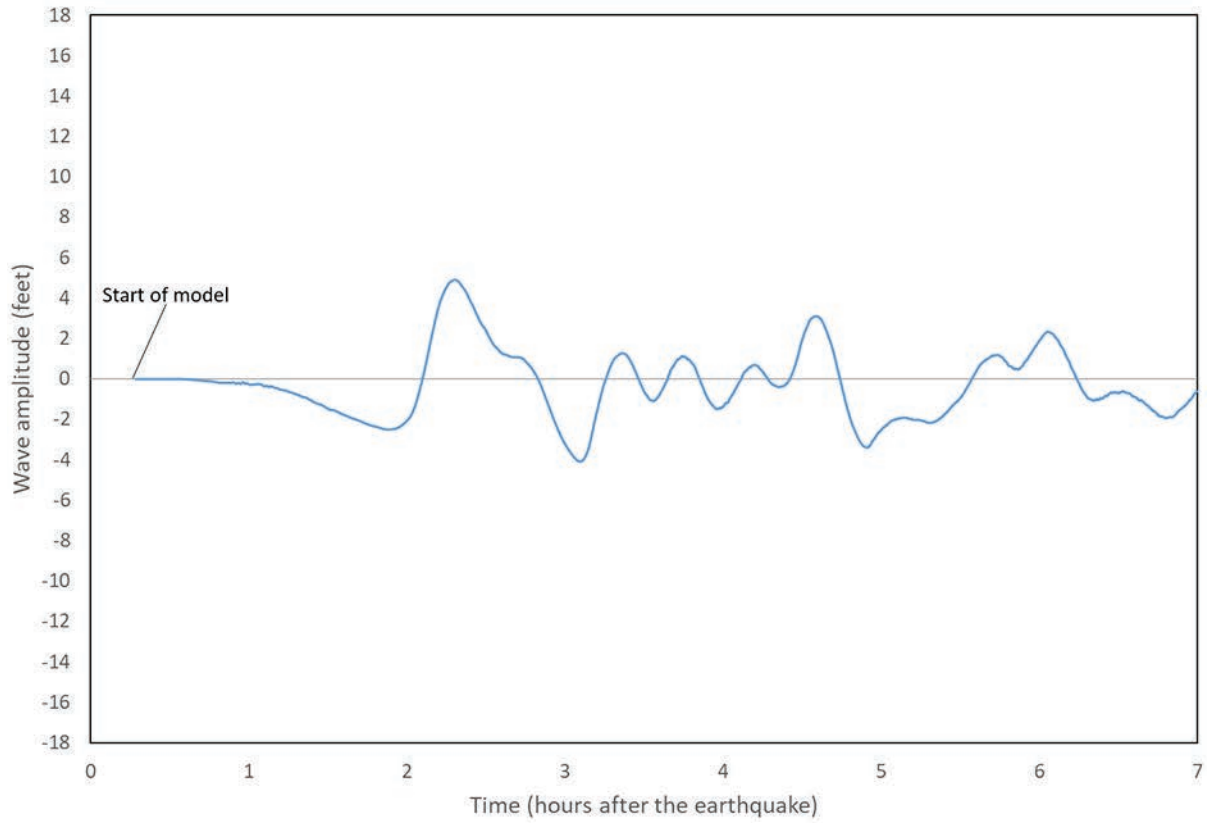
11

Commencement Bay Simulated Tide Gauge



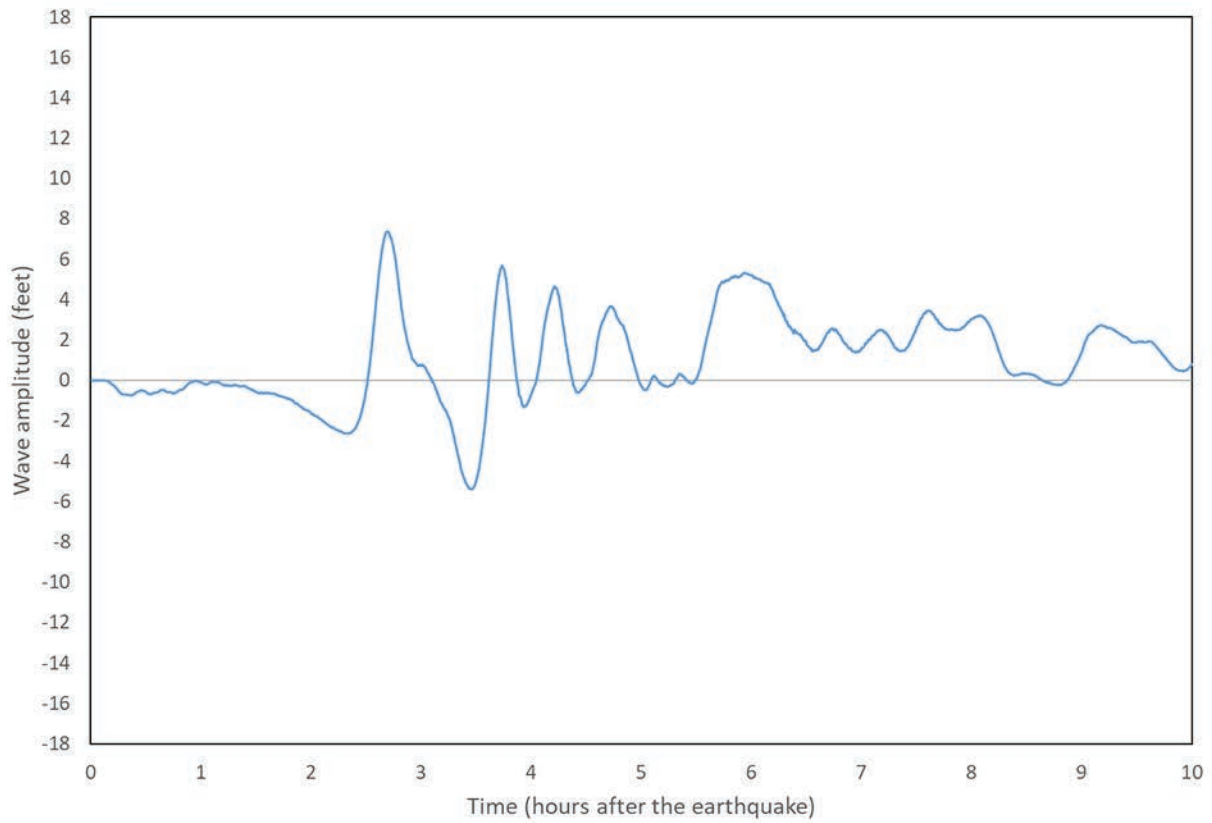
12

Cultus Bay Simulated Tide Gauge



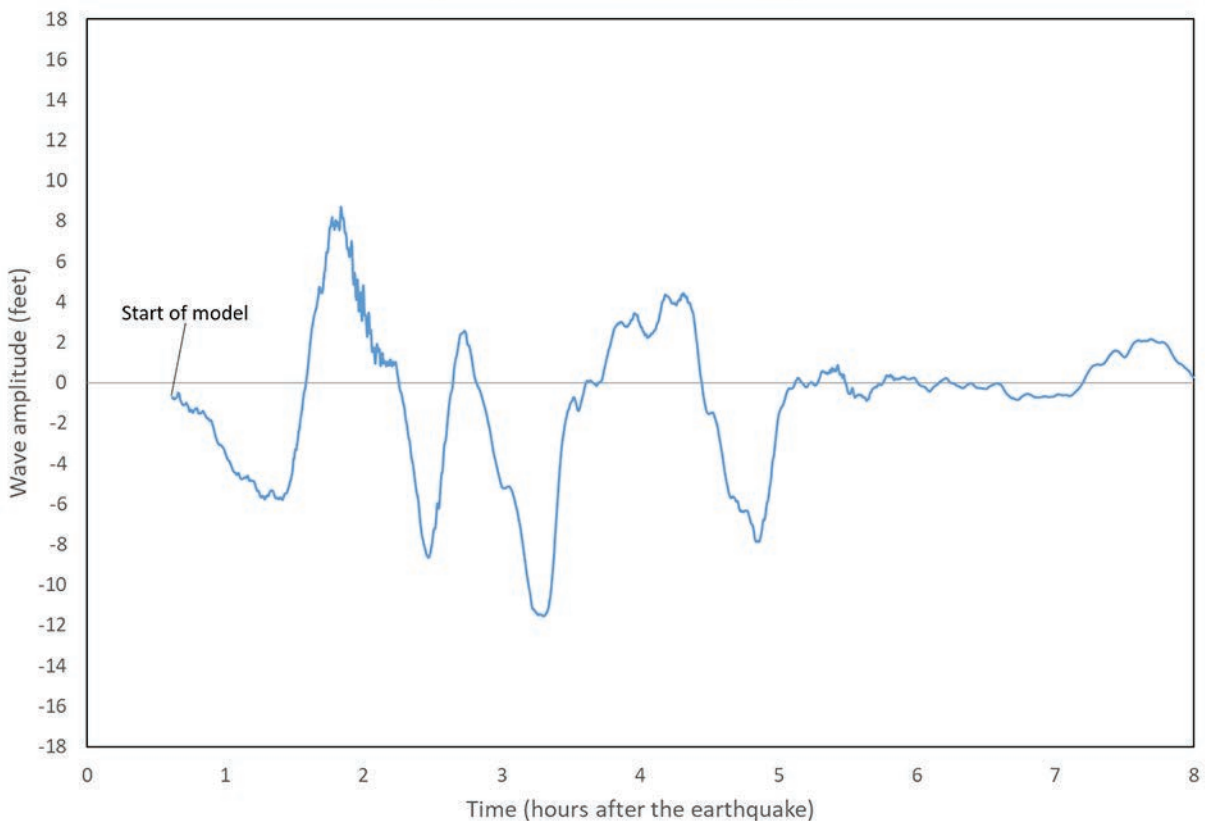
13

Dabob Simulated Tide Gauge



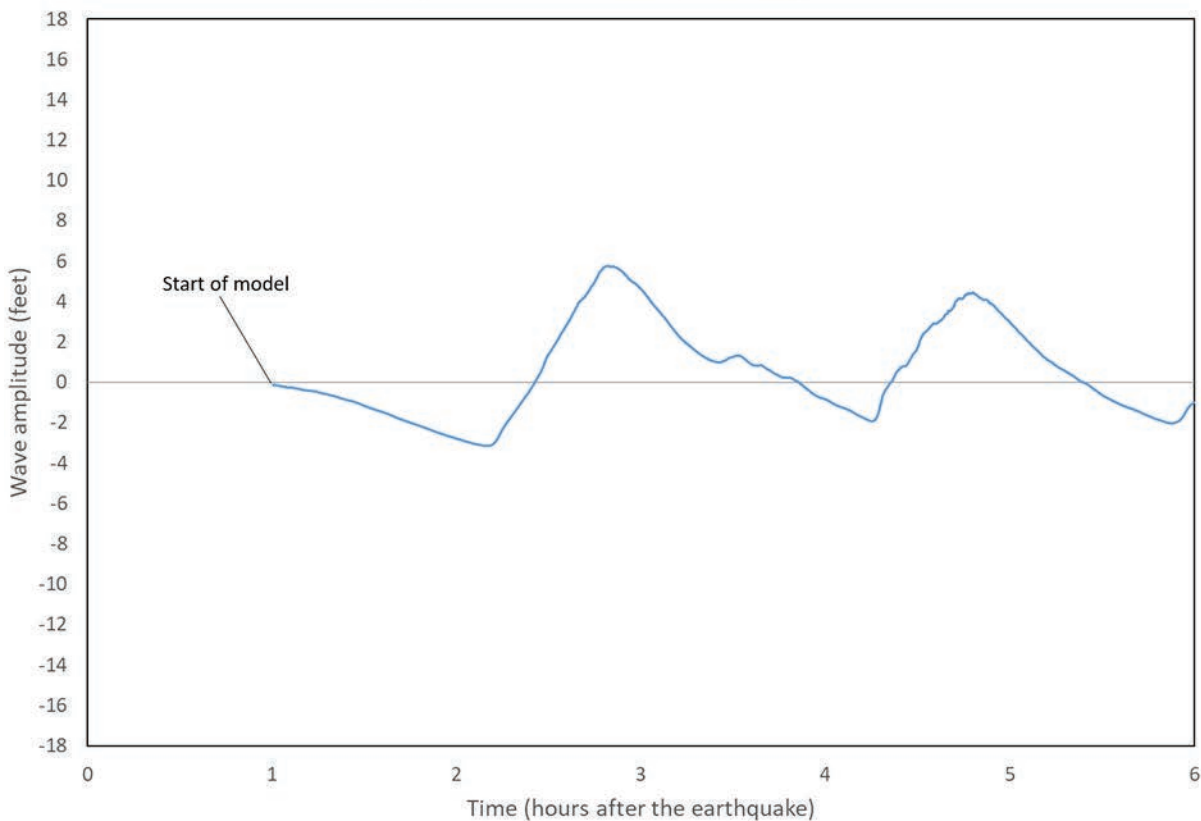
14

Deception Pass Simulated Tide Gauge

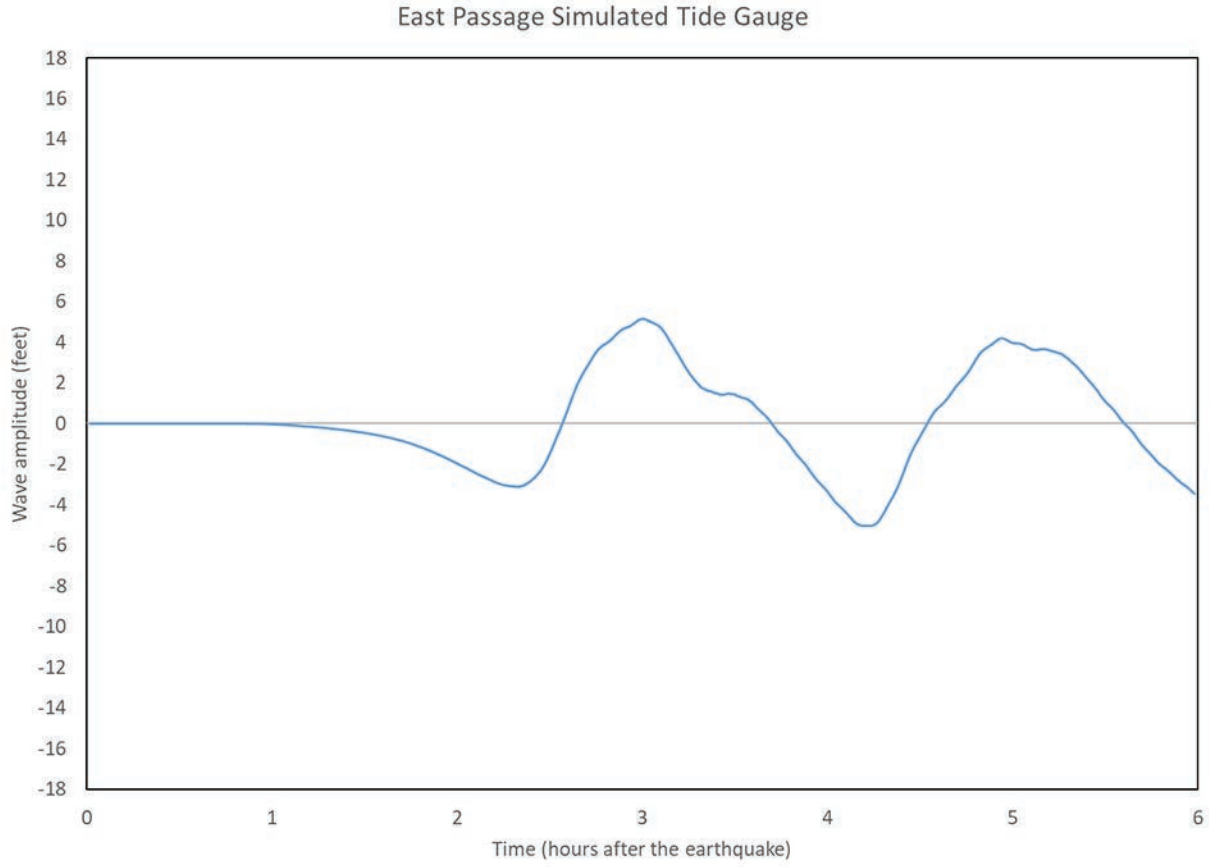


15

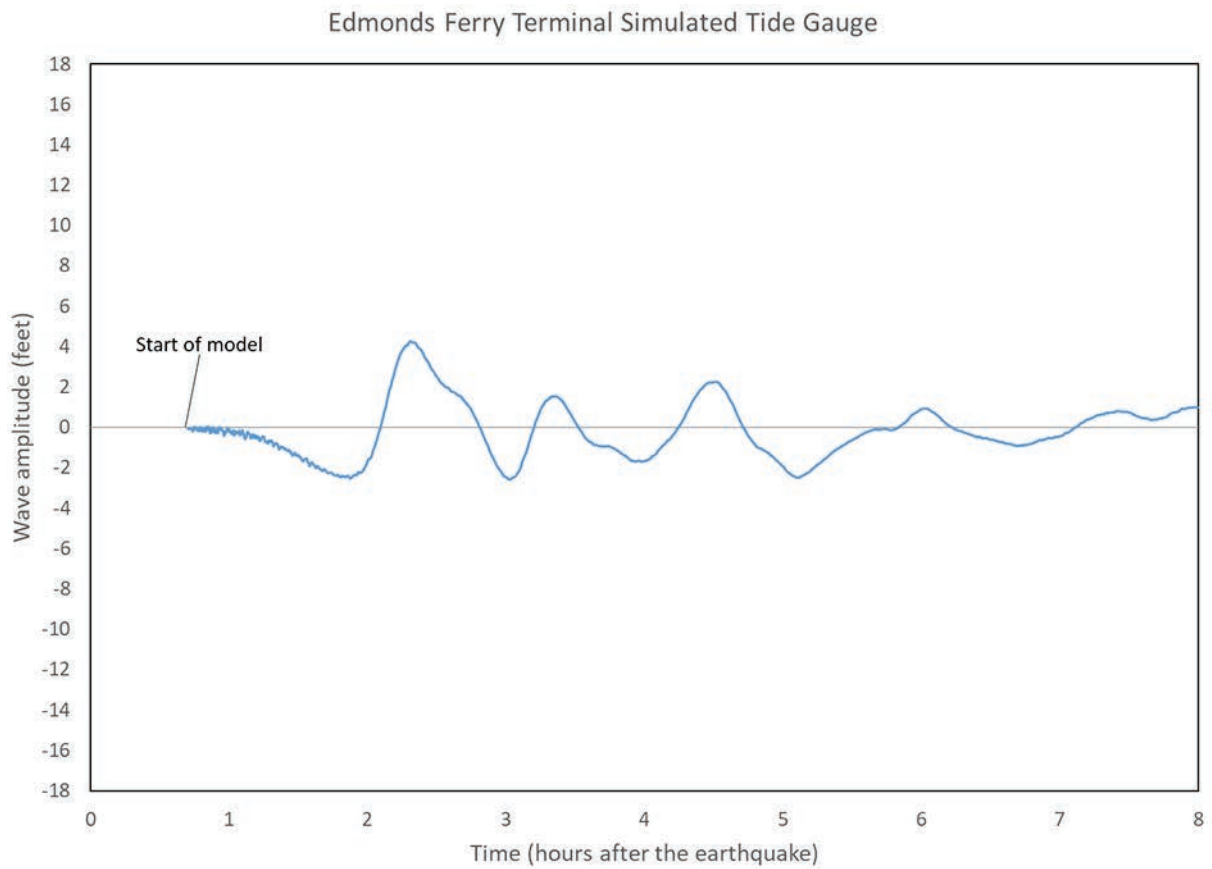
Drayton Harbor Simulated Tide Gauge



16

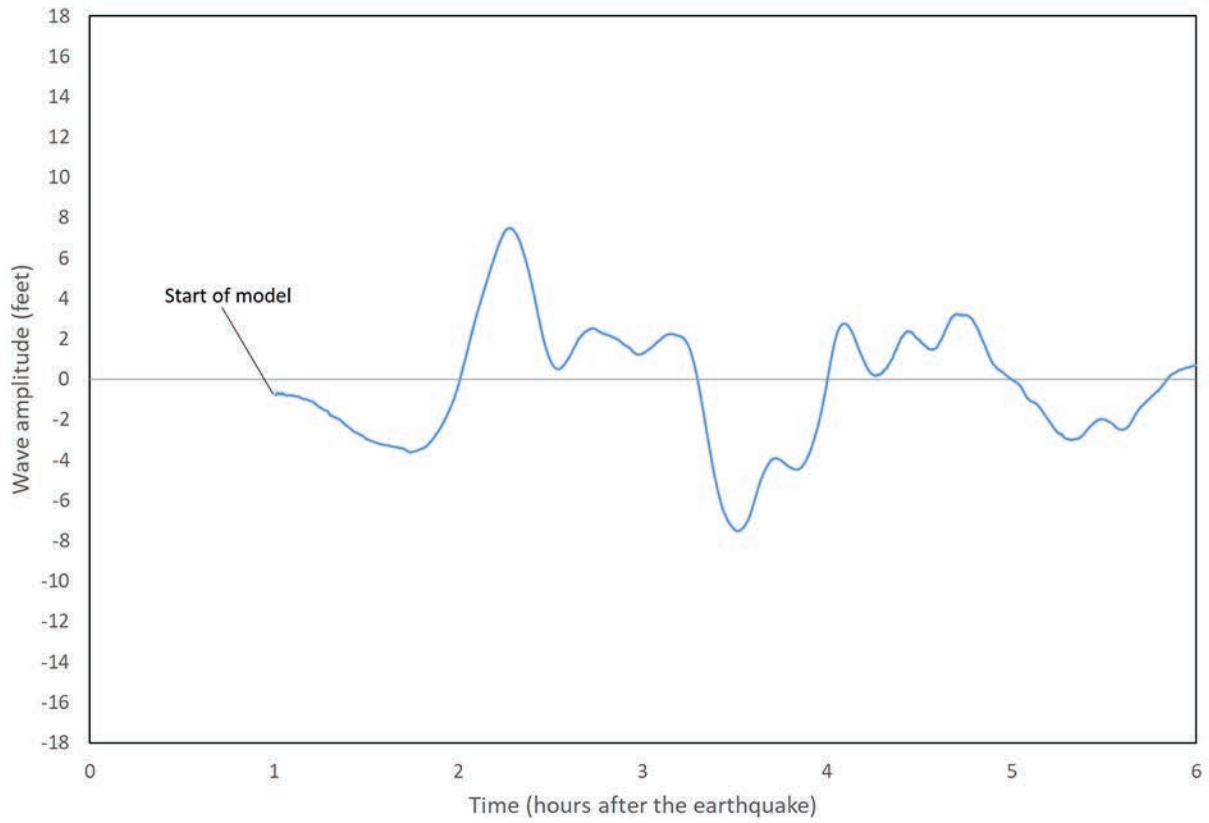


17



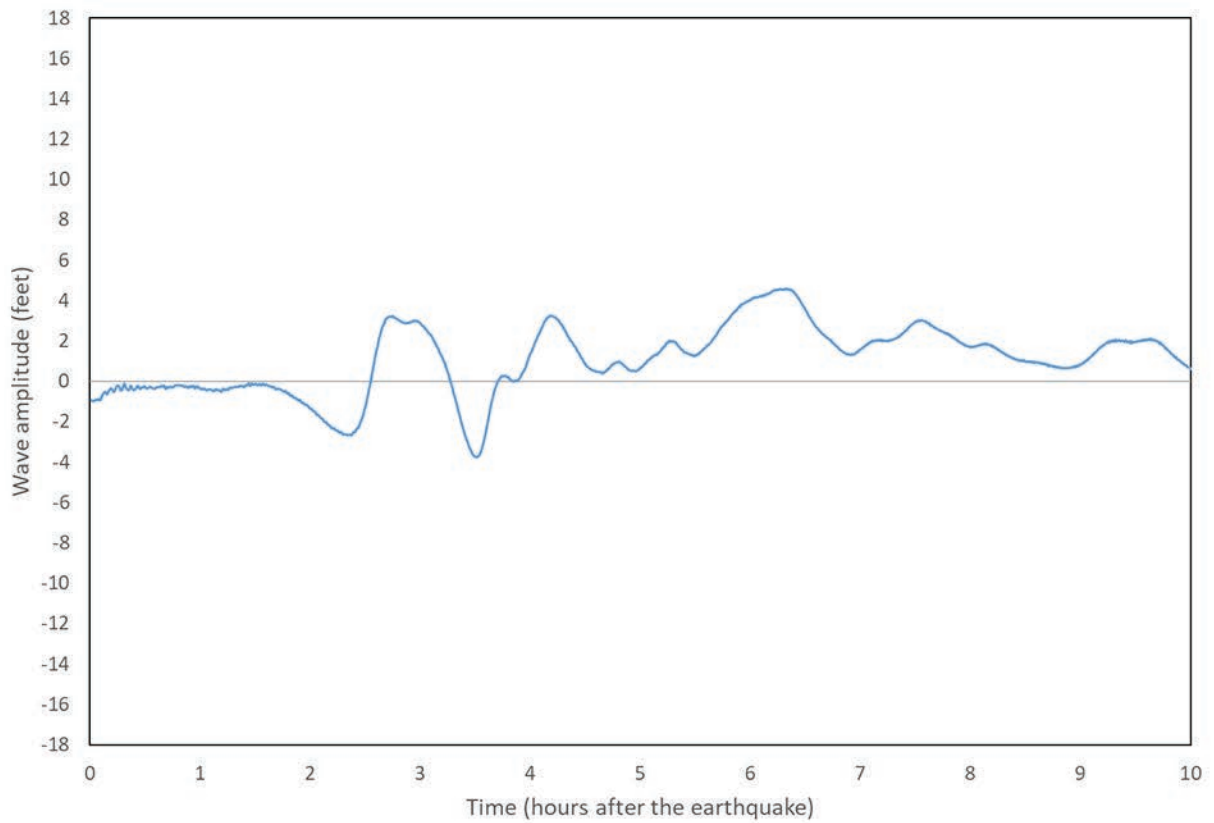
18

Ferndale Simulated Tide Gauge



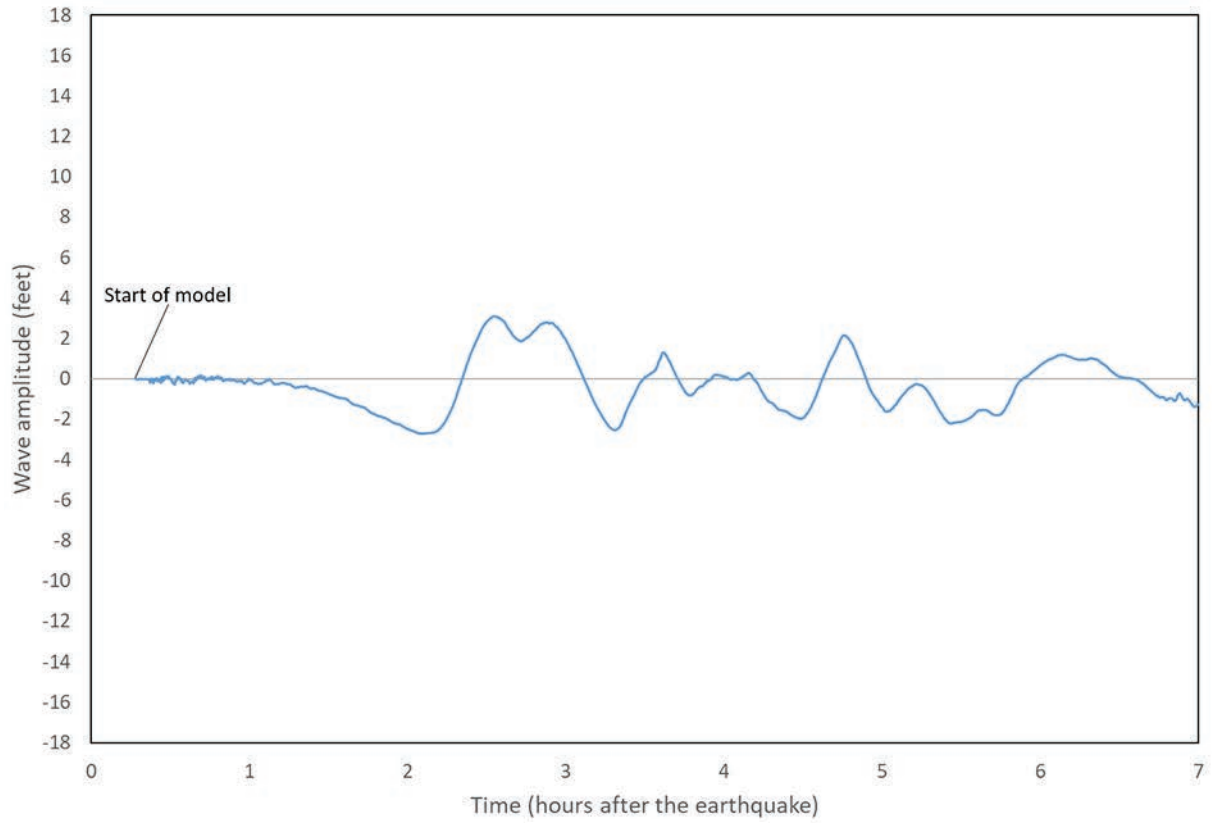
19

Holly Simulated Tide Gauge



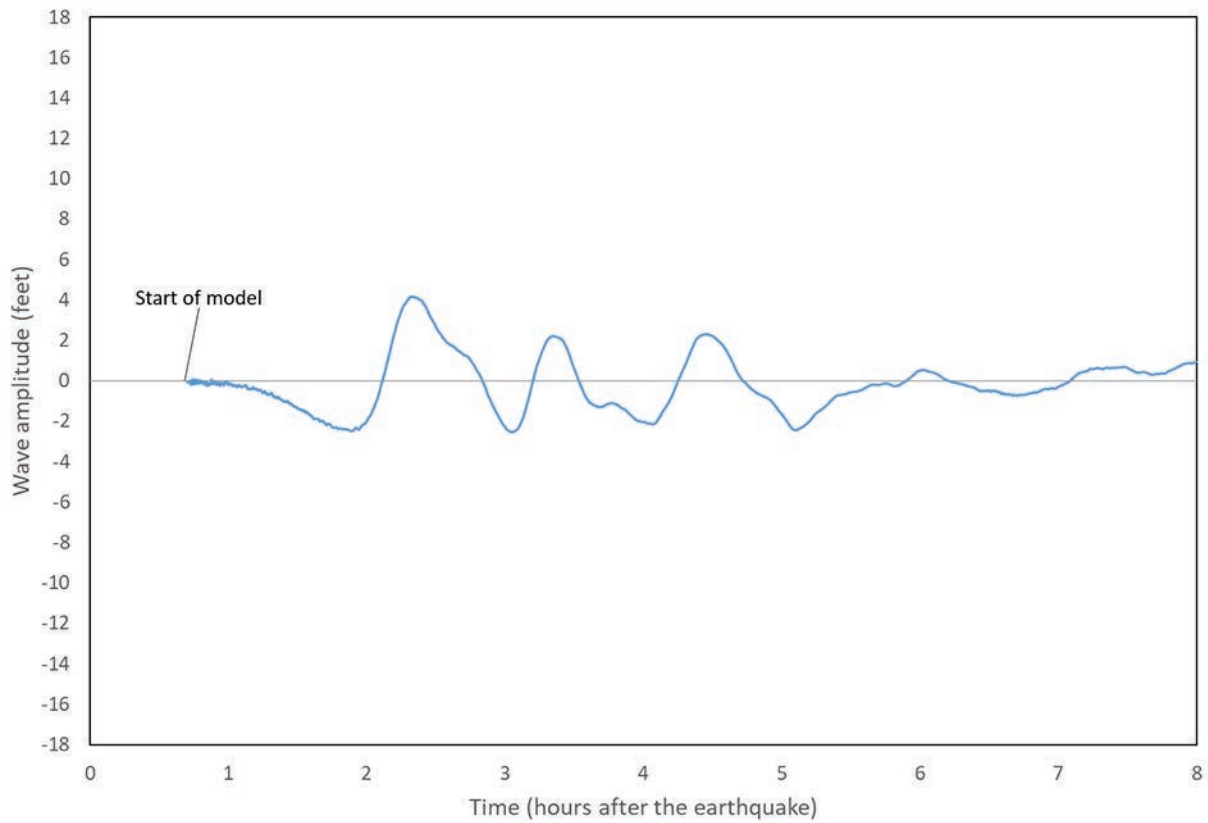
20

Jetty Island Everett Simulated Tide Gauge



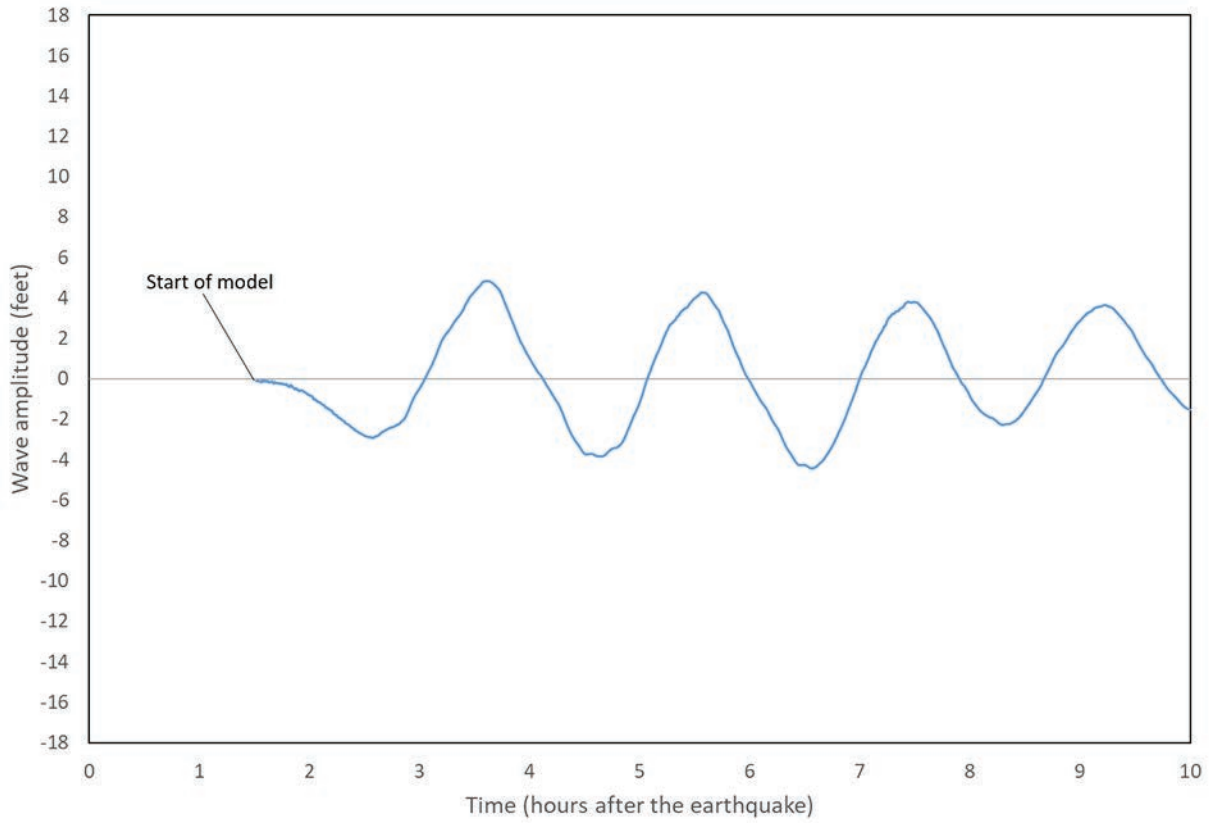
21

Kingston Ferry Terminal Simulated Tide Gauge



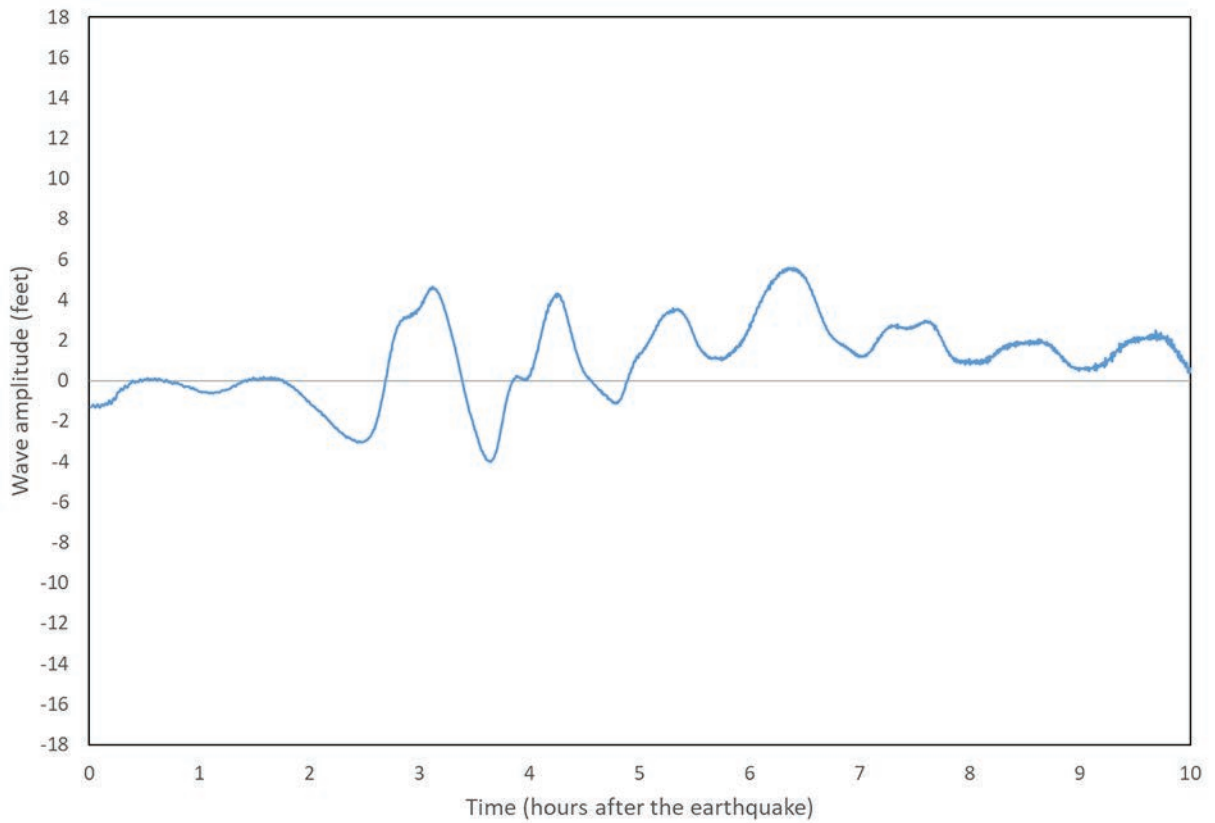
22

Liberty Bay Simulated Tide Gauge



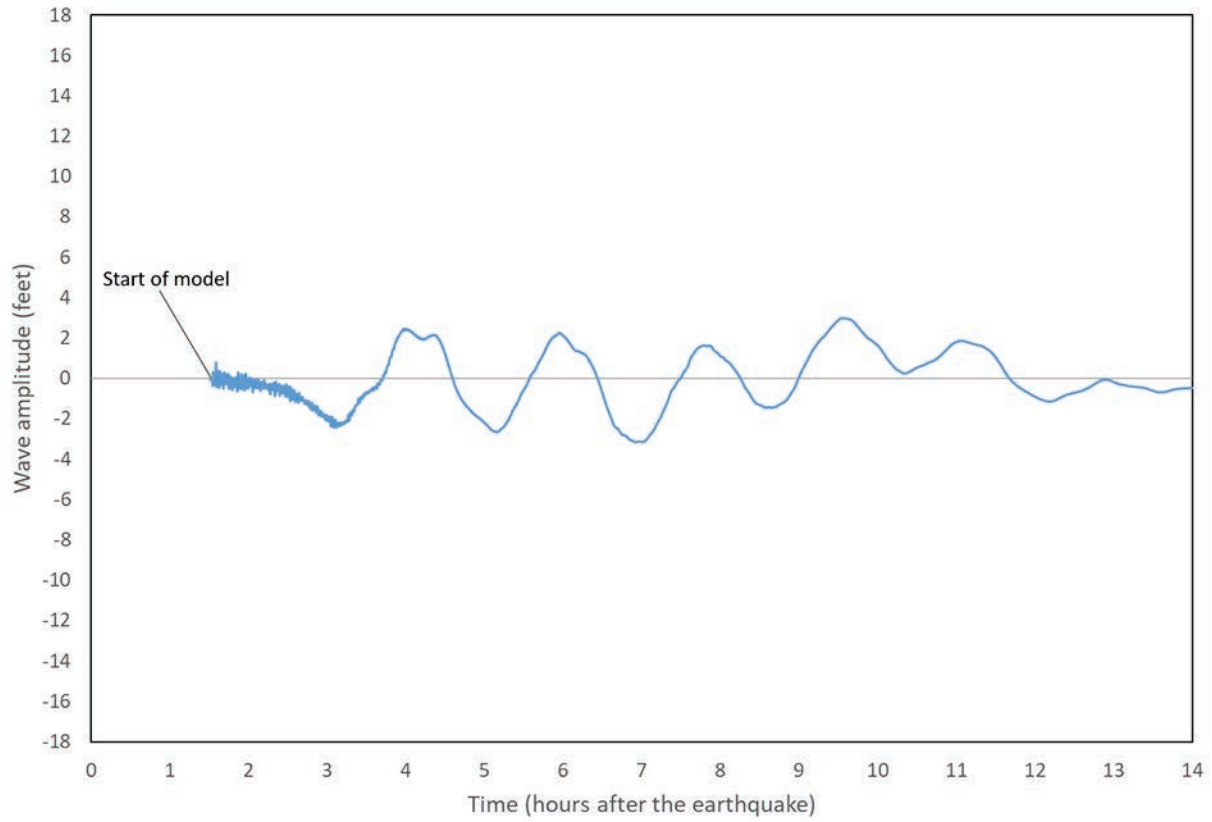
23

Lilliwaup Simulated Tide Gauge



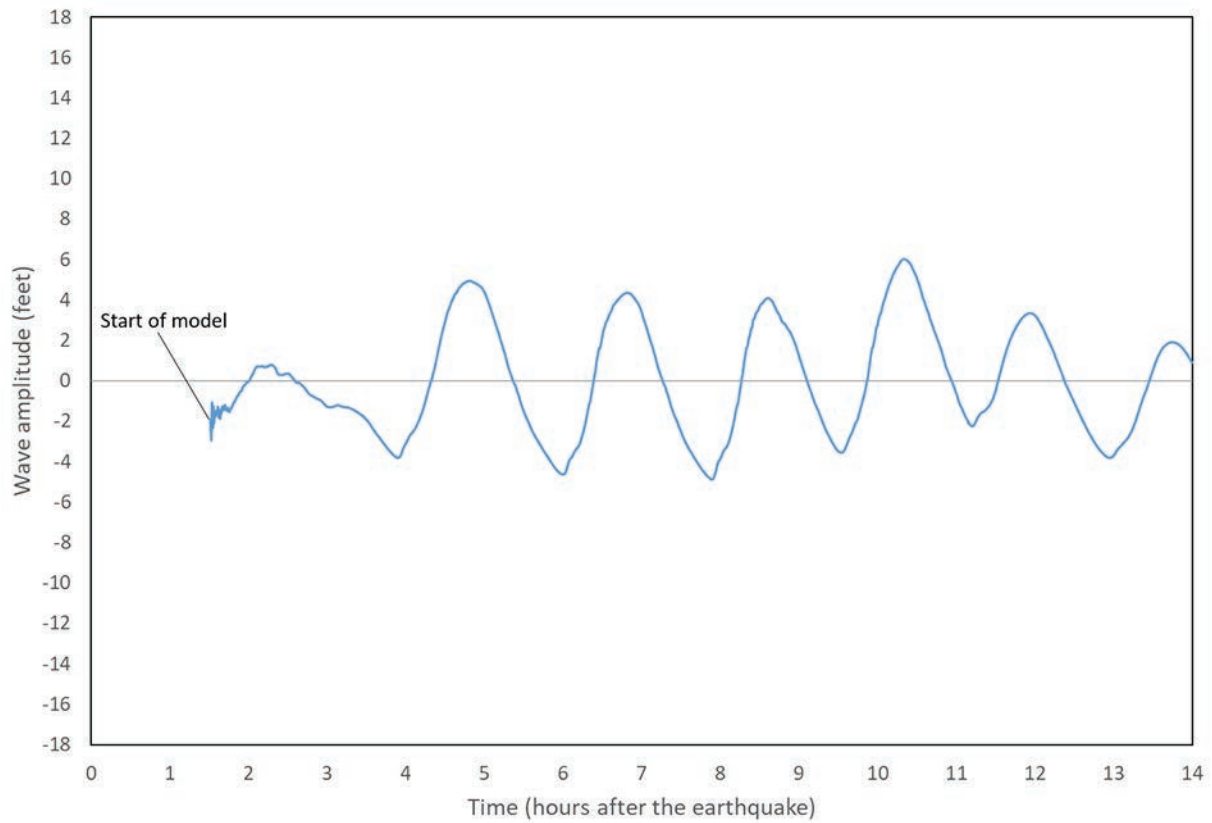
24

McMicken Island Simulated Tide Gauge



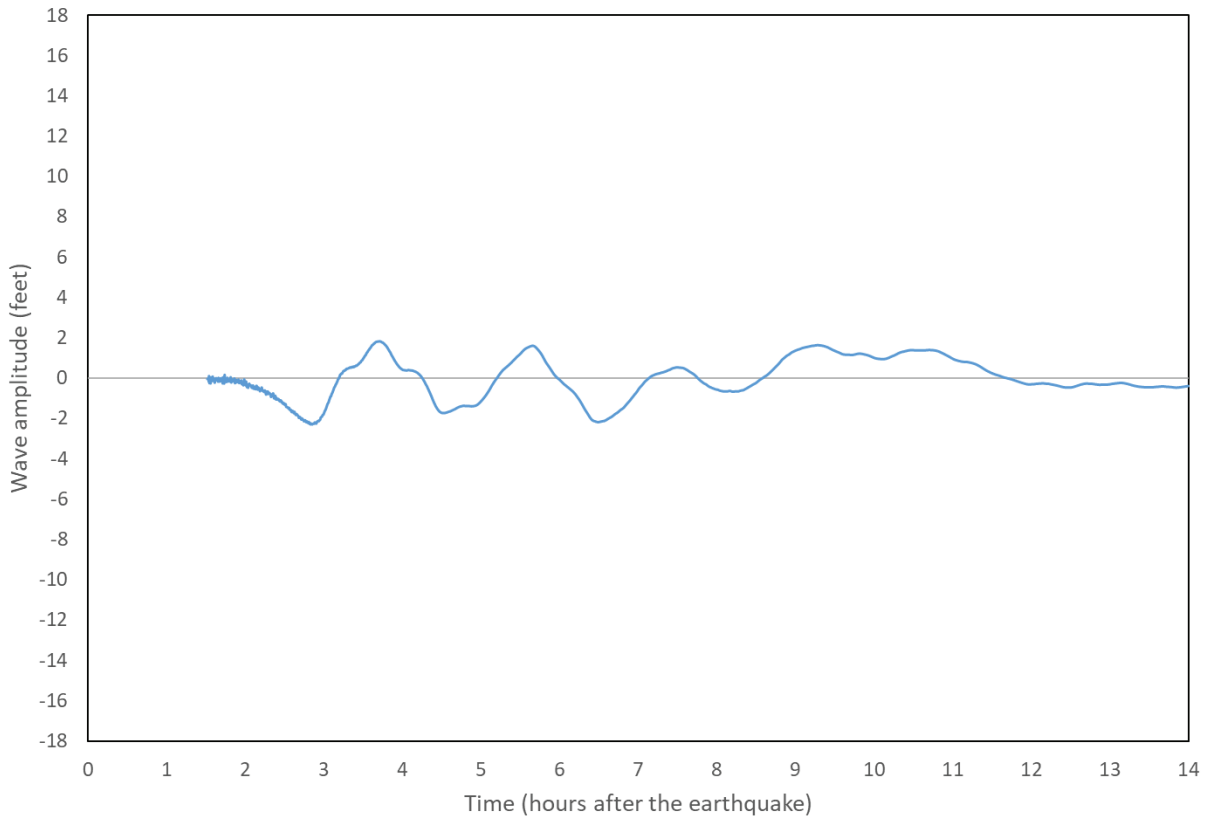
25

Mud Bay Simulated Tide Gauge



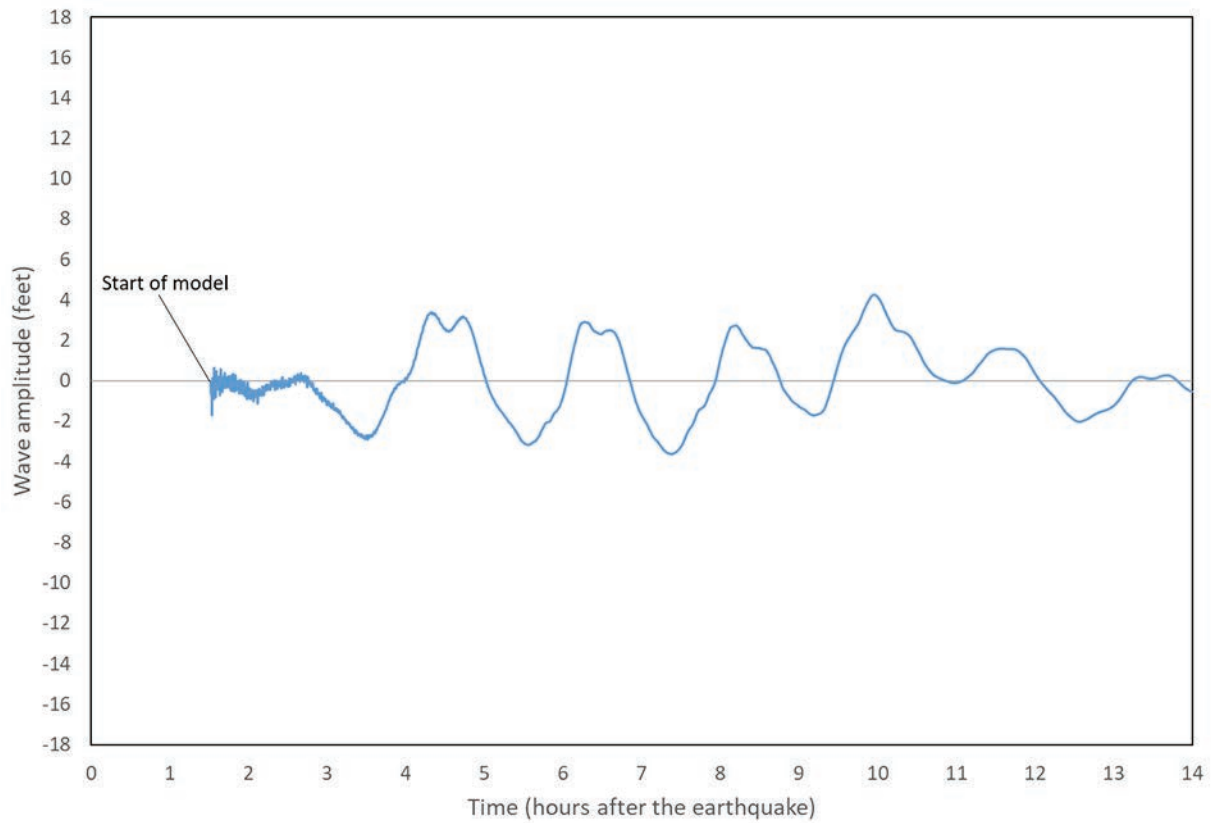
26

Nisqually Reach Simulated Tide Gauge



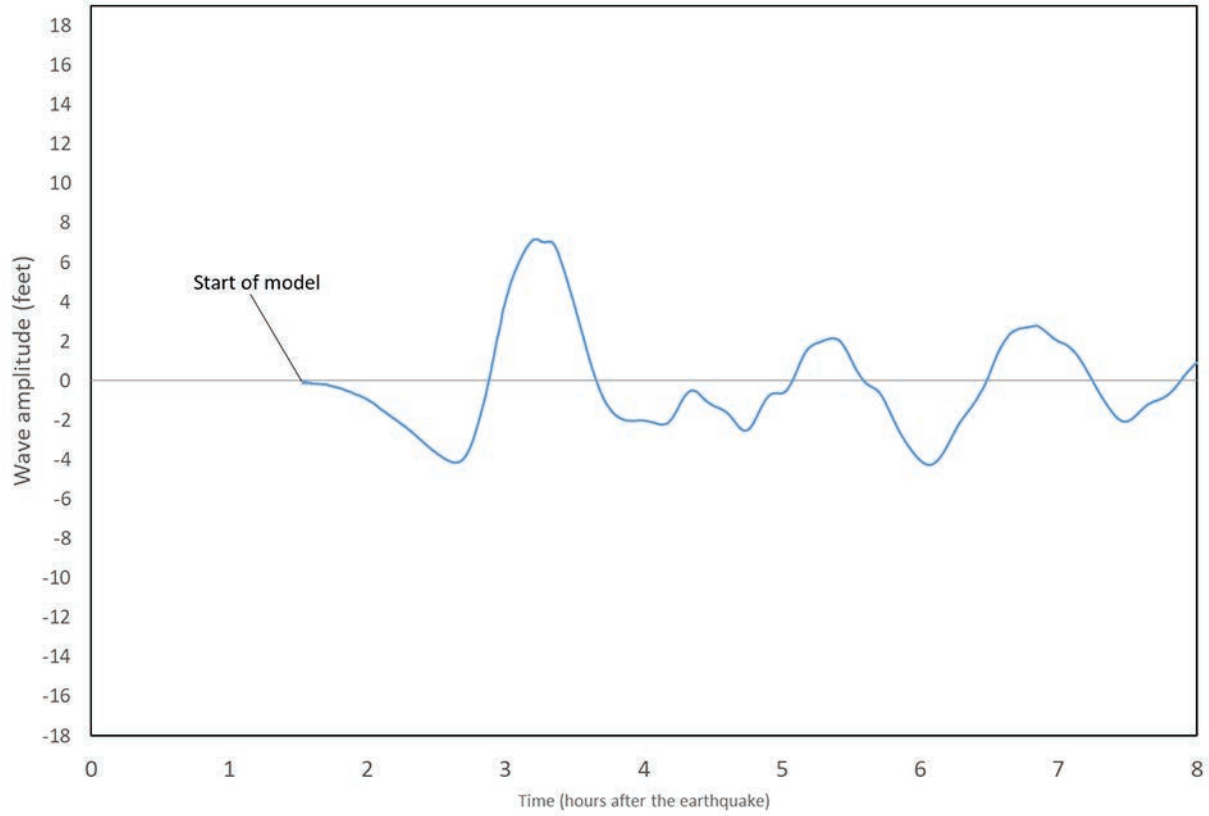
27

North Point Simulated Tide Gauge



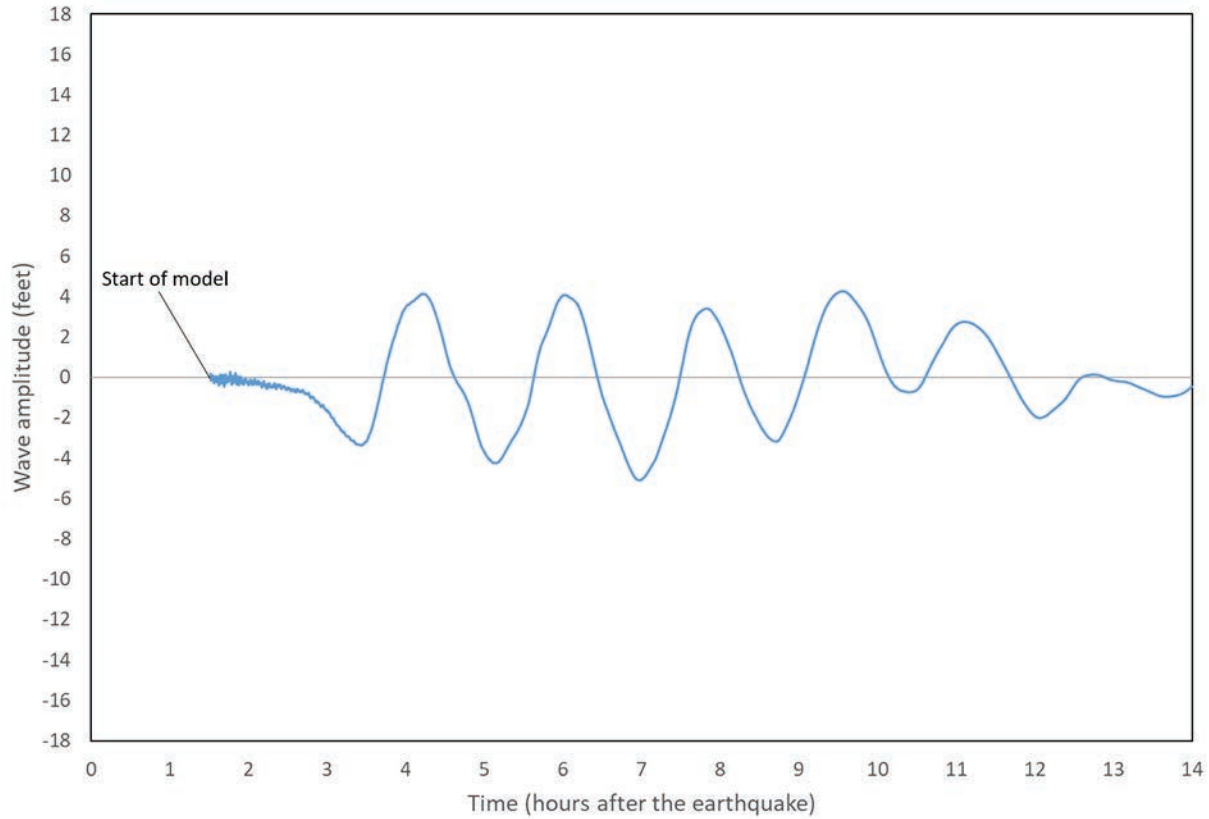
28

Oak Harbor Simulated Tide Gauge



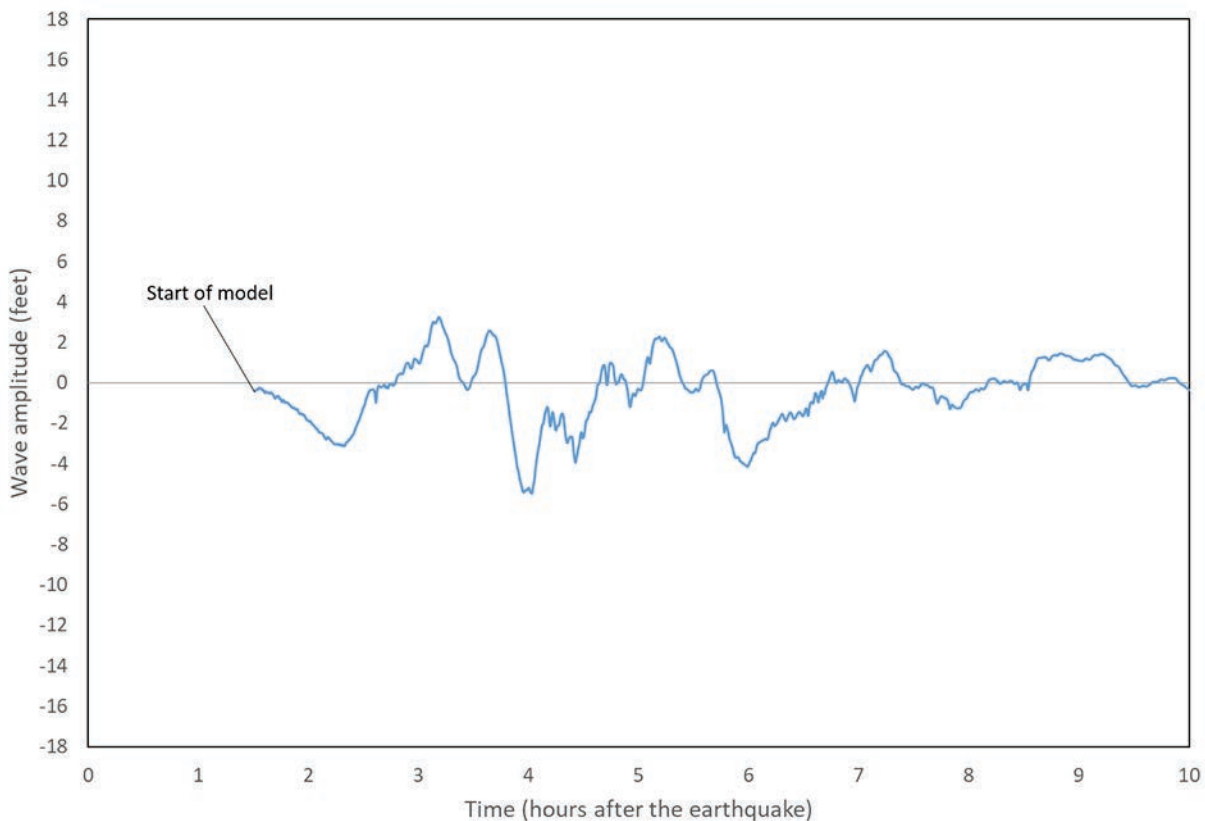
29

Point Victor Simulated Tide Gauge



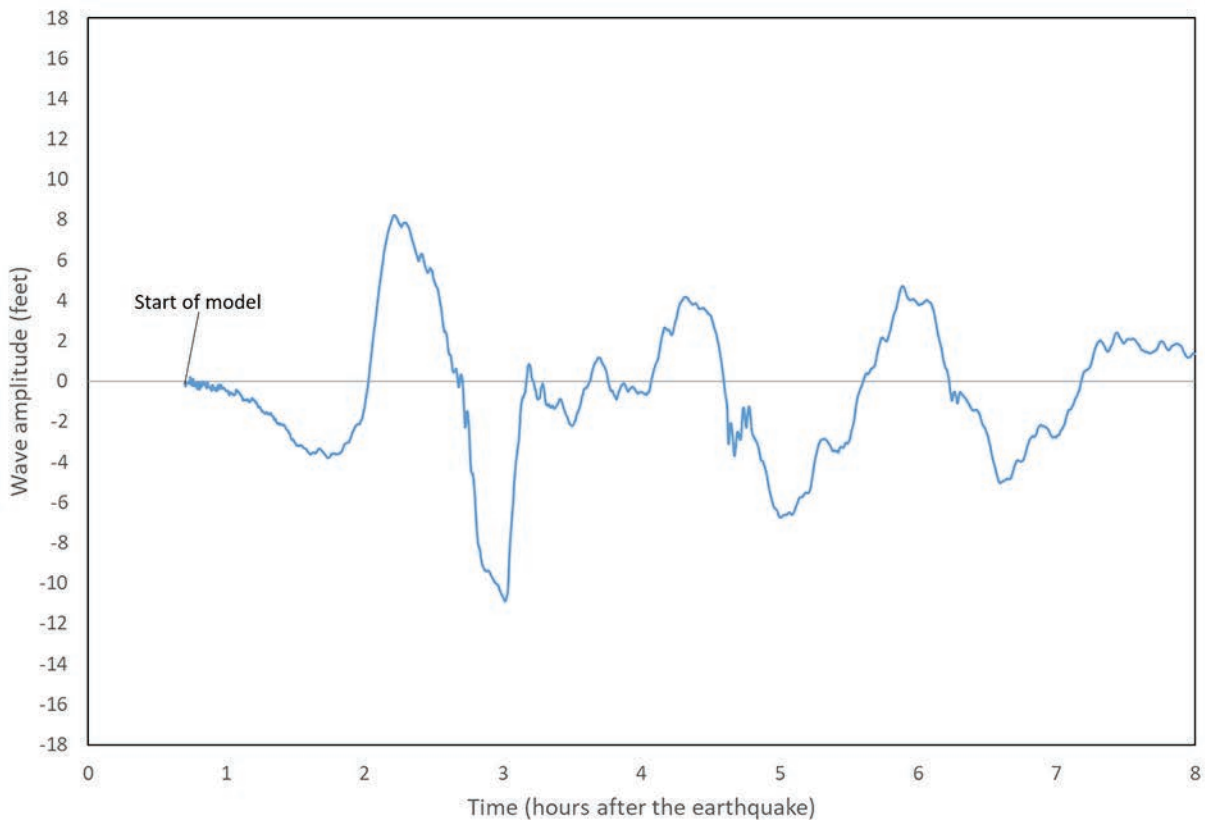
30

Point White Simulated Tide Gauge



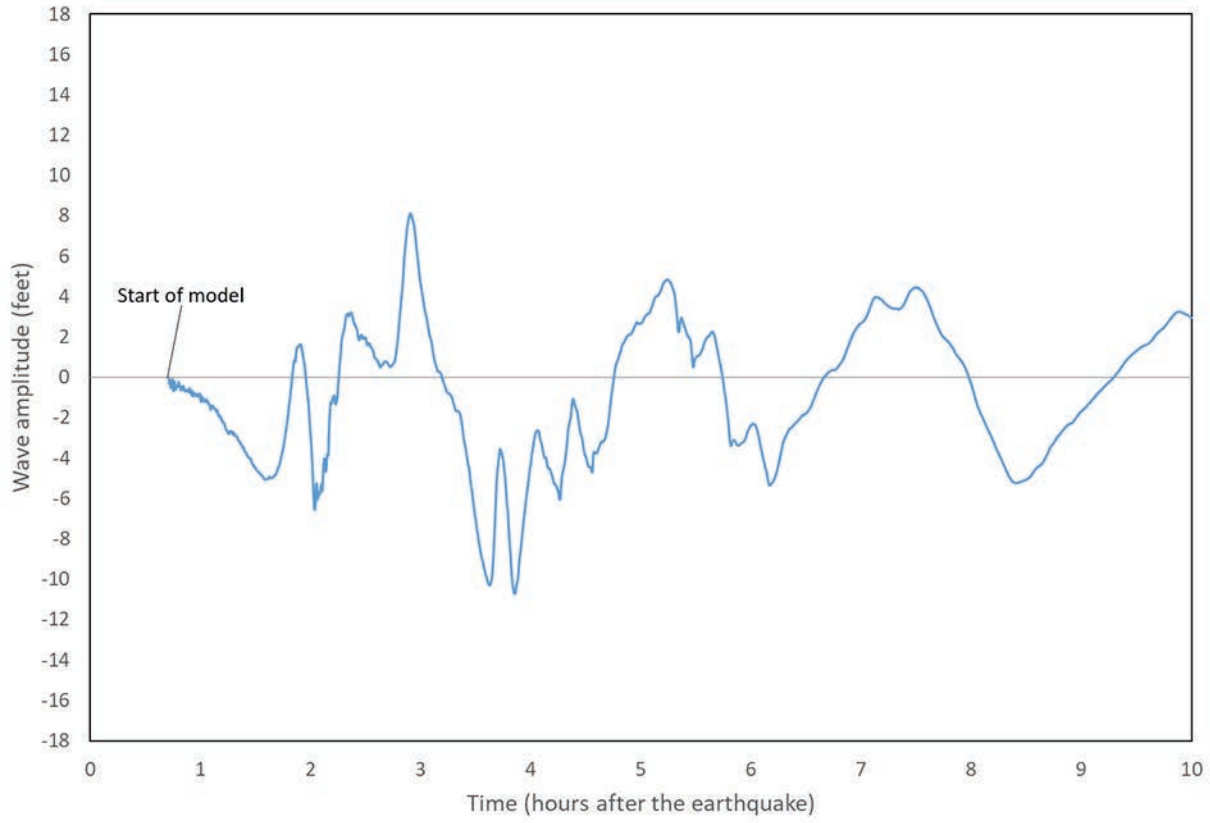
31

Port Gamble Simulated Tide Gauge



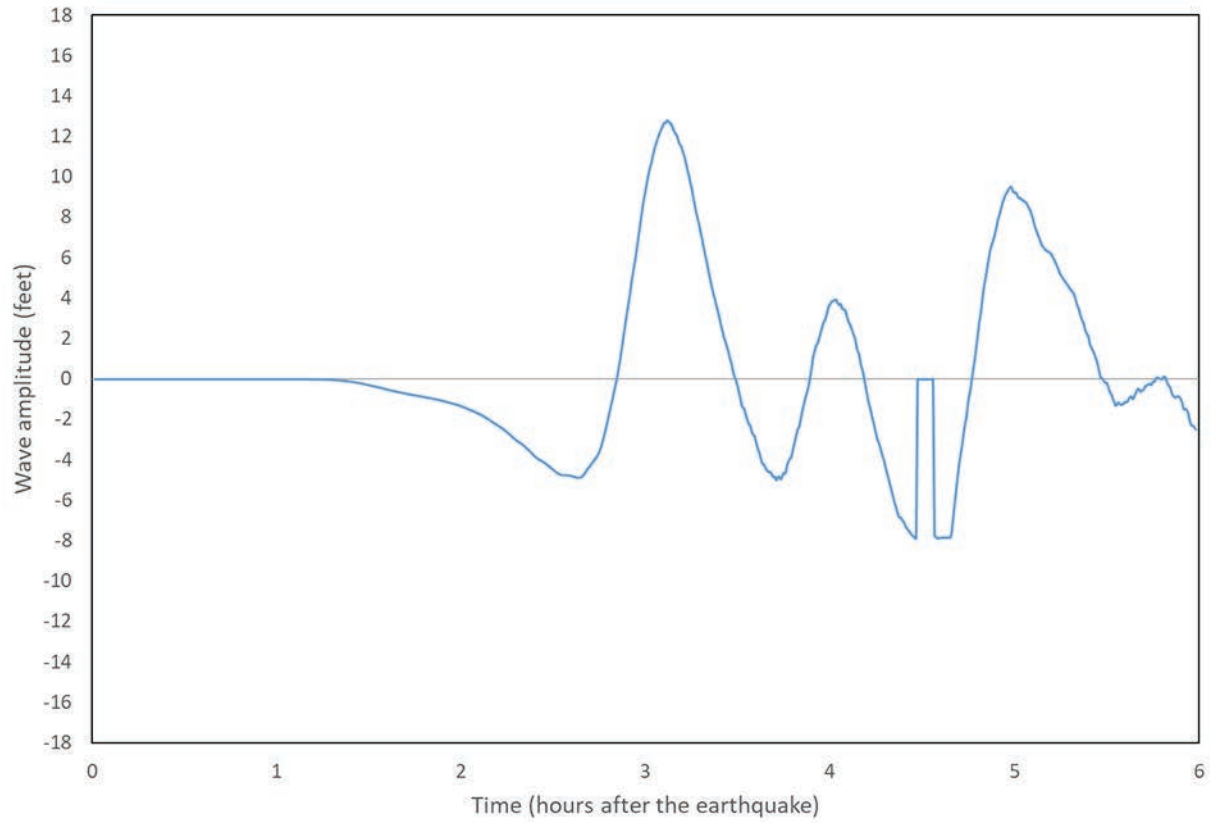
32

Port of Anacortes Simulated Tide Gauge



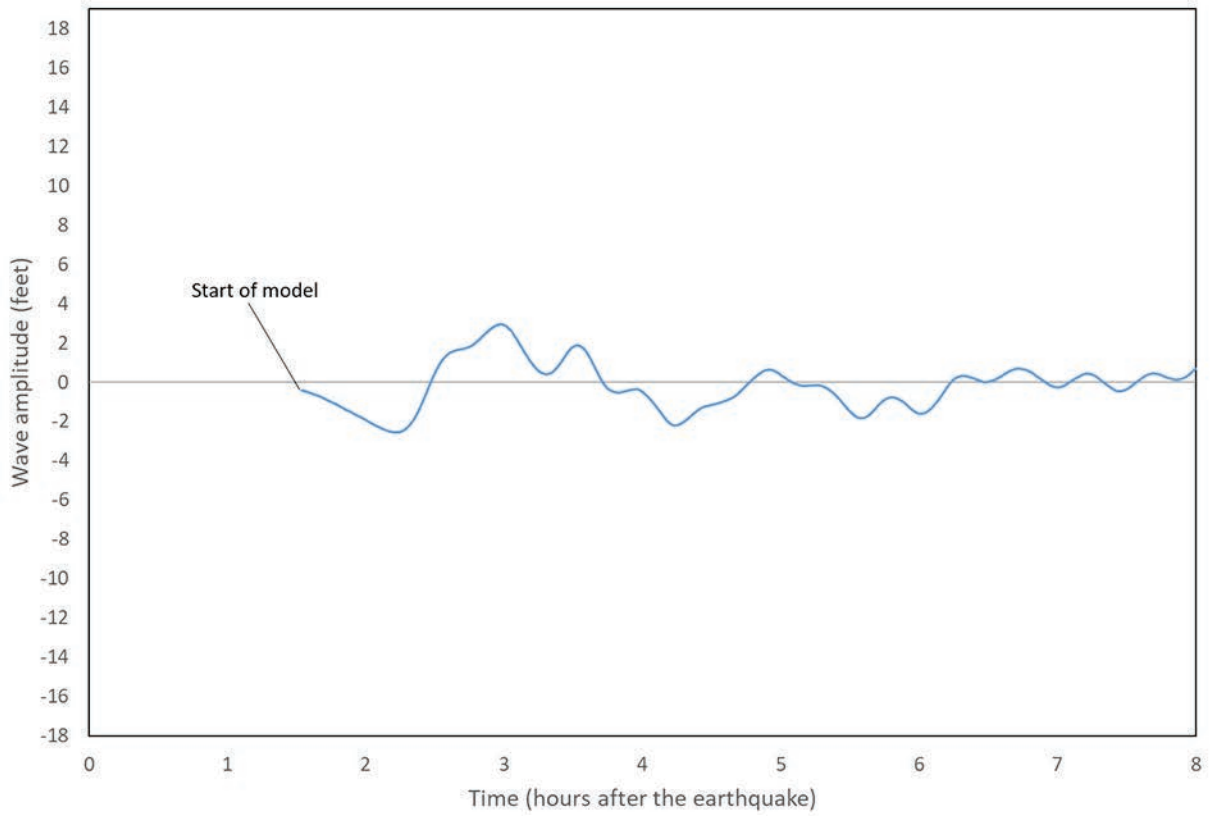
33

Portage Simulated Tide Gauge



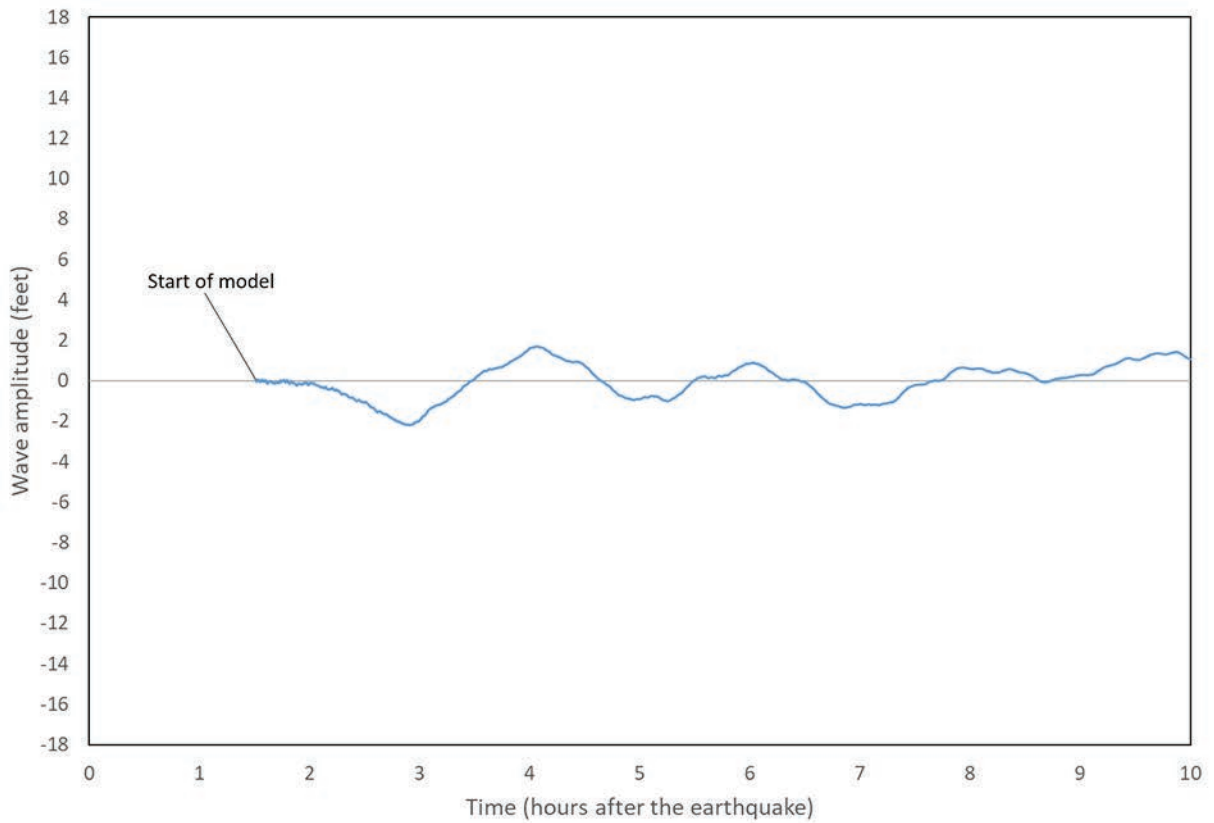
34

Saratoga Passage Simulated Tide Gauge



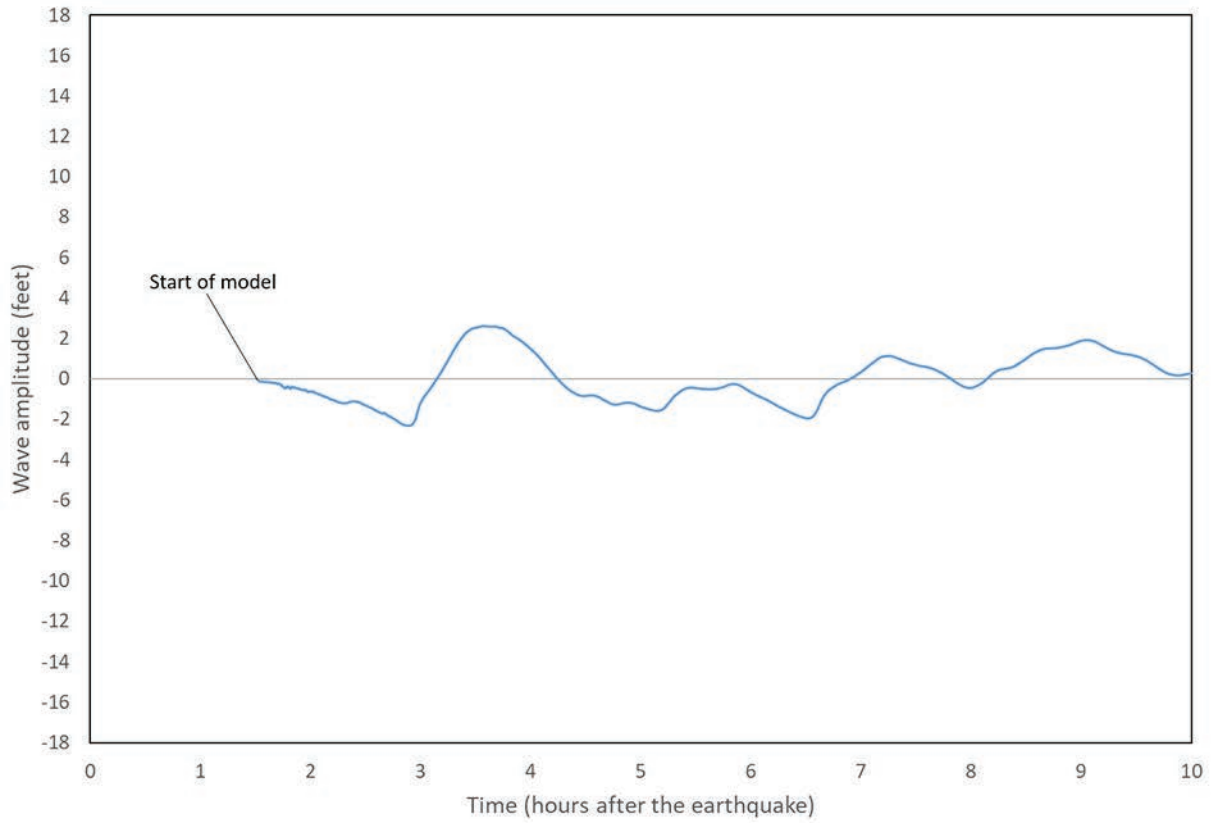
35

Silverdale Inlet Simulated Tide Gauge



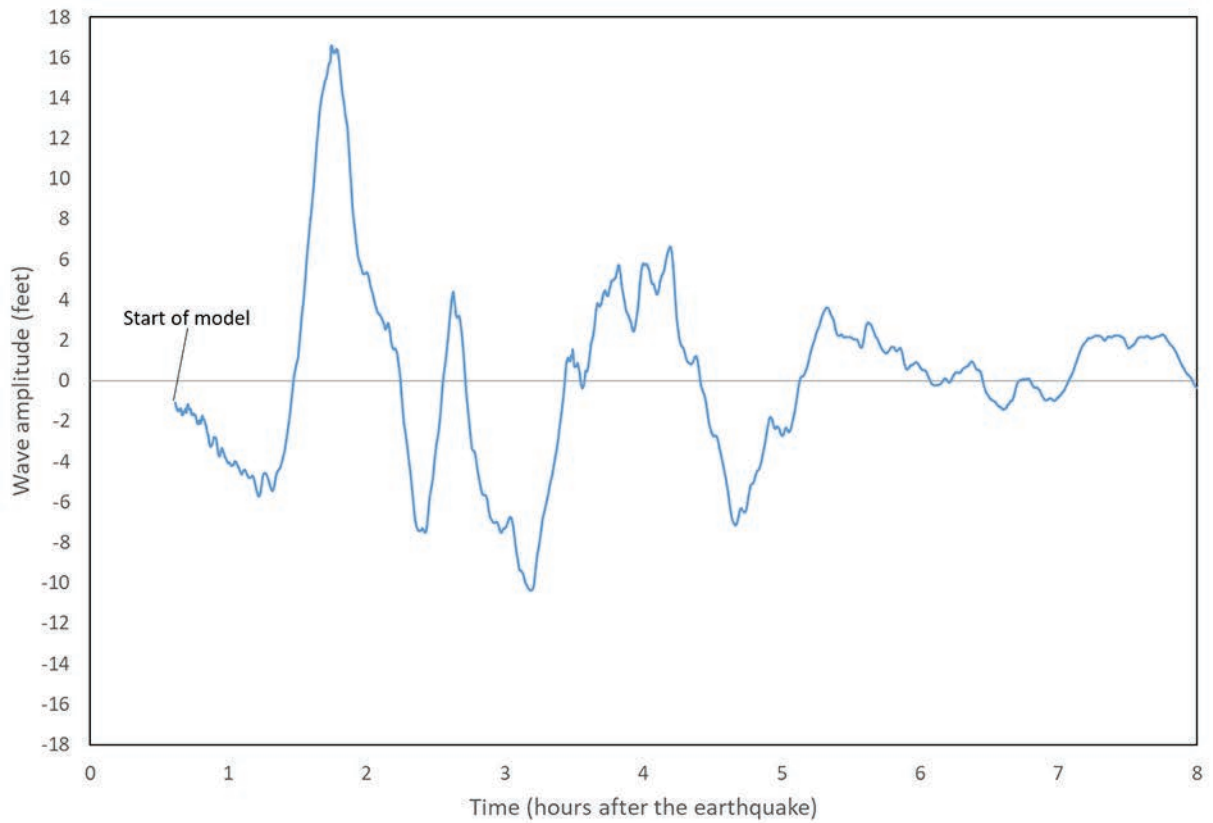
36

Skagit Bay Simulated Tide Gauge



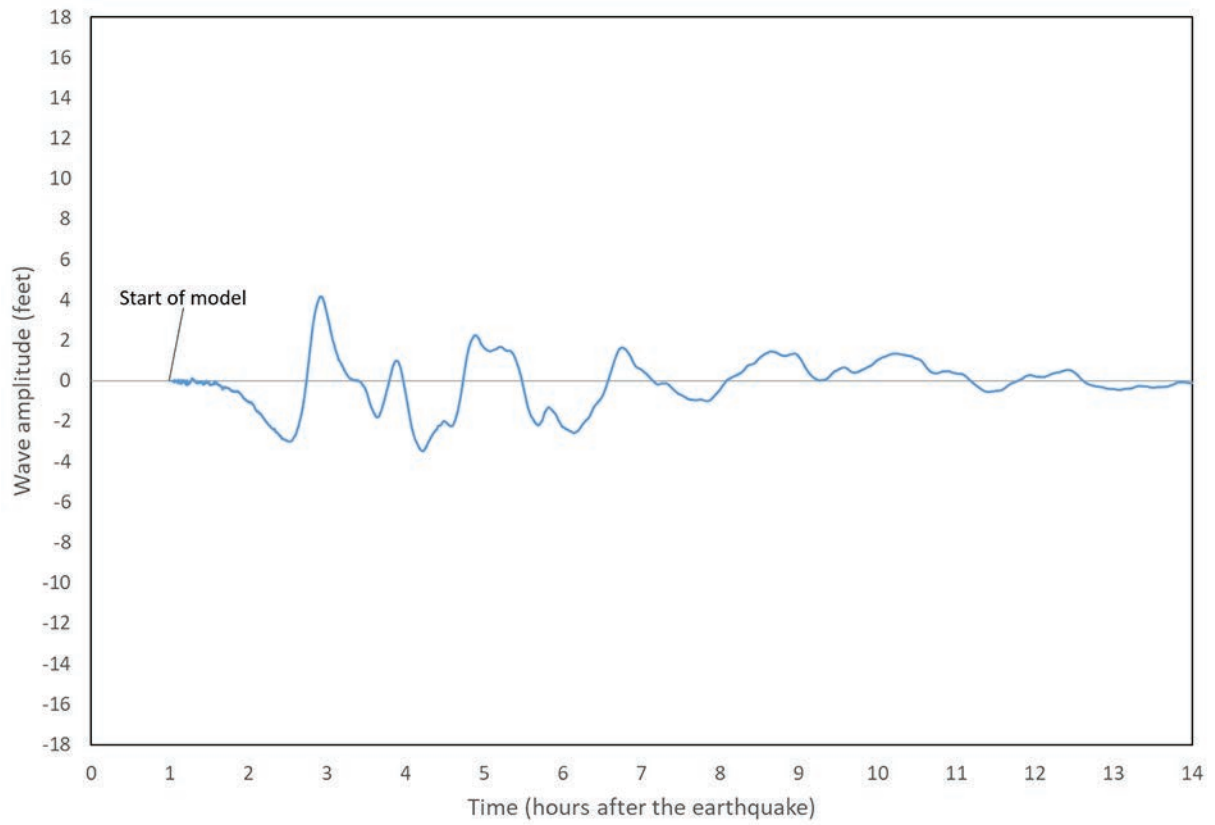
37

Swantown Simulated Tide Gauge



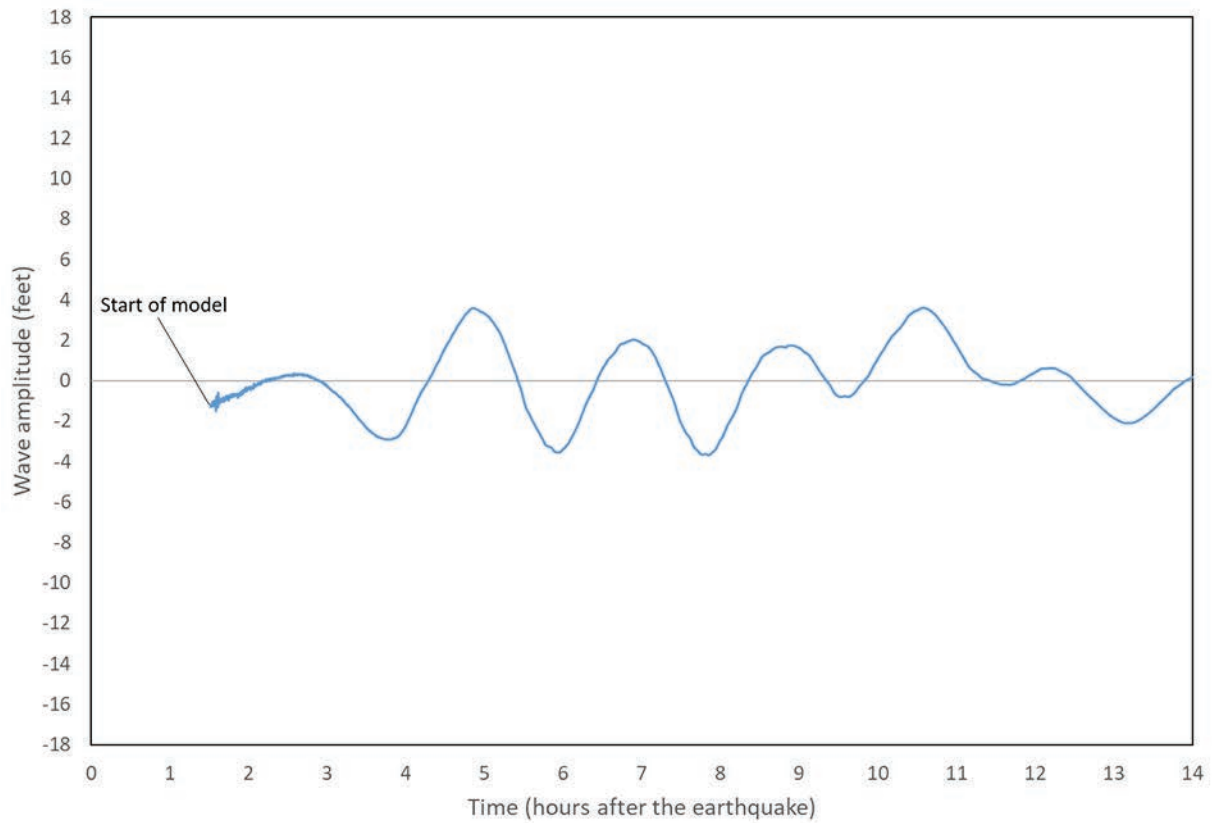
38

Tacoma Narrows Simulated Tide Gauge



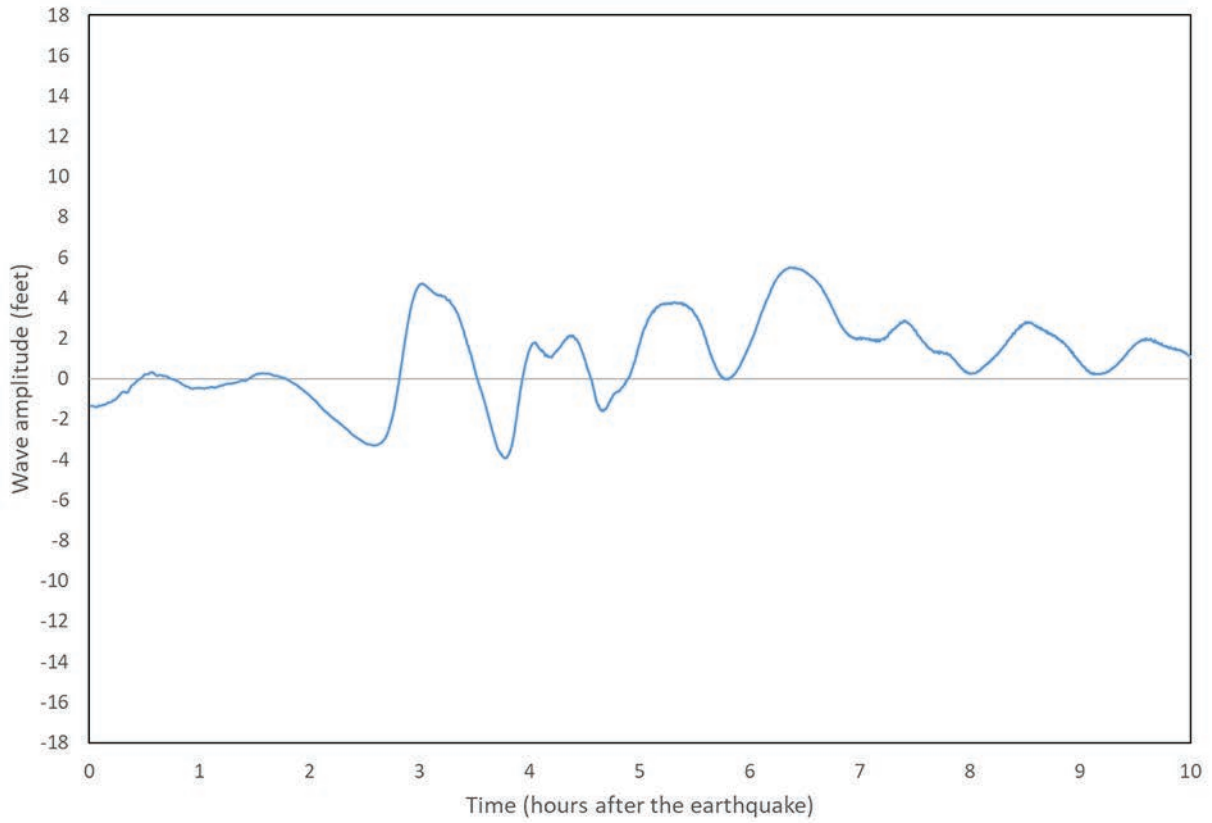
39

Totten Inlet Simulated Tide Gauge



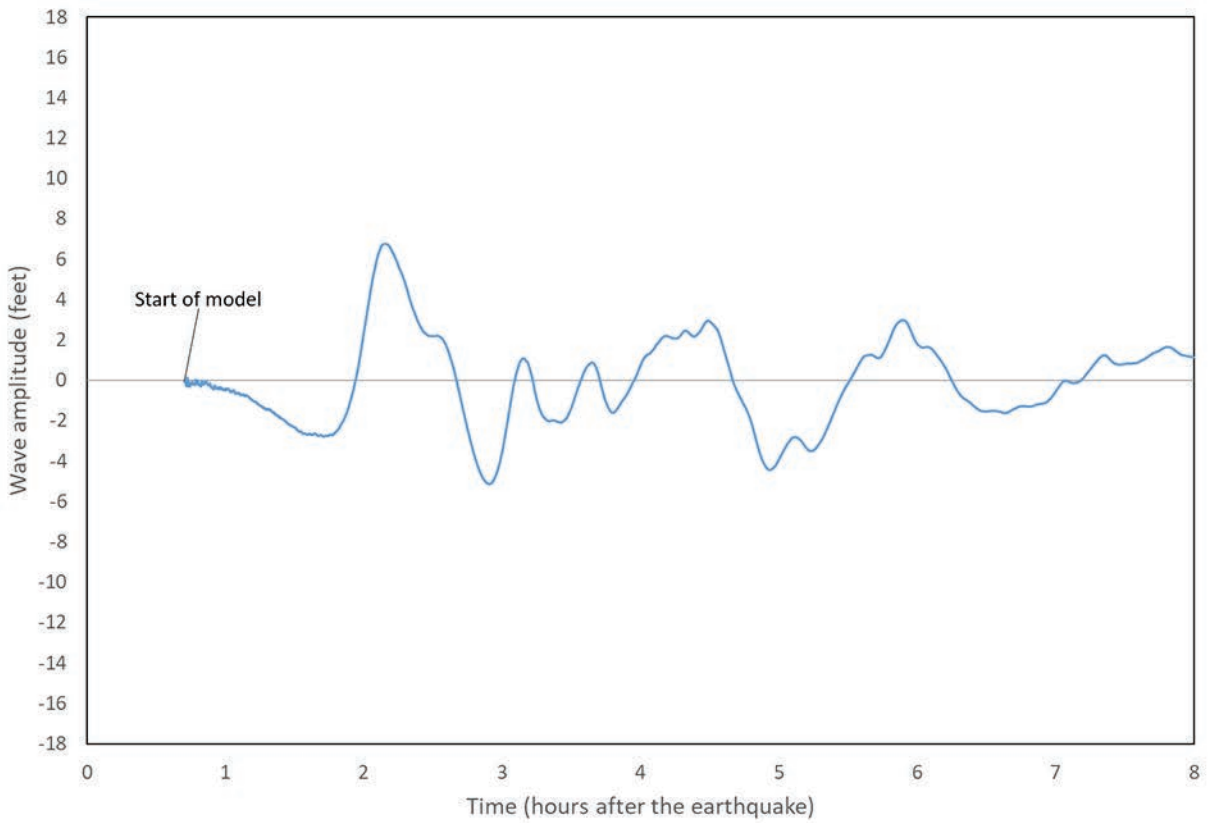
40

Union Simulated Tide Gauge



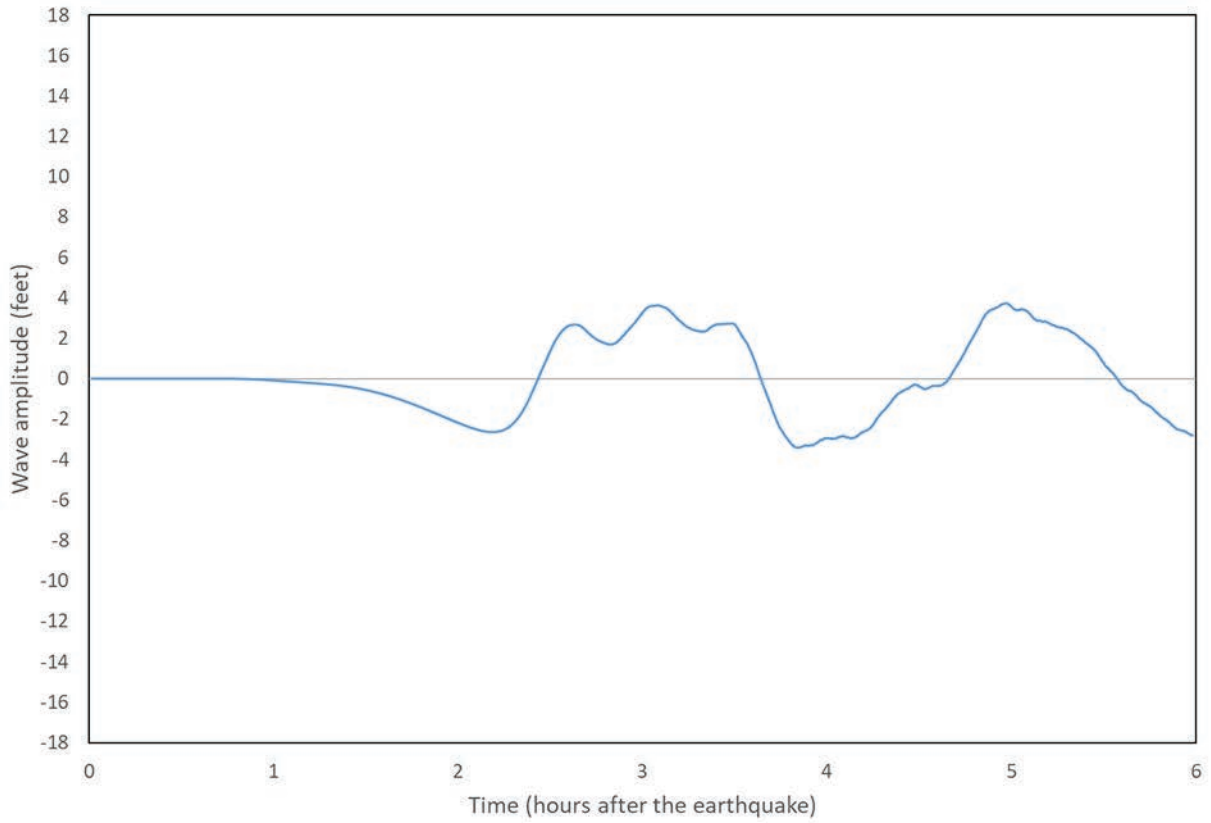
41

Useless Bay Simulated Tide Gauge



42

Vashon Ferry Terminal Simulated Tide Gauge



43

Waterfront Park, Seattle Simulated Tide Gauge

